The Institute of Paper Chemistry

Appleton, Wisconsin

Doctor's Dissertation

The Thermal Conductivity of Dry and Partially Saturated Fiber Beds

David Gerald McMaster

June, 1963

THE THERMAL CONDUCTIVITY OF DRY AND PARTIALLY SATURATED FIBER BEDS

A thesis submitted by

David Gerald McMaster

B.Ch.E. 1958, Georgia Institute of Technology
M. S. 1960, Lawrence College

807 Kingwood Drive
Murfreesboro, Tennessee

in partial fulfillment of the requirements
of The Institute of Paper Chemistry
for the degree of Doctor of Philosophy
from Lawrence College,
Appleton, Wisconsin

June, 1963

TABLE OF CONTENTS

SUMMARY

Drying studies have indicated that a better understanding of the heat transfer characteristics of fibrous materials is required in order to document the drying phenomena of these systems. The mechanisms associated with the heat flow through porous materials have not been completely described, and this study was undertaken in order to elucidate the role played by fiber and bed characteristics and to increase the information available on the thermal properties of highly porous, fibrous systems.

Fiber beds were formed by filtration of dilute suspensions of synthetic fibers—nylon, dacron, and glass. The thermal conductivity of the fiber beds was determined with a single-specimen, guarded hot-plate apparatus which had the hot plate above and the cold plate below. The steady-state heat flux in the specimen was determined with the heat-meter method which utilized a "standard" Plexiglass disk positioned below the fiber bed specimen such that the bed and "standard" were sandwiched between the hot and cold plates.

The two-phase conductivity study consisted of measurements on dry fiber beds and on beds fully saturated with a nonvolatile oil, dioctyl phthalate. The six two-phase systems allowed observation of solid-fluid conductivity ratios in the range of one to forty.

It was concluded from the measurements on the dry nylon fiber beds that

1. The over-all bed conductivity in the 30 to 60°C. temperature range was only an insensitive function of temperature.

2. Changes in fiber length (2.78 to 5.54 mm.) and diameter (19.3 to 45.4 μ) produced no significant alteration of the over-all conductivity of the beds at the same porosity.

The reduction in bed porosity produced an increase in the conductivity of the bed provided the porosity level was not too high. As porosities were increased above 0.93, the conductivity versus porosity relationship began to level off and radiation and convection mechanisms were apparently responsible.

From the observations on the six two-phase systems it was concluded that:

1. Changes in fiber conductivity produced corresponding changes in bed conductivity provided the elastic moduli of the fibers were similar.

2. Changes in fluid conductivity produced corresponding changes in the effective conductivity of the fiber beds.

3. Porosity reductions produced conductivity variations in the fiber bed which were dependent on the compressible nature of the fibers.

Glass fiber beds and nylon fiber beds had approximately the same over-all conductivity even though the glass fiber conductivity was four times that of nylon. However, dacron fiber beds had lower over-all conductivity values than the nylon beds which corresponded to the difference in fiber conductivity. Because the bed porosity was reduced by compression, it was hypothesized that the deformable nature of the fibers permitted significant fiber-fiber contact areas to be present in the nylon and dacron systems, and that these contact areas contributed to the heat flow in the solid structure of the bed.

Application of a compression theory for a single fiber-fiber contact indicated that the nylon and dacron systems had appreciably more contact area between fibers than the glass system in the porosity regions of the study.

Prediction equations derived for two-phase systems with point contacts between particles corresponded quite well with the glass fiber bed results, but underestimated the nylon and dacron results.

An empirical expression was derived which accounted for the heat flow in the contact regions between fibers, and the response of the calculated contact factors for glass and the compressible systems was consistent with the hypothesis of a fiber-fiber contact area contribution.

The partial saturation study allowed the observation of three-phase systems of fiber-oil-air as a function of the liquid saturation of the void spaces in the beds. The introduction of the nonvolatile oil into the nylon system produced a change similar to that of a porosity reduction, because small solid-fluid conductivity ratios and contact areas between fibers were involved. The parallel phase distribution equation adequately predicted the nylon-oil-air conductivity results.

In the partially saturated glass fiber beds, the large change from the glass-air system to the glass-oil system produced a rapid change in the conductivity-saturation relationship as the oil became the predominant fluid in the voids. Consequently, the need for an adequate description of the distribution of the fluids in the void spaces of the beds hampered the correlation of the glass-oil-air system results.

INTRODUCTION

Many fields, including packed column design, petroleum recovery, insulation, refractories, and drying, require heat transfer information on porous systems under widely divergent operating conditions. The thermal properties of most porous materials are not readily available for application in a given situation. Consequently, many difficulties arise. These difficulties stem from a lack of understanding of the contribution of the components in the system to the over-all heat flow, as well as from an inadequate description of the internal geometry and temperature distribution.

In the paper industry, the lack of understanding of the heat-transfer characteristics of a fiber network is no exception. The mechanisms associated with drying phenomena are intimately related to the heat flow in the fiber system. Early workers in this area directed their attention to the apparent simplicity of the drying rate curve. In reality, these curves only masked the inherent complexities involved in such an operation. Further elucidation of the paper drying operations has had limited consideration. However, recent studies (1, 2) have included efforts in the regimes of water and vapor movement, vaporization zones, heat transfer, moisture distributions, and temperature distributions.

A significant contribution to the understanding of the drying phenomena was made by Cowan (3) in his study of the hot-surface drying of glass fiber beds. This simplified fiber system eliminated some of the difficulties associated with the paper system and, as a result, heat and mass balance equations could be applied in the analysis of the drying data. This analysis was extremely comprehensive and it included estimates of surface evaporation, internal evaporation and vapor diffusion rates along with detailed explanations of drying rate curves, moisture and temperature distributions, etc.

The heat-transfer mechanisms involved in the drying of a porous system include the pure conduction heat flow in the components, heat transfer due to radiation and convection, heat transfer by vapor distillation from warm to cold regions of the system, and heat transfer associated with the liquid movement. Obviously, it will require a concentrated effort for many years before an adequate understanding of these mechanisms and their contribution can be obtained.

It is presently believed that the primary contributions in the drying operation are made by the conduction and vapor distillation mechanisms. The object of this investigation was to observe the pure conduction mechanism of heat flow in the fibrous network, without the interference of the other mechanisms suggested above. Obviously, a drying system would not allow this distinction. Therefore, the thermal conductivity of various fiber systems was obtained by a steady-state measurement—impressing a temperature gradient across a specimen and measuring the heat flux.

With a two-phase fibrous system, measurement of the pure conduction thermal conductivity is not complex unless radiation and convection begin to make a significant contribution. With the three-phase system, the important factor is the volatility of the liquid phase. In drying, the volatile water phase produces the vapor-liquid movement. The elimination of this mechanism of heat flow in the pure conduction study was accomplished by using a nonvolatile liquid.

The selection of the fibrous systems to be studied was largely dependent on the fiber and bed characteristics to be varied in the course of the investigation. The use of pulp fiber, although directly applicable to the paper drying studies, would not be consistent with the desire to obtain specific information on the fiber characteristics and their effect on the heat transfer in the network.

Therefore, synthetic fibers with uniform geometry and no intrafiber pores provided a simpler, more basic system than the wood fiber which swells and shrinks, bonds to other fibers, has internal pore structure, and has a variation in the length and diameter dimensions.

The kinds of synthetic fibers which were utilized were determined by considering the variables in the fiber network which were of interest from a pure conduction viewpoint. The list of variables included temperature, fiber size, fiber and fluid conductivity, porosity or void fraction of the bed, and degree of liquid saturation. It was planned that the variables would be adequately studied in the two-phase systems, dry and fully saturated beds, and that the more important ones would be included in the partial saturation or three-phase study.

For the two-phase study, the bed porosity was anticipated to be the primary consideration. Nylon fibers were selected for the main program of study because a porosity range of 0.8 to 0.95 was conveniently obtainable in the nylon fiber beds. Lower porosity values are of particular interest for application to the paper system. However, extremely large pressures are needed to compress the synthetic fiber bed below 0.8 porosity and it was believed that a satisfactory indication of the effect of bed porosity could be obtained in the 0.8 to 0.95 range.

Fiber conductivity was varied by using two additional fibers, glass and dacron. The glass fiber has a conductivity approximately four times that of nylon and a little more than six times that of dacron.

Response to compression was an additional variation introduced by the use of different types of fibers. Consequently, the effect of compression on the fiber network, and, in turn, its effect on the heat flow in the system was of primary interest in the investigation.

The alteration of fluid conductivity was intimately associated with the three-phase study and the variation of the liquid saturation. The selection of a non-volatile liquid was dependent on the characteristic of the liquid desired and also on the properties of the fibers to be utilized. Dioctyl phthalate oil* was chosen because it had an extremely low volatility, produced no changes in the fiber properties, was fluid enough to conveniently saturate the beds, and was not hygroscopic. With the dioctyl phthalate oil, the fluid conductivity in the fully saturated fiber bed would be more than six times the air conductivity in the dry fiber bed.

The investigation was primarily phenomenological in order to assess the importance of the fiber, fluid, and bed characteristics in the purely conductive flow of heat in the fibrous system. The analysis of the more fundamental aspects of the system and the empirical correlation of the experimental results produce a better understanding of the heat-transfer characteristics of fibrous materials and allow an extension of this understanding to other systems with similar characteristics.

*Ohio-Apex specifications
vapor pressure: less than 0.01 mm. Hg at 100°C.
viscosity: 80 centipoises at 20°C.
impurities: 0.01%
specific gravity: 0.986.

LITERATURE SURVEY

Fiber beds fall into the category of high porosity systems (porosities from 0.5 to 0.99). The principal efforts in the area of heat transfer in porous media have been concentrated in the low porosity range, 0.1 to 0.5, which generally includes the granular materials. On the basis of system geometry and over-all porosity, there are some outstanding differences in the characteristics of the granular and the fibrous systems.

There are also other major distinctions in porous systems as a whole and these distinctions are of primary consequence in analyzing their heat-transfer characteristics. The porous systems can be divided into two groups, continuous fluid and continuous solid. The continuous fluid group can be further subdivided into consolidated and unconsolidated systems. For the purposes of this study, the systems of primary interest are in the unconsolidated, continuous fluid group. These materials are composed of solid particles dispersed in a continuous fluid network with no permanent bond between solid particles. In general, the fiber and granular beds are included in this type of system. However, paper might be considered to be a part of the consolidated group.

It is convenient to divide the following discussion into two sections. The first section will deal with the systems composed of two phases, solid-gas or solid-liquid. The second section will be devoted to the three-phase systems, solid-liquid-gas.

TWO-PHASE POROUS SYSTEMS

There is some information available on the mechanisms of heat flow through dry fibrous materials.

Heilman, (4), in discussing insulation, pointed out that, except with materials containing large pore spaces, heat is primarily transmitted by conduction and that the importance of the air conductance is often unrealized. He believed that the relative significance of internal contact resistances was not extremely important, although this was difficult to observe. He indicated that radiation contributed to the heat flow in the insulation when the system contained large diameter pores. With regard to convection, Heilman observed heat transfer with the heat flowing upward and downward through the specimen and concluded that no convection occurred in materials with pore diameters less than 0.2 inch.

Finck (5) studied the mechanism of heat flow in fibrous materials such as bagasse, cornstalk and wood pulp, flax, kapok, cotton, rockwool, etc. His primary efforts were concerned with conductivity variations associated with changes in bulk density. These results may be explained if one assumes that radiation and convection are of primary importance at a low degree of compaction and that conduction becomes increasingly important as the density increases, but the radiation-convection contribution decreases at a faster rate. Thus, a minimum is reached as conduction becomes the predominant mechanism.

Of considerable interest is Finck's work with fiber arrangement at constant density. Using randomly formed flax specimens for control, specimens with fibers arranged perpendicular to the heat-flow direction exhibited a 20% decrease in conductivity, but specimens with fibers arranged parallel to the heat flow gave a 90% increase in conductivity. Other fibers such as glass wool, hair felt, excelsior, wheat straw, etc., showed similar differences between parallel and perpendicular arrangement.

Finck varied the direction of heat flow through a specimen, and he concluded that convection was negligible even at densities of 0.003 g./cc. Radiation was

observed to be affected markedly by dusting the fiber with aluminum powder. At densities of 0.003 g./cc. the dusted specimens had a 17% decrease in apparent conductivity, but at densities greater than 0.016 g./cc. the change was negligible.

These investigations indicate that conduction is the primary mechanism of heat flow in the normal dry fibrous system. It is on this basis that other investigators have attempted to analyze their conductivity results by utilizing the so-called phase distribution equations (6, 7).

The phase distribution equations are the simplest and most straightforward method of predicting the conductivity of a composite system. When conduction is the only mechanism of heat flow, the maximum conductivity for the system can be obtained by considering the components to be thermally in parallel in the direction of the heat flow. This gives the parallel phase distribution equation,

$$K = \epsilon K_g + (1-\epsilon)K_s, \qquad (1)$$

where ϵ is the porosity and K, K_g, and K_s are the thermal conductivities for the composite, fluid phase, and solid phase, respectively.

If the components are considered to be thermally in series in the direction of the heat flow, the series phase distribution equation results:

$$1/K = \epsilon/K_g + (1-\epsilon)/K_s \qquad (2)$$

The series model predicts the minimum composite conductivity.

Bogaty, et al. (6) utilized a combination of the parallel and series models in order to analyze the effect of fiber arrangement on the thermal properties of textiles made from wool, cotton, orlon, and viscose. The conductivity relationship,

commonly referred to as the Schuhmeister expression for a two-phase composite, was

$$K = A[\epsilon K_g + (1-\epsilon)K_s] + BK_sK_g/[\epsilon K_s + (1-\epsilon)K_g] \qquad (3)$$

where A and B are taken to be the effective fraction of the fibers parallel and perpendicular to the heat flow. Applying Equation (3) to the various parallel and perpendicular arrangements studied by Finck (5), surprisingly good agreement with the experimental values was observed. In the analysis of their results for the conductivity-density relationships for the various fabrics, they concluded that the relative fiber arrangements as indicated by A and B were altered as the fabrics were compressed. These changes were also dependent on the fiber conductivity.

Since these investigations and analysis of the thermal properties of dry fibrous materials do not provide an extensive background for the study of the heat-transfer mechanisms associated with porous materials, a review of the work that has been accomplished utilizing two-phase granular systems is necessary.

Wilhelm, et al. (8) discussed the reaction rate and heat transfer in a fixed-bed catalytic converter and also included a correlation for the thermal conductivity of a static bed (flow absent) and an estimate of the radiation effect. They stated, "a complete mathematical description of a bed of particles ..., is difficult if not impossible, and attempts to compute theoretically the thermal conductivities of such systems have not proved notably successful." They summarized the status of knowledge of heat transfer in systems of solid particles as follows:

1. Heat transfer is almost purely conductive provided particle size, gas pressure, or temperature are not too high (upper limits: 3-4 mm. diameter, 8-10 atm., 300°C.).

2. Effective conductivity is more dependent on the continuous phase than the discontinuous phase.

3. Bed conductivity approaches that of the solid phase when the porosity is small.

4. The thermal conductivity of granular systems exhibits a pressure dependence which sets in at much higher gas pressures than ordinarily observed for gases in unpacked containers. This is attributed to the interstitial distances which approach the mean free path of the gas molecules.

This summary coincides with the conclusions made by Waddams (9) in his analysis of several investigations (10-14).

Woodside and Messmer (15) have recently made an extensive study of the thermal conductivity of unconsolidated media—sand, glass beads, lead shot—with air, n-heptane, and water as the saturating fluids. They reported:

(a) The conductivity variation with porosity was greater the higher the conductivity of the saturating fluid.

(b) The effect of larger solid conductivities was increased when the conductivity of the saturating fluid was increased.

(c) The effective conductivity of the media increased as fluid conductivity increased.

(d) In vacuo conductivities were one-hundredth of the conductivity of the solid particles.

(e) The part of the gas phase which was important in heat conduction extended from the contact points to a distance of one-sixth of the particle radius.

The usual granular systems have certain characteristics which make a theoretical analysis of the heat-transfer characteristics of the system plausible:

1. Conduction is the primary mechanism.
2. Particle size and shape are uniform.
3. Internal structure is a fairly regular array.
4. Point contacts exist between particles.

Consequently, the relationships derived for the prediction of the thermal conductivity of a composite material normally involve three parameters associated with the individual components: (1) thermal conductivity, (2) volume concentration, and (3) phase distribution. The distribution of the components in a two-phase system provides a wide variation in the type and applicability of the derived prediction equation.

Maxwell proposed a model system composed of spherical particles randomly dispersed in a continuous phase. These particles were so far apart as to have no influence on one another. The conductivity of such a model is given by

$$K = K_g[2\epsilon K_g + (3-2\epsilon)K_s]/[\epsilon K_s + (3-\epsilon)K_g] \qquad (4)$$

The conductivity results for an actual granular system are greatly underestimated by this noninteracting system of spheres.

Several authors have attempted to modify Maxwell's basic equation in order to obtain predictions consistent with the experimental results for granular materials. Strickler (16) utilized two factors which were functions of surface area and solid conductivity in his adaptation of Equation (4). This adaptation produced satisfactory predictions for the effective conductivities of powder and glass sphere systems (17). Strickler (18) also published calculated results which compared favorably with the experimental values for granular beds (19).

A better modification of Maxwell's equation was made by deVries (20). He attempted to compensate for the differences in the temperature gradients which existed in the solid and fluid components by incorporating a particle shape factor in his analysis. The expression for a two-phase system is

$$K = [\epsilon K_g + (1-\epsilon)F_1 K_s]/[\epsilon + (1-\epsilon)F_1] \qquad (5)$$

with $$F_1 = (1/3)\sum_{i=1}^{3} [1 + g_i(K_s-K_g)/K_g]^{-1}$$

and $$\sum_{i=1}^{3} g_i = 1,$$

where g_i is the particle shape factor ($g_1 = g_2 = g_3$ for the spherical particles of Maxwell's equation).

A different type of phase distribution and analysis has been proposed by several authors. These systems are composed of particles arranged in a cubic lattice. Russell (21) and later Topper (22) utilized an array of cubical voids with the void faces perpendicular to the heat flow. Both arrived at the same solution for the continuous solid system by assuming the heat flow lines in the model were parallel. If the system is altered such that the fluid phase is continuous, the following conductivity equation is produced

$$K_g/K = 1 - (1-\epsilon)^{1/3} + \frac{(1-\epsilon)^{1/3}}{(K_s/K_g)(1-\epsilon)^{2/3} + 1 - (1-\epsilon)^{2/3}} \qquad (6)$$

Woodside (23) and Webb (24) also utilized the cubic lattice model for spherical particles in a continuous fluid phase. Using the assumptions of pure conduction and parallel heat flow lines, the thermal resistance of the model was evaluated to give

$$\frac{K_g}{K} = 1 - \left[\frac{6V_s}{\pi}\right]^{1/3} \left[1 - \frac{a^2-1}{a} \ln \frac{a+1}{a-1}\right] \qquad (7)$$

with

$$a = [1 + 4/\pi\ (K_s/K_g - 1)(6V_s/\pi)^{2/3}]^{1/2},$$

where V_s is the solid fraction, equivalent to $(1-\epsilon)$.

Conductivity predictions calculated on the basis of the cubic lattice models have produced satisfactory correlations with the experimental results for certain granular systems.

The derivation which has proved to be the most applicable to a wide range of two-phase granular systems has been presented by Kunii and Smith (25). In their detailed analysis of heat transfer in a bed of unconsolidated spherical particles, they assumed the following mechanisms:

1. Heat transfer through the fluid in the void space by conduction and radiation.

2. Heat transfer through the solid phase.
   a. Conduction through the contact surfaces.
   b. Conduction through the stagnant fluid near the contact surfaces.
   c. Radiation between surfaces of the solid particles.
   d. Conduction through the solid particles.

The over-all mechanisms 1 and 2 were assumed to be in parallel while mechanism d was in series with the combined result of parallel mechanisms a, b, and c. At ordinary temperatures and with small particles, the radiation terms can be omitted and the derived expression becomes

$$\frac{K}{K_g} = \epsilon + \frac{\beta(1-\epsilon)}{\frac{1}{(1/\phi)+(D_p h_c/K_g)} + \gamma \frac{K_g}{K_s}}, \qquad (8)$$

where h_c is the heat transfer coefficient at the contact and D_p is the particle diameter. Neglecting the heat flow through the contact surfaces of the particles, Equation (8) becomes

$$K/K_g = \epsilon + \beta(1-\epsilon)/(\emptyset + \gamma\, K_g/K_s) \qquad (9)$$

where β, γ, $\emptyset$ are parameters for the distances between particle centers, and the effective length in the direction of heat flow of the solid particle, and the fluid filaments adjacent to the contacts, respectively.

Other relationships have been proposed (14, 26) and utilized (8, 27) with good success for certain granular systems under specific conditions. Austin (28) has presented an extremely comprehensive discussion concerning the conductivity of nonmetallic two-phase systems, including those of high porosity, and he reviews the effect of porosity, temperature, system geometry, and component conductivity on composite apparent conductivity.

In attempting to apply the information concerning the heat transfer characteristics of granular materials to the fibrous systems, one is confronted with differences in porosity, particle shape, and particle contact. The various models utilized in the analysis of the granular beds can be applied to the composite systems over the entire porosity range. Also, component concentration in the system is generally believed to be more important than the individual shape of a specific particle. This leaves the contact between particles as a major distinction between the fiber and granular systems, primarily because the fiber beds are compressed in order to reduce the porosity.

The magnitude of the contact areas between fibers in a bed and the effect of significant contact on heat flow in the system is not known. It should be noted

that consolidated granular systems have much higher conductivities than unconsolidated beds (21). Therefore, any contact area between fibers in the solid structure of the bed would produce a system analogous to the consolidated particles and an alteration in the flow of heat would be expected.

THREE-PHASE POROUS SYSTEMS

The three-phase systems retain all of the difficulties associated with the two-phase network and introduce the additional complexity related to the geometrical configuration of the liquid phase in the pore spaces and its influence on the heat flow in both the void volume and the solid structure of the system.

All of the information available on the heat-transfer characteristics of three-phase materials are related to systems in which water is the liquid phase. In these systems the vapor and liquid movement contribute to the heat flow in the network. Therefore, any analysis of a system's conductivity when the liquid phase is volatile must account for the heat flow by vapor distillation as well as by conduction.

The liquid-vapor movements associated with a partially saturated porous material on which a temperature gradient has been impressed has been the subject of recent controversy and discussion. The most comprehensive analysis of the phenomena has been presented by Philip and deVries (29). They critically analyzed (a) the large value of the apparent vapor transfer in comparison with the simple theory prediction, (b) the effect of moisture content on net moisture transfer, and (c) the transfer of latent heat by distillation. Their prediction equation for the effective conductivity of partially saturated sand took the form of deVries' (20, 30) modification of Maxwell's expression for three-phase systems. They utilized an

apparent conductivity, K_v, which can be attributed to the transfer of latent heat of vaporization by vapor diffusion through a wetted pore space under the influence of a temperature gradient. This apparent conductivity can be expressed for the saturated vapor conditions as

$$K_v = D\lambda [P_a/(P_a-p_o)][d\rho_o/dT] \qquad (10)$$

where D is the molecular diffusion coefficient for water vapor in air, λ is the latent heat of vaporization, P_a is the total pressure, p_o is the partial pressure and ρ_o is the density of the saturated water vapor.

Philip and deVries simply added the apparent conductivity due to vapor distillation, K_v, to the conductivity of the air, K_g, and used the total result for the air phase in their calculations. The results of this type of analysis were consistent with the conductivity of partially saturated sands as determined by a transient line heat source method (20, 30). Woodside, et al. (31, 32) also utilized this approach and found good agreement with the conductivity results for sands and clays as measured with a guarded hot plate technique.

A different approach was taken by Herminge (33) in his investigation of the conductivity-moisture characteristics of partially saturated glass fiber fabrics by the dynamic Angstrom method (measurement of the propagation velocity of a heat wave in the material). His correlation equation was a combination of the parallel and series phase distribution equations for three components. The apparent conductivity due to vapor distillation, K_v, was applied to that fraction of pore space which contained water. The two parameters expressing the fractional amount of parallel and series contribution were determined from the dry and completely saturated fabric conductivities. The resulting conductivity equation predicted results which coincided with the partially saturated fabric conductivities.

Gemant (34) has proposed a conductivity expression for a model system of spherical particles saturated up to 20% of the total void volume. However, this expression has been severely criticized (35, 36) because of its neglect of the air phase conductance and for its use of artificial chipped areas of contact between the particles. In addition, Gemant did not consider the effect of vapor movement in his system.

The remainder of the information on the heat transfer characteristics of three-phase systems has been derived from drying studies. It is difficult to evaluate some of these conductivity results because of the dynamic conditions associated with the drying phenomena.

Nissan, et al. (37, 38) computed apparent conductivities for partially saturated wool fiber mats from temperature-time relationships observed during air drying studies.

Han and Ulmanen (2) utilized a heat balance at the hot surface of pulp beds during drying in order to calculate the apparent conductivity at the moisture content of the hot-surface region. Cowan (3) pointed out that these values were artificial due to the neglect of the hot-surface evaporation rate. Realizing the difficulty in predicting the mass movement during drying, Cowan proposed a heat balance in a region in the bed where liquid and vapor movement was negligible. Such were the conditions in the central regions of the glass fiber beds during the constant-rate drying period because the moisture gradient and the temperature gradient were small. However, since mass movement appeared to depend on the actual drying rate, no generalized apparent conductivity-saturation relationship could be acquired. The specific apparent conductivity-saturation data for the central region of the glass fiber bed and also some of the values reported by Herminge (33) are shown in Fig. 1.

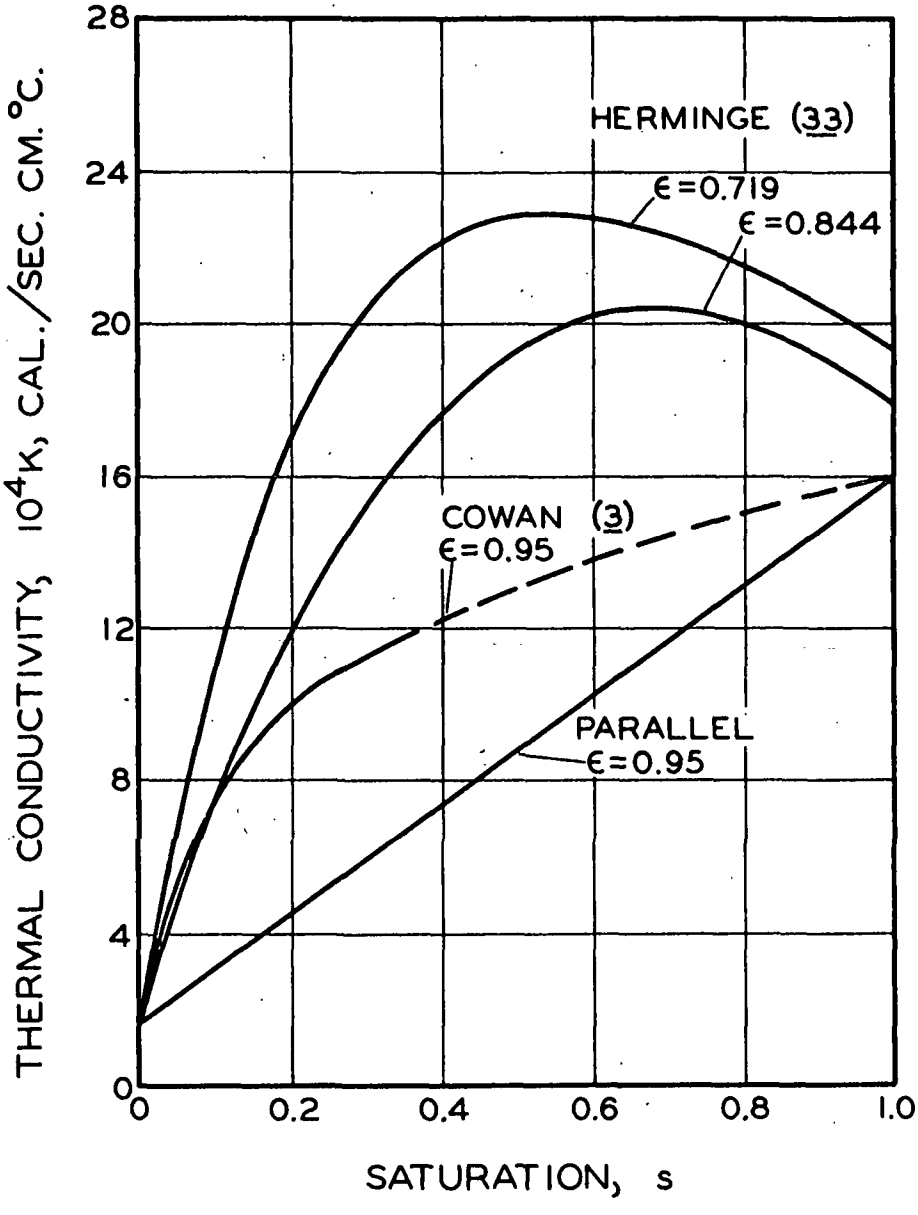

Figure 1. Conductivity of Glass-Water-Air Systems at ca. 70°C.

The parallel phase distribution equation for a three-component system is included in Fig. 1 in order to indicate the maximum conductivity for the material in which conduction is the only mechanism of heat flow. A discussion of the apparent conductivity-saturation curves will provide a better insight as to the complexities associated with heat transfer in a system with a volatile liquid phase.

Looking at Fig. 1, as the water enters the bed, the vapor diffusion from hot to cold regions in the system immediately produces a significant rise in the over-all apparent conductivity. Once a continuous liquid network is formed, the return liquid flow by capillary forces balances a portion of the heat flow by vapor diffusion. As a result, the apparent conductivity-saturation relationship levels off. As the saturation level increases further, the air space in the bed decreases and restricts the vapor movement until the apparent conductivity and pure conduction curves converge at total saturation.

CONDUCTION EQUATIONS FOR COMPRESSIBLE SYSTEMS

A theoretical treatment of the thermal characteristics of a porous system is confronted with numerous difficulties, which leads most investigators to conclude that such an analysis is impossible. The actual composite system consists of some distribution of components. With unconsolidated systems this distribution is dependent on the size and shape of the particle involved and must be defined in order to continue with the analysis. With some systems an idealized, geometrically definable structure may be utilized as a model. However, with a fiber bed, where the fibers assume a random distribution in the x-y plane of the bed, a useful mathematical description of such an array presents vast problems.

The consideration of the heat flow through a system with the complex geometry leads to insurmountable difficulties. With a two-component system of particles and fluid having an imposed steady-state temperature gradient, the description of the temperature distribution in the structure would have to be revealed in order to provide the boundary conditions for any derived equations for either or both components. The temperature distribution is dependent on the individual system. The factors of component conductivity and system geometry immediately illustrate that the temperature within the structure is a function of the location in the bed and that variation of these factors induces variation in the temperature distribution.

A graphic illustration of the above statements is provided by Woodside and Kuzmak (39) who measured the temperature gradient in the pore space of a model porous system. Their results are shown in Fig. 2. With their system of spherical particles, the solid conductivity was larger and the porosity was lower than with

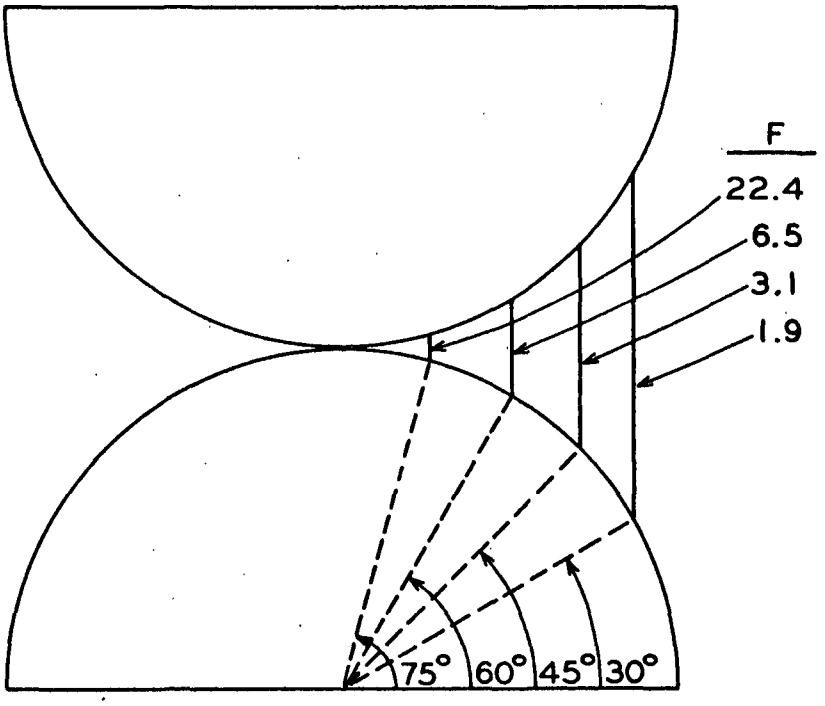

$$F = \frac{\text{PORE TEMPERATURE GRADIENT}}{\text{OVER-ALL BED TEMP. GRADIENT}}$$

BED POROSITY = 0.47

COMPONENT	MATERIAL	CONDUCTIVITY
SOLIDS	MARBLE SPHERES	46×10^{-4}
VOIDS	SILICA AEROGEL	0.58×10^{-4}

Figure 2. Temperature Gradients in Pore Space [Woodside and Kuzmak (39)].

the fibrous system. Nevertheless, the wide variation in the temperature distribution in the pore space is evident. The rigorous application of the general case is difficult and, therefore, simplifying assumptions associated with the temperature distribution and system geometry are usually incorporated in order to make any headway in the analysis of the porous system. The assumptions are widely divorced from the actual conditions and the resulting solutions are unsatisfactory for the general case.

The treatment of the type of heat-transfer mechanisms which occur in the porous systems also produces additional difficulties when high porosity systems are involved. Conduction is the major mechanism, but strict analysis must regard the contribution of convection and radiation as the pore volume becomes large.

TWO-PHASE EQUATION

Because of the successful efforts of Kunii and Smith (25) with their derivation for spherical particles, the initial efforts to predict the fiber bed conductivity results of this study were directed toward a similar relationship for cylindrical particles. These efforts were not entirely successful, but the treatment for aligned cylinders was completed and is presented in Appendix I. The aligned-cylinders configuration should produce the maximum effective conductivity provided the solid-solid contact contribution is negligible and the assumption of parallel heat flow lines is valid.

The analysis of the crossed cylinders in the manner of Kunii and Smith was confronted with geometrical descriptions which were impractical. Modification of the method and the resultant simplification allowed an analysis of the crossed-fiber system to be accomplished. The treatment which is presented in Appendix II was limited by the evaluation of the extent of the contact region.

In a compressible system, such as the fiber bed, consideration has to be given to the decreased resistance in the contact region because of a finite contact area. Ideally, the heat flow in the fluid surrounding the contact and the heat flow through the solid-solid contact should be separated in the analysis. For the initial case, it was assumed that the mechanisms of heat transfer in the compressible, porous system were:

1. conduction in the continuous fluid phase
2. conduction in the solid structure
   a. conduction in the solid particle
   b. conduction in the contact region.

Mechanism 2a and 2b were considered to be in series with each other, and the combined result for the solid structure in parallel with Mechanism 1. The derived expression (similar to the derivation in Appendix I) for the conductivity of the model system was

$$K/K_g = \epsilon + [1-\epsilon]/[(K_g/K_s) + K_g/D_f(h_c\alpha)] \qquad (11)$$

where $\underline{h_c}$ is the heat transfer coefficient for the contact region and α is the ratio of the area of the contact region to the solid cross-sectional area. The effective length of the solid particle in the direction of heat flow was taken to be the fiber diameter. The area of the contact region as defined by the fraction α consists of the solid-solid contact area as well as the area of the fluid filament which contributes to the heat transfer in the solid phase.

Equation (11) satisfies the necessary conditions for a porous material: (a) The effective conductivity of the composite approaches the fluid conductivity when the porosity approaches unity, and (b) The composite conductivity approaches the solid conductivity as the porosity approaches zero, since the contact area becomes large and the contact term $(\underline{K_g}/\underline{D_f}\underline{h_c}\alpha)$ becomes negligible.

THREE-PHASE EQUATION

A description of the distribution of the fluid phases in the porous network presents insurmountable problems. However, at the intermediate levels of saturation, both fluid phases can be considered to be continuous and the following mechanisms of heat flow are assumed:

1. Conduction in the gas phase.
2. Conduction in the liquid phase.
3. Conduction in the solid phase.
   a. Conduction in the solid particle.
   b. Conduction in the contact region.

The contact region in this case includes both the fluid filament adjacent to the contact and the solid-solid contact area.

If Mechanism 1, Mechanism 2, and the combined series result of Mechanisms 3a and 3b are considered to be in parallel, a conductivity expression for three phases can be derived (similar to two-phase derivation in Appendix I),

$$K = \epsilon\,(1-s)K_g + \epsilon s K_\ell + \frac{(1-\epsilon)}{(1/K_s) + (1/D_f h_c \alpha)} \qquad (12)$$

where s is the saturation which is defined as the fractional amount of the void volume which is occupied by the liquid with a conductivity of K_ℓ. The heat transfer coefficient, h_c, and contact area fraction refer to the entire contact region. The effective length of the fiber in the direction of the heat flow is considered to be D_f.

When the contact resistance term $(1/D_f h_c \alpha)$ is small, Equation (12) reduces to the parallel phase distribution equation for three components.

FIBER-FIBER CONTACT AREA

The consideration of the number of fiber-fiber contacts in a fiber bed has not been satisfactorily resolved since the experimental determination of the number of contacts and, therefore, the verification of any of the theoretical calculations has not been accomplished. Likewise, the evaluation of the contact area is controversial in nature, and direct measurement of this parameter in the fiber bed has met with dubious success.

With a lack of sound experimental evidence, estimates of the contact areas in the fibrous systems of this study were acquired by combining two theoretical treatments along with available compression data.

The total number of fiber-fiber contacts in a fiber bed was determined with the equation of Onogi and Sasaguri (40)

$$C_t = 64W^2/\pi^4 D_f^3 \rho^2 HA \qquad (13)$$

where C_t is the total number of contacts between fibers, W is the weight of the fiber bed, D_f is the fiber diameter, ρ is the density of the fiber, H is the thickness of the bed, and A is the cross-sectional area of the bed.

The contact area for a single fiber-fiber contact was calculated utilizing the equations derived by Finch (41) for the response of identical cylinders contacting at any angle, ω. The elliptical contact area is described in terms of the semi axes, a and b as follows:

$$a = m[3NR(1-\xi^2)/2E]^{1/3} \qquad (14)$$

and

$$b = n[3NR(1-\xi^2)/2E]^{1/3} \qquad (15)$$

where m and n are transcendental functions depending on the auxiliary angle τ, N is the total load per contact, R is the radius of the cylinders, E is the modulus of elasticity, and ξ is Poisson's ratio (assumed to be 0.5). For cylinders contacting at right angles, $\omega = 90°$, the auxiliary angle τ is equal to 90°, and m and n become equal to unity. Therefore, the contact area, A_c, with the above conditions becomes πa^2.

The fiber bed is assumed to be composed of a number of layers, L, which have a thickness equivalent to the fiber diameter. Therefore, $L = H/D_f$. The number of fiber-fiber contacts per layer, C_L, becomes equal to C_t/L. If each layer is assumed to support the total compressional load on the bed, G, at a given porosity, then the average load at each contact, N, becomes G/C_L. Therefore,

$$N = GH/C_t D_f \qquad (16)$$

Substituting Equation (16) into Equation (14) and utilizing the value of C_t as expressed by Equation (13), the resulting expression for contact area becomes

$$A_c = 2.83[PD_f^3/E(1-\epsilon)^2]^{2/3} \qquad (17)$$

where P is the compressional stress on the fiber bed at porosity, ϵ, ($P = G/A$). The contact area as a function of porosity for the fibers of this study are shown in Fig. 3. The compressional data of P versus ϵ was taken from the work of Jones (42). Comparison of the contact areas of the fibers at the porosity levels of this investigation indicates that the nylon and dacron values are much larger than those for the glass system.

From the standpoint of heat transfer through the fiber structure of the bed, a better basis for comparison is acquired if the total contact area of a layer is

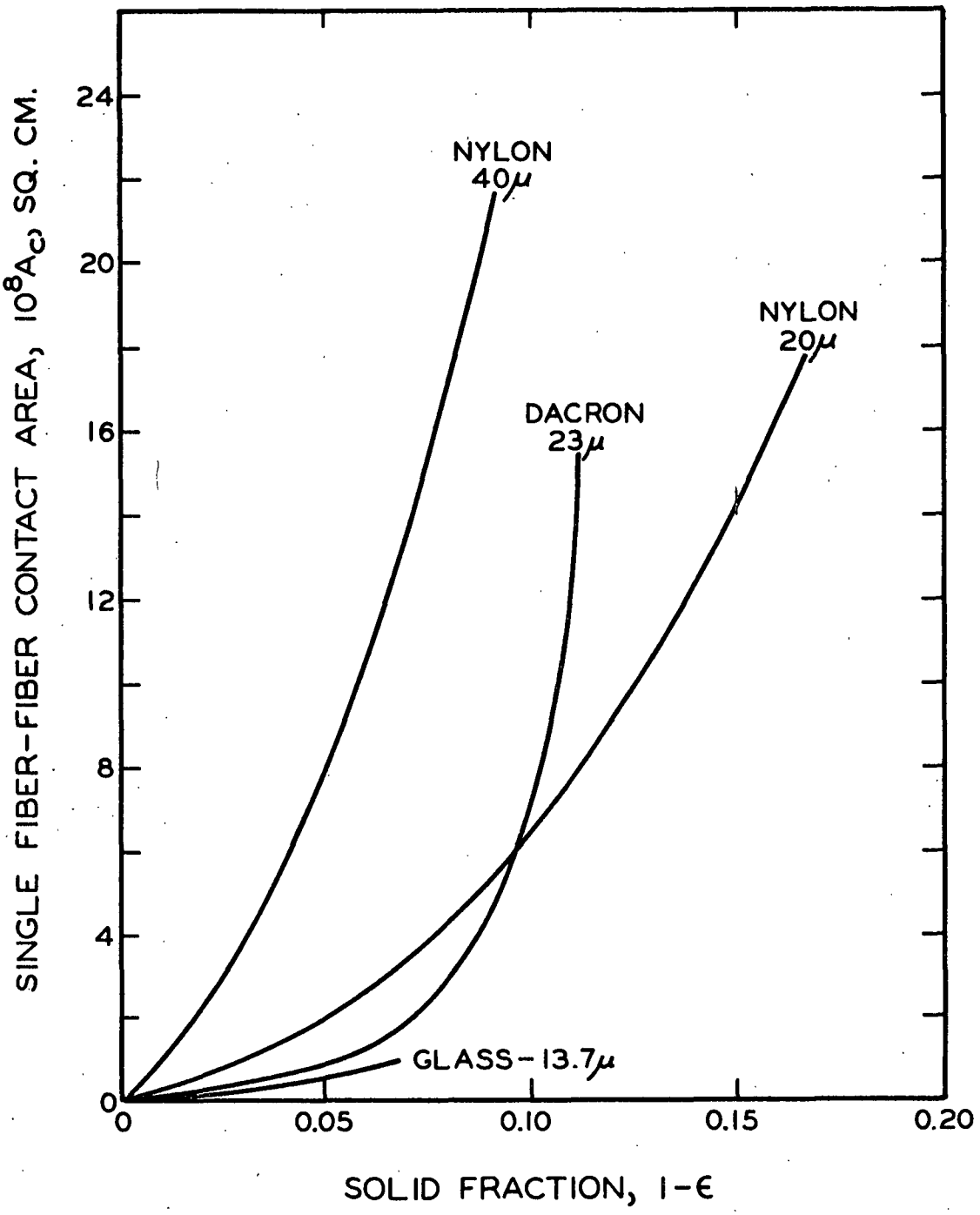

Figure 3. Single Fiber-Fiber Contact Area Response

considered as a fractional portion of the cross-sectional area of the layer which is solid fiber. Therefore,

$$\alpha' = A_c C_L/(1-\epsilon)A \tag{18}$$

where α' is the contact area fraction. Substituting the previously derived expressions into Equation (18) gives

$$\alpha' = 1.86[P/E(1-\epsilon)^{1/2}]^{2/3} \tag{19}$$

The calculated results for the contact area fraction are presented in Fig. 4.

It is apparent that the contact area fraction for a given fibrous system is dependent only on the compressional characteristic of the system. Jones (42) reported that the fiber size did not alter the compressional characteristics of the fiber bed when the length-to-diameter ratio was above a certain critical range. Therefore, if the compressional stress on a given type of fiber bed is assumed to be a function of porosity, then the contact area fraction is dependent only on the bed porosity.

The contact area fractions as calculated should be qualified by the assumptions associated with the stress distribution at the contacts and the angle relationships of the fibers. However, as a basis for comparison, the calculated values provide a verification that the contact areas in nylon and dacron systems at the porosity levels involved are larger than the glass system values at the porosity levels of this study.

The actual magnitude of these contact areas are yet to be verified, and the additional question arises as to whether the contact areas of even the magnitude calculated could contribute significantly to the heat transfer in the fiber bed.

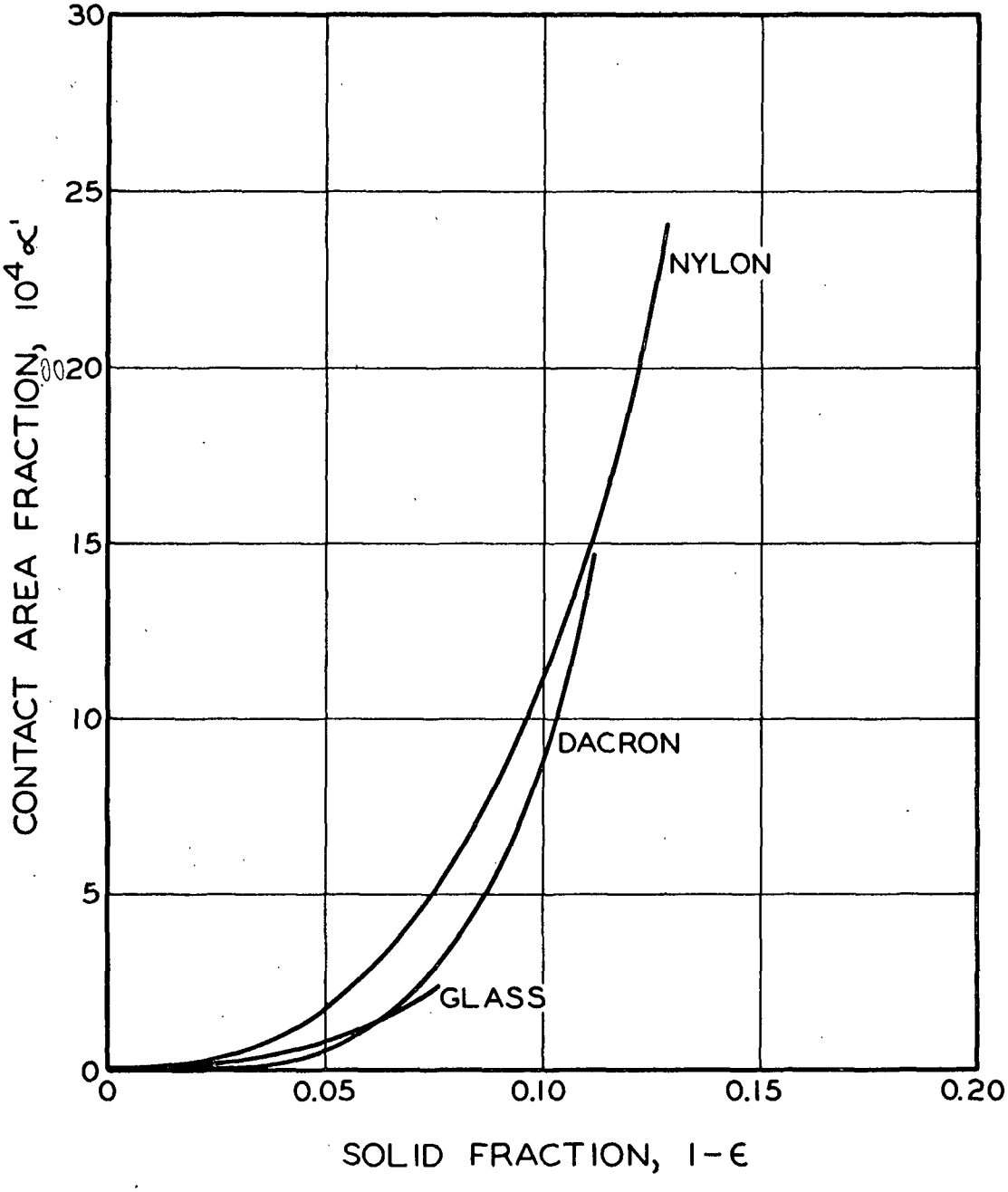

Figure 4. Solid-Solid Contact Area Response

Considering the observations of Woodside and Kuzmak (39) as was shown in Fig. 2, one realizes that even a small area of fiber-fiber contact could maintain a significant heat flux due to the increased temperature gradient in the region of the contact surface. Therefore, the contact areas as calculated might well contribute significantly to the over-all heat-transfer mechanisms associated with the compressible fiber systems.

EXPERIMENTAL FIBER SYSTEMS

FIBER PREPARATION AND CHARACTERIZATION

Nylon, dacron, and glass fibers were obtained as continuous multifilament strands and were cut to the desired lengths utilizing the method and equipment of Jones (42). The continuous fiber was unwound from the bobbin onto a hexagonal wheel, the filaments glued together and cut to produce a six-foot skein. The skein was placed on a board backed with blotters and cut to precise fiber lengths with a razor blade, gang cutter which was forced through the fibers with a hydraulic press. After cutting, the glass fibers were cleaned with 30% hydrogen peroxide overnight in order to remove the starchlike binder on the fibers (42, 43).

Fiber length distributions were determined with the Finnish Fiber Length Recorder (44). From 100 to 150 fibers were counted from each sample and a few duplicate measurements were made. All of the samples had very narrow fiber length distributions and the arithmetic average length was utilized in all calculations.

Fiber diameters were measured microscopically with a calibrated eyepiece. Ten to twenty fibers were measured and very little diameter variation was observed.

Fiber density, conductivity, and elastic modulus values were taken from information provided by the manufacturers and from other available data.

Table I gives a summary of all fiber samples and their properties.

FIBER BED FORMATION AND PREPARATION

An ideal fiber bed composed of layers of fiber randomly oriented in the two-dimensional plane of the layer should result from the filtration of a perfectly

dispersed, fiber slurry. The general technique and filtration apparatus described by Cowan (3) was utilized for the formation of fiber beds involved in this study.

TABLE I

FIBER CHARACTERISTICS AND PHYSICAL PROPERTIES

Fiber	Denier	Diameter, μ	Average Fiber Length, mm.	Density, g./cc.	Thermal Conductivity, $10^4 K_s$, cal./sec.cm. °C.	Modulus of Elasticity, $10^{-7} E$, g./sq.cm.
Nylon	3	19.3	2.78	1.14[a]	5.9[b]	0.9[c]
	3	19.3	5.54			
	15	45.4	2.49			
Dacron	5	23.0	2.04	1.39[a,d]	3.8[e]	14.7[d]
	5	23.0	5.30			
Glass	-	13.7[f]	2.76	2.55[f]	24.8[g]	72.0[d,g]

[a] DuPont (45)
[b] DuPont (46)
[c] Wilder (47)
[d] Jones (42)
[e] Pritulsky (48)
[f] Arnold (43)
[g] Owens-Corning (49)

The required weight of fiber (9 to 14 grams) was dispersed in 12-15 liters of deionized water and placed in 4-liter suction flasks. The fibers were de-aerated under vacuum for a sufficient length of time (until the fibers settled).

The formation was accomplished by slowly pouring the fiber slurry into the upper formation tube of the filtration apparatus as deaerated water flowed through the system. The fibers were deposited on a 150-mesh septum screen covered with

tea bag stock. The formed, five-inch diameter bed was then removed from the system and dried at 105°C. in an oven. Tea bag stock was retained at both surfaces of the bed to facilitate handling. The bed was weighed and then stored for the conductivity measurements.

PARTIAL SATURATION TECHNIQUE

After dry bed formation and preparation were accomplished, the fiber bed was saturated with the nonvolatile dioctyl phthalate oil. Several techniques were attempted and the most successful means simply allowed the oil to drip slowly into the fiber bed over a period of eight to ten hours. The sides and bottom of the bed were enclosed with an aluminum foil or plastic shell which prevented the oil from escaping the saturated porous network of the bed. All evidences indicated that a fully saturated system was acquired.

The removal of the oil in order to acquire a specific level of partial saturation was accomplished by two methods, both utilizing the capillary forces involved. The more complex method incorporated the porous-plate, capillary pressure apparatus (3). With the apparatus filled with oil and the porous plate saturated with oil, the saturated bed was placed atop the porous plate. The mercury leg was then lowered to apply capillary suction and thereby remove a certain portion of the oil in the bed. The oil remaining in the bed was assumed to be retained in a uniform liquid network.

An easier means of accomplishing the same results utilized pulp blotters. The saturated bed was placed atop several blotters and the oil allowed to flow from the bed into the blotters.

The two methods were used alternately in the initial, partial saturation studies, and, apparently, if any differences in the nature of the produced liquid

network were present, they did not alter the conductivity response of the fibrous system. Consequently, the blotter technique was utilized in the majority of the saturation studies.

THERMAL CONDUCTIVITY APPARATUS

GENERAL CONSIDERATIONS

Both steady-state and transient methods were available for the conductivity measurements on the fibrous systems to be utilized in this investigation. The transient methods have generally been adopted in cases where mass movement occurred or when confined specimens were impractical. The obvious advantage of such methods are the brief testing times involved. However, the assumed or partially valid boundary conditions for most techniques limit the accuracy of the results unless one resorts to difficult, often empirical, correction procedures. The transient, line heat source method (15) has been used most often for partially saturated, porous materials, but the large temperature gradients associated with such a method may override any advantages which accompany the method's speed.

The classical, steady-state, thermal conductivity methods involve the simultaneous measurement of the steady-state heat flux and the temperature gradient in the test samples. Since mass movement was eliminated in the partially saturated system due to the nonvolatile oil, it was decided that one of the steady-state methods was more advantageous to this study than any of the transient techniques.

The approved ASTM C177-45 method for work with homogeneous solids utilized two heat sources, one of which physically surrounds or guards the central or testing source. Heat from the testing zone has no tendency to escape when the outer guard source is maintained at the same temperature as the test source. The heat input is measured electrically and the temperature gradient across the specimen, as well as between sources, is measured with thermocouples.

Since the test specimens were to be porous materials rather than solids, and since the majority of the investigation would utilize partially saturated beds,

the usual ASTM design was not considered acceptable. This was due primarily to the necessity of having the heat flow downward through the specimen in order to prevent convection due to density gradients in the fluid. Also, two test specimens were required which would magnify difficulties in the preparation procedures.

A single-specimen assembly, using an uppermost hot plate and single cooling plate, was considered most advantageous. Such designs had been used successfully for thermal conductivity measurements on liquids (50), air (51), and textiles (52). The heat flow in such an apparatus could be determined by one of three methods:

(1) measurement of the heat input to the cooling water flowing in the cold plate,

(2) use of a material of known conductivity, heat meter (53), and,

(3) measurement of electrical input to the hot plate.

It appeared from the literature (54-57) that the primary apparatus problems arose in acquiring heat flow lines normal to the specimen, measuring interface temperatures, and determining the heat flux in the specimen. The flow-lines problem is not easily solved, but it appears that an adequate guard-ring system, properly operated, can make this factor almost negligible. If the direction of heat flow is not a problem, then the measurement of the heat flux becomes less of a difficulty.

The surface-to-surface temperature drop in the specimen must be measured precisely in order to acquire the temperature gradient. Since thermocouples at the interface between the plate and specimen must lie in the isotherm of the surface in order to measure the surface temperature, many discrepancies can arise. Several authors (55, 56) discuss this problem, and it would appear that a butt-welded thermocouple (like a cylinder), lying in accurately formed grooves in the surfaces, lies in the isotherm of the surface.

GUARDED HOT-PLATE APPARATUS

The circular, guarded hot-plate apparatus design is presented in an exploded diagram in Fig. 5.

The 0.5-inch brass backing plate (C) for the hot plate assembly was milled 3/16 inch deep in order to contain the 3/16-inch copper plates (G and H). The Western Electric heating elements (E and F) were constructed from closely spaced, high-resistance wire which was embedded in silicone rubber. The elements were bonded to the copper hot plates by the manufacturer. The backing plate was recessed 0.05 inch in the areas of the heating elements in order to maintain a level, hot-plate surface. The test section (G) of the hot plate was attached to the backing plate with a single, brass screw. The guard ring (H) was attached by several screws along the circumference of the backing plate. A 1/32-inch gap was maintained between the test and guard sections. The outside diameter of the hot-plate assembly was 9 inches.

The test section (J) of the cold plate was milled from a 0.5-inch copper disk. The 5/32-inch channels in the test section were concentric and continuous such that water entering and leaving the test section flowed in alternate channels. The 3/16-inch brass backing plate (L) for the cold plate was attached with several screws and sealed with vacuum grease to prevent leakage. The circumference of the test plate was beveled such that a 1/32-inch gap was maintained at the upper edge.

The guard section (K) of the cold plate was composed of a 3/16-inch copper plate to which was soldered 0.25-inch copper tubing (M). The tubing was doubly wound to give concentric, alternate flow channels similar to the test section.

The cold-plate assembly was recessed into a 1-inch Micarta base (N) such that the upper, copper surfaces remained level.

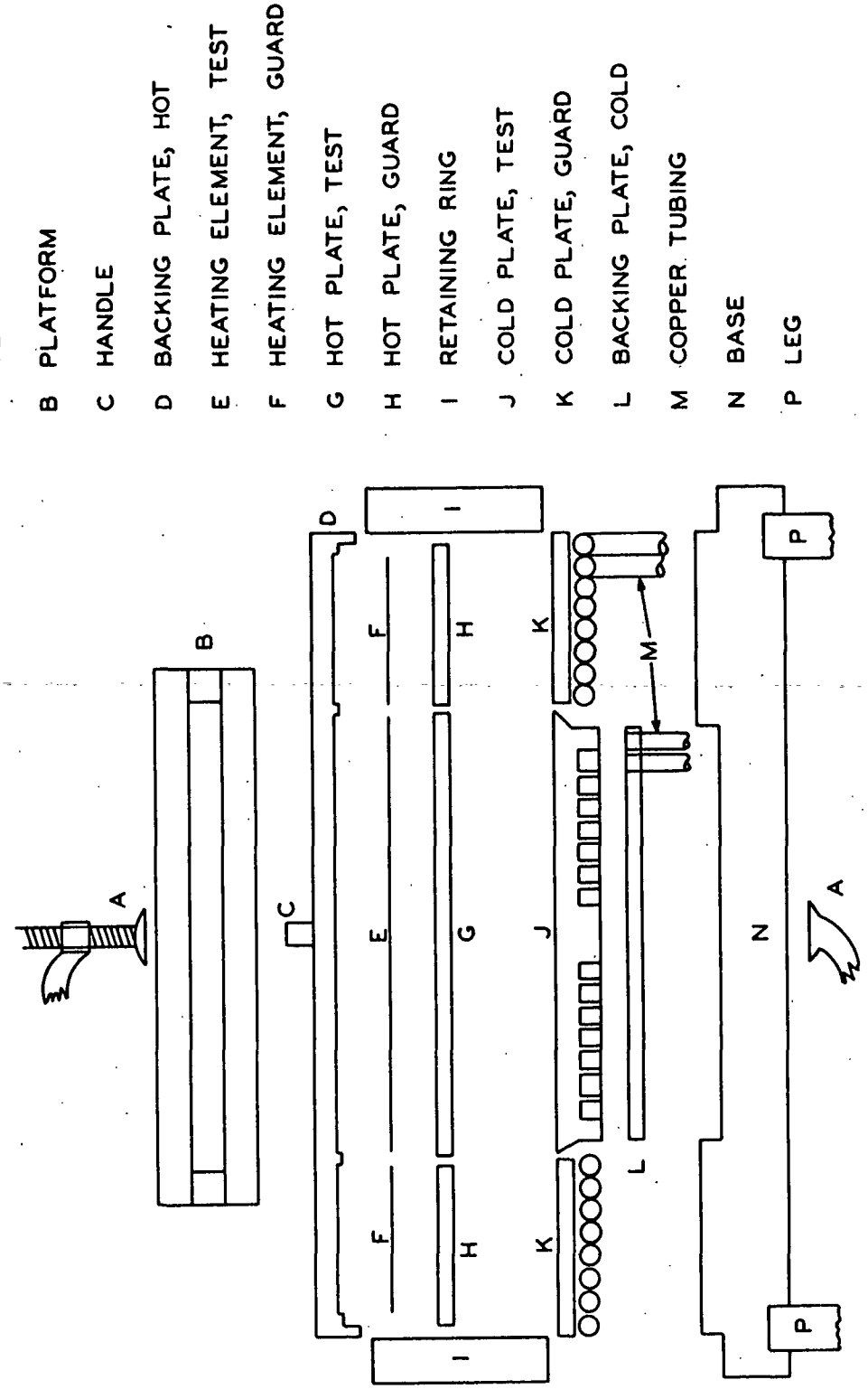

Figure 5. Guarded Hot Plate Apparatus

The hot and cold-plate assemblies were confined in a 9-inch Plexiglas ring (I). The 2-inch high ring was recessed 0.25 inch into the Micarta base. A handle (C) allowed the removal of the hot plate assembly from the retaining ring in order to place the test specimen between the plates. A brass platform (B) was used in most of the measurements. The platform sat atop the hot plate and evenly distributed the pressure applied by the large, deep-throat, C-clamp (A).

Photographs of the guarded hot-plate apparatus are shown in Fig. 6 and 7.

THERMOCOUPLE LOCATION AND TEMPERATURE MEASUREMENT

The thermocouples utilized in the temperature measurements were constructed from 28-gage Chromel and Constantan wires. The thermal wires were insulated with enamel and cotton braid. Junctions were formed by twisting the two wires together and dipping in silver solder. Excess solder and wire ends were clipped away, and the junction was carefully hammered until a continuous cylinder was formed.

The manufacturer's calibration curve for the Chromel-Constantan junction was checked by immersing the thermals in a well-stirred oil bath along with a thermometer calibrated by the National Bureau of Standards (NBS). The measured electromotive forces (e.m.f.s)' were identical to the reported values and an average calibration of 0.0165°C./μvolt was utilized for the 15 to 70°C. temperature range.

The thermocouples were installed in the guarded hot plate apparatus at the following locations:

(a) center area of hot-plate test section,

(b) center area of cold-plate test section,

(c) copper tubing of inlet cooling water,

(d) across the inlet and outlet tubing of the cooling water,

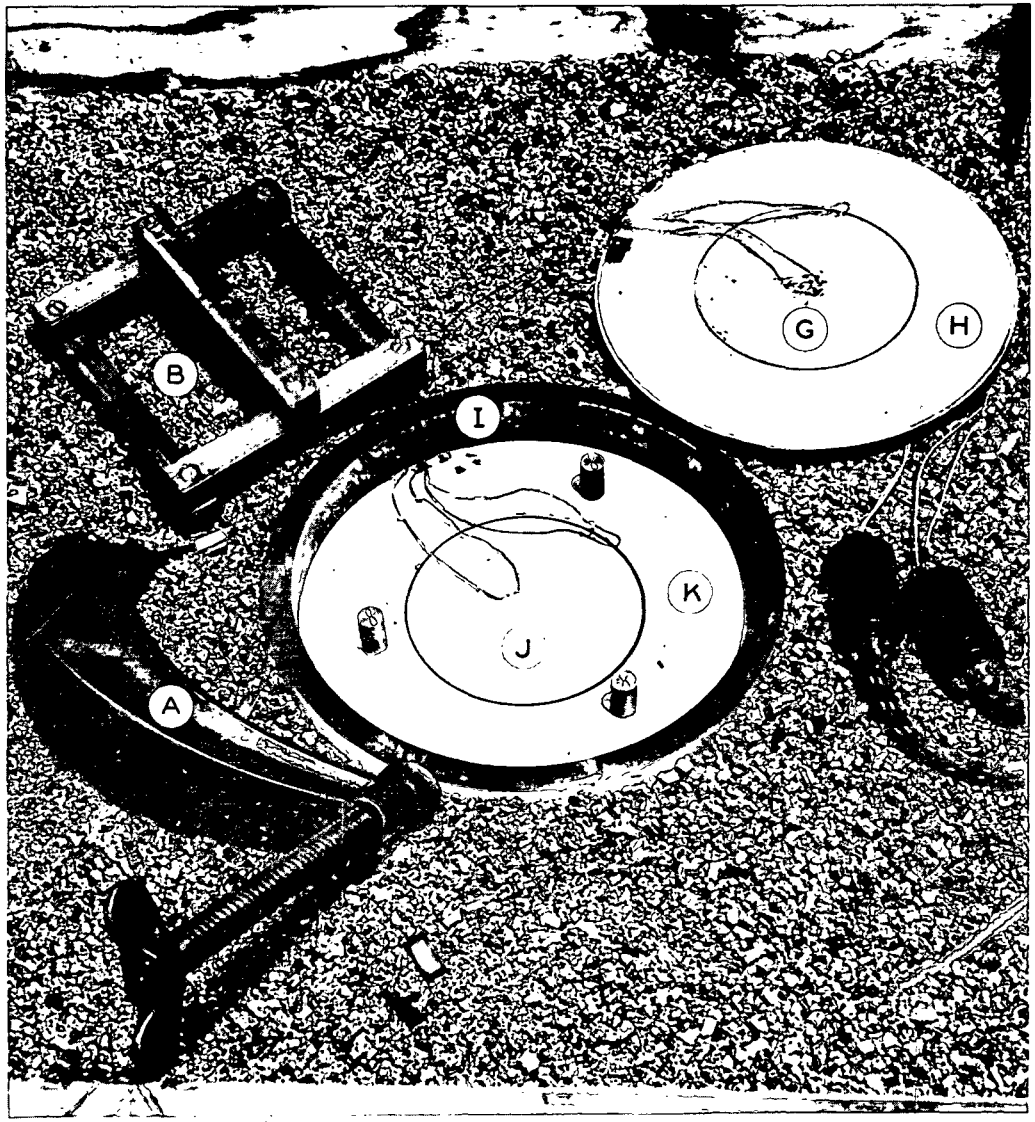

Figure 6. Guarded Hot Plate Apparatus, Open

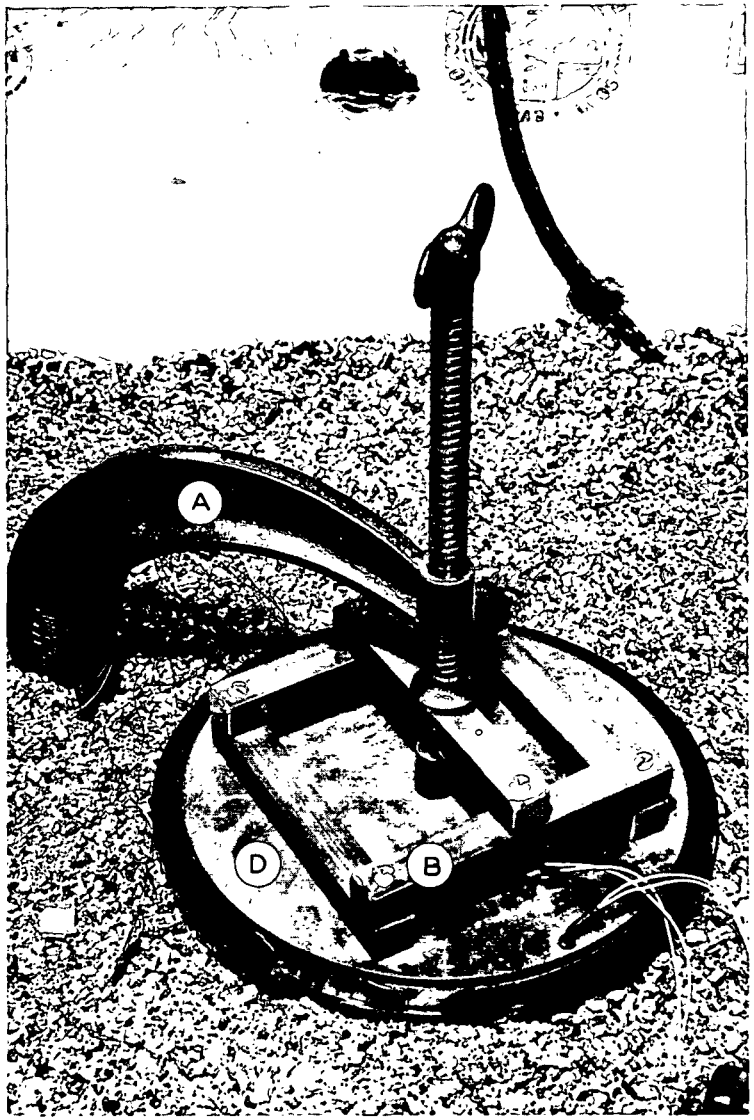

Figure 7. Guarded Hot Plate Apparatus, Closed

(e) across the guard-to-test gap of the hot plate, and

(f) across the guard-to-test gap of the cold plate.

Also, thermocouples were prepared for differential measurements on the test specimen and standard as will be explained in a later section.

The thermals measuring the temperature of the hot plate and cold plate were attached to a Honeywell, six-point, automatic recorder. The cold junctions were placed in mercury wells submerged in an ice-distilled water bath. E.m.f.s. could be measured with the recorder to $\pm$ 5 μvolts.

The differential thermocouples and the inlet cooling water thermocouple were attached directly to a Thermo-Electric, six-junction rotary switch. The switch was attached to a manual potentiometer circuit containing a Leeds-Northrup 2430a galvanometer, Leeds-Northrup student potentiometer, and accompanying standard cell, four-dial rheostat, tap keys, and dry cells. E.m.f.s. could be read to $\pm$ 1 μvolt with this installation.

The thermocouples were attached to the copper plates of the apparatus by cutting a small groove slightly larger than the thermal wire, placing the junction in the groove, and peening the metal against the wire until the junction was firmly secured. The thermocouples in the cooling-water copper tubing were attached with epoxy resin.

HEATING AND COOLING REGULATION

A schematic diagram of the thermal conductivity assembly is presented in Fig. 8.

The heating elements were connected to the 110-volt circuit through variable transformers which could be regulated in approximately 1-volt intervals. The heating elements in the guard and test sections were regulated separately.

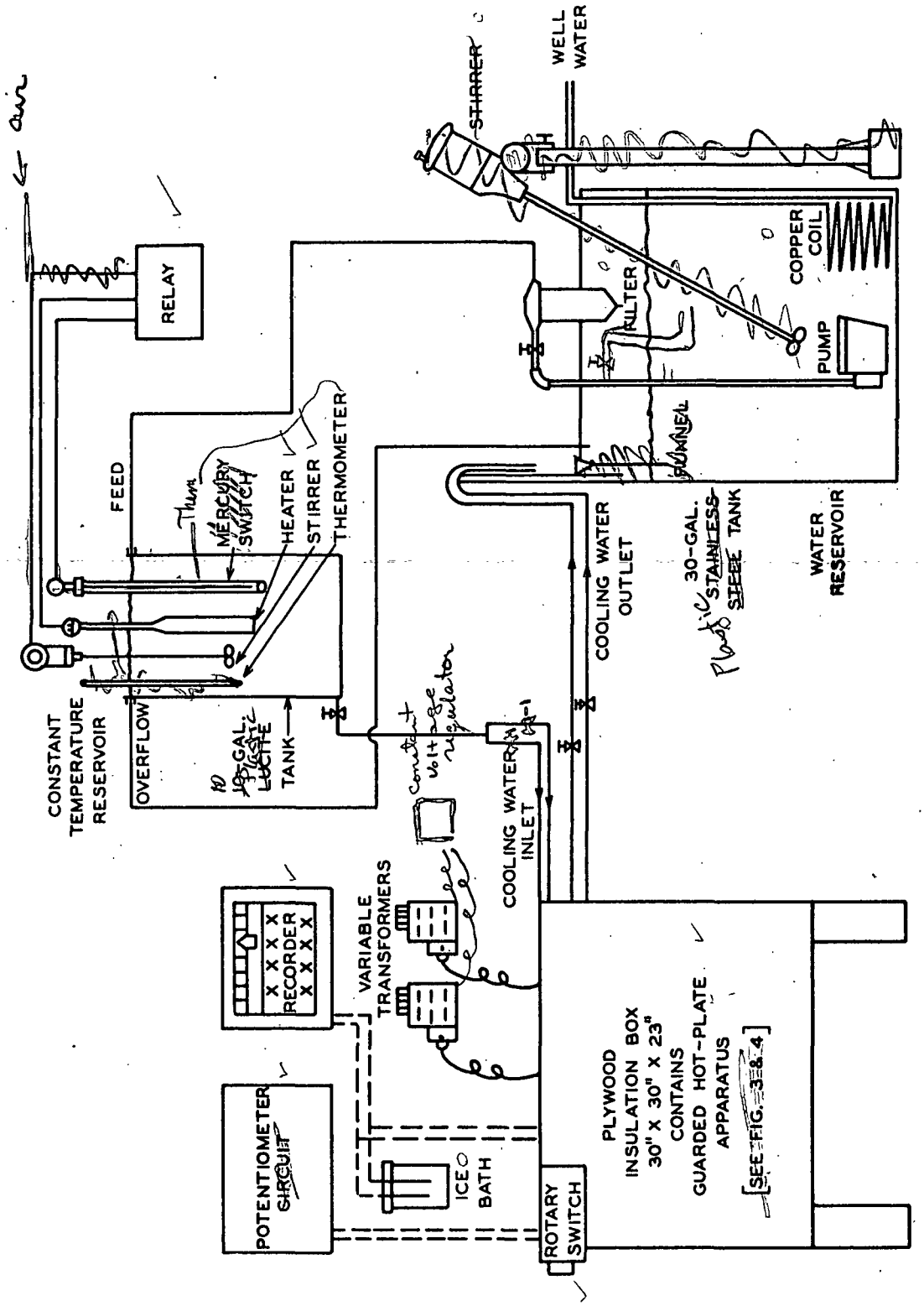

Figure 8. Schematic Diagram of Thermal Conductivity Apparatus

The control of the cold plate temperature and thermal balance was maintained with the flow rate of the cooling water. Deionized, deaerated water was stored in the main reservoir where its temperature was maintained at a low level by allowing well water to pass through the copper cooling coil. The cooled water was pumped to the constant temperature reservoir where the temperature was adjusted and controlled to $\pm$ 0.05°C. with the usual heater-mercury switch-relay system.

From the constant temperature reservoir the water flowed by gravity from the reservoir through the cooling channels of the cold plate. Flow adjustment was maintained with compression clamps on the rubber tubing, with the insertion of capillary tubing, and with alteration of the water head.

Flow rates were determined with graduated cylinder and stop watch and could be maintained and regulated to $\pm$ 0.001 cc./sec. under normal flow conditions which were 0.3 to 0.4 cc./sec. in the test section and 3 to 4 cc./sec. in the guard section.

INSULATION OF APPARATUS

The guarded hot plate apparatus was placed in the center of a 30 by 30 by 23-inch plywood box. Loose Vermiculite insulation filled the lower half of the box to the level of the Plexiglas retaining ring. Fiberglass batting in 30 by 15 by 3-inch strips was placed on top of the apparatus to finish filling the box. The batting could be removed easily when introduction of a test specimen was required. (See Fig. 6 and 7).

THERMAL CONDUCTIVITY DETERMINATION

HEAT FLUX MEASUREMENT

The design of the thermal conductivity apparatus allowed three possible means of heat flux measurement to be considered. Two of the techniques appeared to be most feasible: (1) measurement of heat flow into test section of cold plate, and (2) heat-meter method.

With the first method, adequate maintenance of the guard-to-test thermal balance insured uniform heat flow through the specimen and into the cold plate. Therefore, the important consideration was associated with the accurate measurement of the heat input to the cold plate. This consideration involved the accurate determination of the temperature rise in the cooling water flowing in the test section, the measurement of the water flow rate, and the prevention of heat loss to the surroundings via the insulation below the cold plate.

This "calorimetric" method was tested in preliminary studies in which a Plexiglas disk was utilized as a "standard." After numerous measurements, it became increasingly evident that the measured heat flux input to the cooling water was dependent on the water flow rate as well as on the heat flux through the standard into the test section. It was then obvious that the position of the differential thermocouple in the inlet and outlet channels of the test section did not allow the true temperature change in the cooling water to be measured. Considerable time would have had to be spent in trial and error movement of the thermocouple in order to find the correct location for proper measurement. Also, other modifications of the cooling plate design would probably have been necessary in order to insure proper measurement. In addition, once a satisfactory location and apparatus design was obtained, considerable effort would have been required

to check properly and calibrate all conditions of heat flux and water flow rates. It was decided that the "calorimetric" technique would be abandoned in favor of the heat-meter method.

The heat-meter method involves placing a material of known conductivity in a region of heat flux identical to that of the test specimen. Comparison of the temperature gradients, $\Delta T/H$, in the materials allows a calculation of the unknown conductivity, K_t, from the known value, K_o, in the following manner:

$$Q = K_o[\Delta T/H]_o = K_t[\Delta T/H]_t \tag{20}$$

Therefore,

$$K_t = K_o[\Delta T]_o H_t/[\Delta T]_t H_o \tag{21}$$

where Q is the heat flux and H is the thickness.

The heat-meter method was checked in preliminary work by using two Plexiglas disks of known conductivity. Differential thermocouples were attached to the surfaces of the disks with epoxy resin. The disks were then stacked between the hot and cold plate test sections, and the apparatus brought to steady-state conditions at various temperatures and several temperature gradients. Arbitrarily, the lower 0.240-inch disk was designated as the "standard" and the upper 0.264-inch disk as the specimen. The conductivity of the "standard" was taken as the value for Plexiglas as reported by the NBS*. The results of the heat-meter trials are given in Table II and thermal conductivity versus temperature for the "standard" and the test specimen is plotted in Fig. 9.

*The thermal conductivity value for Plexiglas as reported by the NBS was based on conductivity measurements on a 1-inch thick Plexiglas sheet.

TABLE II

HEAT-METER RUN CONDITIONS

Plexiglas Standard—0.240-inch thick —
Plexiglas Test Specimen—0.264-inch thick

Run No.	Thermal Balance, cold, μv.	Thermal Balance, hot, μv.	Test Specimen, ΔE.m.f., μv.	Test Specimen, $\Delta\bar{T}$, °C.	Standard, ΔE.m.f., μv.	Standard, $\Delta\bar{T}$, °C.	ΔE.m.f. Ratio	Av. Temp. Test, °C.	Av. Temp. Stand., °C.	Test Conductivity, $10^4 K_{\bar{t}}$ cal./sec.cm.°C.
9	0	-17	600	9.9	534	8.8	1.124	41.9	32.1	4.210
9	12	4	645	10.6	575	9.5	1.122	43.7	33.2	4.202
9	4	4	637	10.5	567	9.4	1.123	43.4	33.0	4.208
10	4	4	921	15.2	820	13.5	1.123	51.9	36.9	4.216
11	-20	4	591	9.8	527	8.7	1.121	48.3	38.8	4.213
11	225	5	661	10.9	589	9.7	1.122	52.0	41.3	4.223
11	23	5	615	10.1	547	9.1	1.124	50.0	40.3	4.227
12	-10	-20	1074	17.7	954	15.7	1.126	62.8	45.3	4.246
12	19	2	1122	18.5	1000	16.5	1.122	66.1	47.7	4.236
12	10	-3	1100	18.1	982	16.2	1.120	65.0	47.1	4.228
13	37	5	180	3.0	161	2.7	1.118	38.0	35.1	4.194

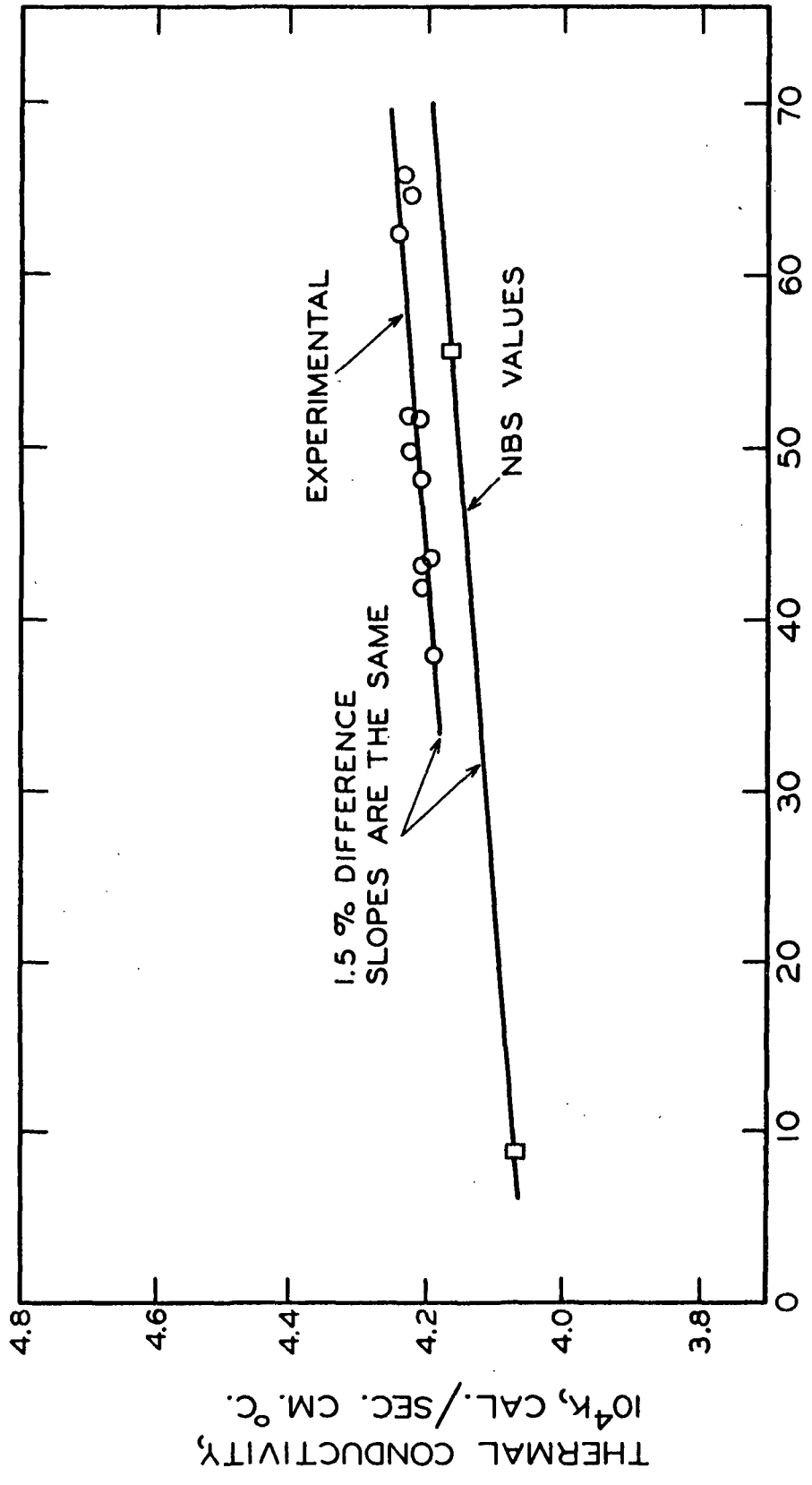

Figure 9. Conductivity of Plexiglas (Heat-Meter Method)

The results of the trial indicated that the heat-meter method would be more than suitable for use in the thermal conductivity measurements. The very small slope of the conductivity-temperature curve for Plexiglas was measured very accurately in comparison with the NBS results. The 1.5% difference in conductivity, which was calculated, was wholly acceptable as the error involved in the installation of the thermocouples at the material's surfaces. However, the two disks were not from the same Plexiglas sheet and the NBS reported some variation in Plexiglas conductivity.

Of additional interest was the observation that the calculated conductivity of the test specimen was essentially independent of the guard-to-test thermal balance (Table II). This occurred because the test and standard materials were of approximately the same conductance, $\underline{K}/\underline{H}$. This concept will be discussed more fully in the next section.

Because acceptable limits of accuracy and reproducibility could be maintained with the heat-meter method, it was adopted for heat flux measurements during the investigation.

OPERATIONAL PROCEDURES

FIBER BED CONDUCTIVITIES

The "standard" for the heat flux determination during the measurements on the fiber beds was a 5-inch diameter disk of Plexiglas which was 0.475-inch thick. A differential thermocouple was laid in 0.01-inch deep grooves on each surface of the disk and attached with epoxy resin. The Plexiglas disk was then placed over the test section of the cold plate, and the thermal wires were run through the retaining ring directly to the rotary thermocouple switch.

The fiber bed test specimen was placed on top of the "standard." A differential thermocouple, with junctions attached to sheets of aluminum foil (5-inch diameter, 0.001-inch thick), was placed on the surfaces of the fiber bed and the thermal wires were run to the rotary switch. Attaching the thermal junctions to the foil allowed positioning of the junction and also aided temperature distribution at the bed surface. The foil also allowed a low-emissivity (0.05) surface to be maintained at the surfaces of the bed.

With the test specimen in place, three spacers (Fig. 6) were positioned in the guard section. The spacers were made from 0.5-inch drill rod and machined to $\pm$ 0.0005 inch length in order to control accurately the separation of the hot and cold plates and thereby fix the specimen thickness. Expansion of the spacers and the Plexiglas standard was negligible under run conditions.

The hot plate was then placed atop the specimen and spacer studs while being positioned by the retaining ring. A diagram of the apparatus containing standard and specimen is shown in Fig. 10.

In order to fix the thickness of the bed, pressure was applied to the hot plate until contact with the spacers was acquired. Initially, the C-clamp pressure was applied to the handle attached to the backing plate. However, better pressure distribution was obtained with the platform arrangement, shown in Fig. 6 and 7, although no differences in the conductivity measurements were observed.

With the conductivity apparatus ready for operation, the fiberglass insulation was put in place, and the voltages to the heater elements and the cooling water flow rates were adjusted. Most of the measurements were made at an average bed temperature of 55°C. and the required heater voltages and water-flow rates

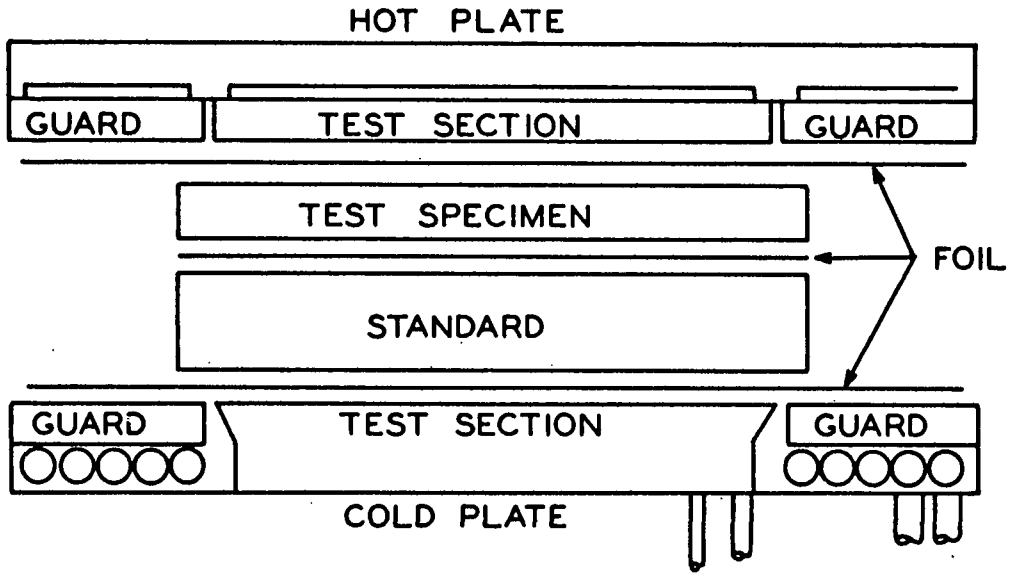

Figure 10. Standard and Specimen Position in Apparatus

were quickly obtained. Heating-up periods of six to eight hours were required if the apparatus was initially at room temperature. Generally, measurements immediately followed one another before the apparatus was allowed to cool. As a result, the normal heating-up period was only three to four hours.

After the equipment reached the approximate operating conditions, adjustments were made in the voltage input and the water-flow rates in order to attain a thermal balance between the guard and test sections. Obviously, such adjustments would be very time-consuming if a perfect balance condition was required. Consequently, the NBS procedure for obtaining a perfect balance condition was adopted. This procedure consisted of observing several imbalance points on either side of the perfect balance condition, drawing a curve through the points and reading off the perfect balance value.

The balance conditions which were plotted were the ΔT ratio of the specimen to the standard versus the arithmetic average of the guard-to-test differential

thermocouple readings for the hot and cold plates. The imbalance guard-to-test readings when the guard ring was hotter than the test section were considered positive, and when the test section was hotter the readings were negative. Generally, the imbalance conditions in the hot plate and the cold plate produced similar changes in the ΔT ratio. Several balance plots are shown in Fig. 11 which indicate the usual response for various specimen and standard conductance ratios.

Adjustments were made to bring the balance e.m.f.s. in the range of $\pm$ 20 μvolts around the balance point. When in this range, adjustments of 4 to 5 μvolts were made every one to two hours until enough points were acquired. The plotted curves were consistent and reproducible within this range, and generally one to two days was a satisfactory length of time for measurement.

Obviously, initial measurements required longer periods in order to acquire information concerning the time necessary to reach a steady-state condition, the variation of temperature at constant heating and cooling settings, and the effect on the conductivity results. Runs were continued for as long as thirteen days without any change in the apparatus conditions and the calculated conductivities which were acquired the first day. In fact, the calculated conductivities acquired during the latter stages of the heating-up period were usually only 2-3% lower than the final steady-state values. Apparently, this is due to the use of the heat-meter method which allowed the response of the standard and specimen to a given heat flux condition to be consistent.

The maximum and minimum ΔT ratios measured over the $\pm$ 20 μvolt range differed only by about 2% (Fig. 11) for most of the conductance ratios observed in the study.

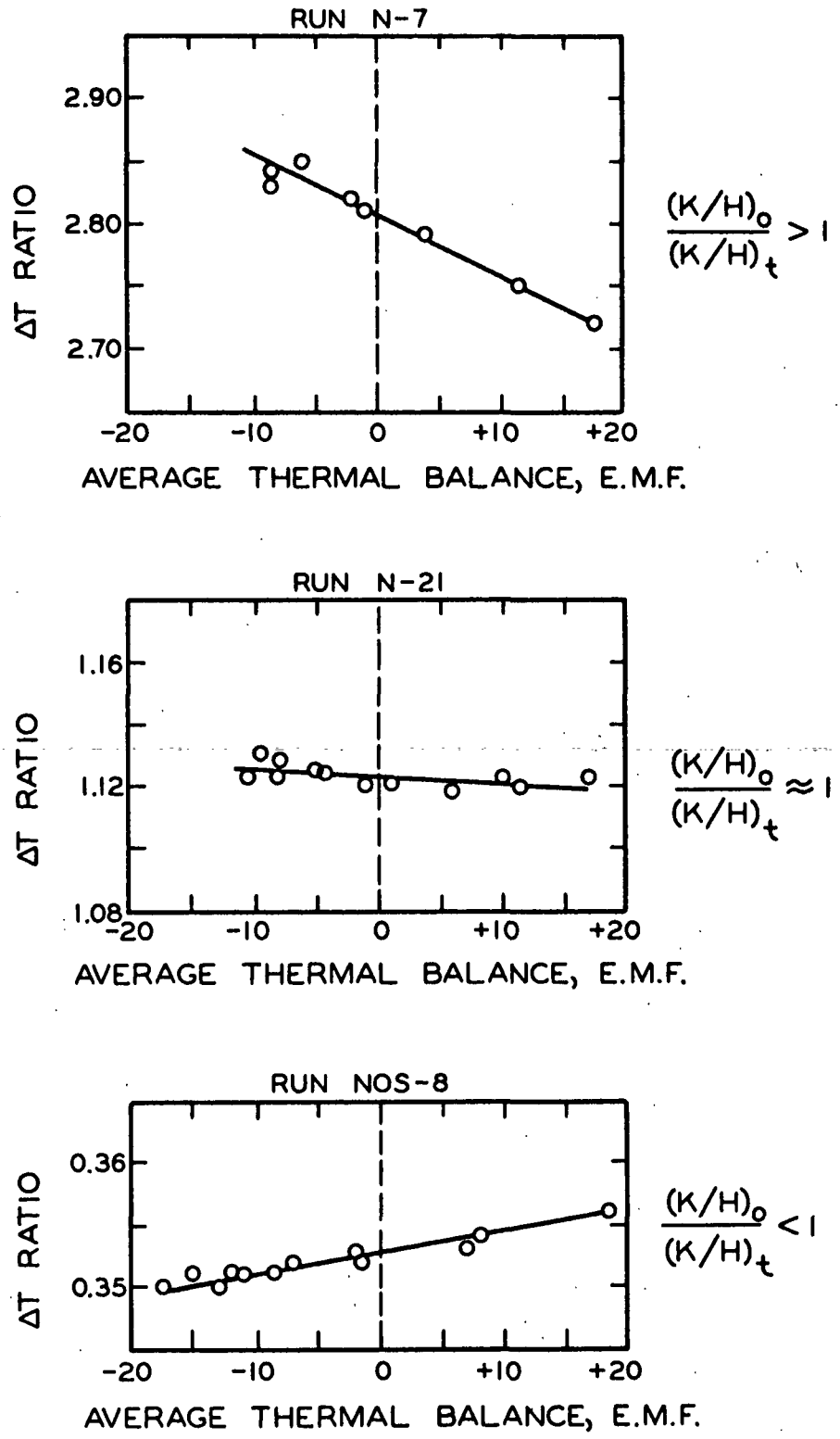

Figure 11. ΔT Ratio Versus Guard-to-Test Thermal Balance

LIQUID CONDUCTIVITY

The procedures utilized for the measurement of the thermal conductivity of the dioctyl phthalate oil were identical to those for the fiber bed determinations. However, the necessity for retaining the liquid, so that conductivity measurements could be made, required certain modifications of the standard-specimen relationship.

A 0.270-inch retaining wall was constructed on a Plexiglas disk (0.475-inch thick, 5.5-inch diameter). Thermocouples were attached to the upper and lower surfaces of the standard and were connected to the automatic recorder.

For conductivity measurements, deaerated oil was poured into the retaining bowl atop the standard, and the hot plate was placed on the disk. The measurements were then conducted as described previously. The conductivity results for the oil are given in Table III.

TABLE III

THERMAL CONDUCTIVITY OF DIOCTYL PHTHALATE

Temperature, °C.	$10^4 K_{\ell}$, cal./sec. cm. °C.
46.0	3.75
55.5	3.77
56.5	3.78
58.0	3.78
65.0	3.78

TWO-PHASE CONDUCTIVITY RESULTS

The experimental work can be conveniently divided into two studies: (1) two-phase systems, and (2) three-phase systems. The results of the dry and fully saturated fiber beds will be presented in this section. It should be noted, however, that the fully saturated beds were considered as terminal conditions for the three-phase systems during the experimental observations. The presentation and discussion of the three-phase systems will follow the discussions and analysis of the two-phase measurements.

The two-phase presentation consists primarily of the investigation of the component and bed characteristics which influence the over-all thermal conductivity of the fibrous systems. Also, information as to the effect of temperature and other operating variables is discussed along with an estimate of the errors associated with the work.

The porosity, used in the experimental discussions, is an over-all value for the bed which is calculated from the bed weight, $\underline{W}$, thickness, $\underline{H}$, cross-sectional area, $\underline{A}$, and the fiber density, ρ, by $\epsilon = 1-(\underline{W}/\rho\underline{H}\underline{A})$.

DRY NYLON FIBER BEDS

The operating conditions and conductivity results for the nylon beds are presented in Table IV.

The nylon fiber beds formed from the 3-denier, 2.78 mm. fibers comprised the primary fibrous system which was studied. The initial work with these nylon beds involved the investigation of the effect of the average bed temperature on the over-all bed conductivity. Figure 12 shows the results for Bed N-1 at a porosity of 0.922 utilizing various hot and cold plate temperatures and several heat flux conditions.

TABLE IV

DRY NYLON FIBER BED STUDIES

Run No.	Fiber Bed Temp., °C.	Fiber Bed ΔT, °C.	$\frac{\Delta T}{}$ Ratio	Porosity	Bed Conductivity, $10^4 K$, cal./sec.cm.°C.
Bed N-1—3 Denier—2.78 mm. Length—9.68 g. Weight					
N-7	34	13.8	2.81	0.922	1.04
N-8	38	20.3	2.78	0.922	1.05
N-12	42	24.3	2.75	0.922	1.06
N-9	45	27.3	2.86	0.922	1.02
N-13	46	21.7	2.69	0.922	1.09
N-6	47	26.8	2.88	0.922	1.02
N-15	48	27.5	2.80	0.922	1.04
N-10	53	34.9	2.84	0.922	1.03
N-11	57	39.4	2.81	0.922	1.04
N-14	61	26.1	2.66	0.922	1.11
N-16	62	26.5	2.63	0.922	1.12
Bed N-2—3 Denier—2.78 mm. Length—9.52 g. Weight					
N-17	55	40.1	3.09	0.923	0.945
N-18	45	29.6	3.13	0.923	0.93
N-23	63	29.5	1.06	0.852	1.43
N-24	55	24.7	1.07	0.852	1.41
N-25	65	25.5	0.801	0.820	1.56
N-26	56	20.5	0.807	0.820	1.55
N-27	65	21.2	0.643	0.796	1.72
N-28	56	17.5	0.648	0.796	1.70
Bed N-3—3 Denier—2.78 mm. Length—9.64 g. Weight					
N-19	55	40.8	3.10	0.922	0.94
N-21	63	30.9	1.12	0.850	1.35
N-22	66	23.2	0.681	0.793	1.63
Bed N-6—3 Denier—2.78 mm. Length—9.43 g. Weight					
N-35	61	39.8	2.12	0.905	1.105
Bed N-7—3 Denier—2.78 mm. Length—9.03 g. Weight					
N-37	57	46.1	3.97	0.938	0.871
N-38	56	45.2	3.96	0.938	0.872
N-39	55	41.7	3.20	0.925	0.892

TABLE IV (Continued)

DRY NYLON FIBER BED STUDIES

Run No.	Fiber Bed Temp., °C.	Fiber Bed $\Delta\underline{T}$, °C.	$\frac{\Delta T}{\text{Ratio}}$	Porosity	Bed Conductivity, $10^4\underline{K}$, cal./sec.cm.°C.
Bed N-10—3 Denier—2.78 mm. Length—9.31 g. Weight					
N-40	55	41.4	3.155	0.923	0.903
Bed N-4—3 Denier—5.54 mm. Length—9.70 g. Weight					
N-29	56	41.5	2.90	0.922	1.01
N-30	55	24.0	1.07	0.849	1.41
N-31	56	17.6	0.672	0.792	1.64
Bed N-5—15 Denier—2.49 mm. Length—10.53 g. Weight					
N-32	55	39.5	2.79	0.915	1.05
N-33	54	22.5	0.995	0.836	1.52
N-34	55	16.5	0.625	0.774	1.76

In the temperature range from 30 to 60°C., the conductivity-temperature relationship for the nylon bed was masked by scatter in the data. Apparently, this scatter was the result of changing the temperature drop across the fiber bed. This situation was connected with the operating conditions since the lower levels of heat flux (lower temperature drops across the bed) produced the larger conductivity values at specific temperatures, i.e., 46 and 61°C. Once the heat flux level reached a certain minimum (a temperature drop of approximately 25°C. for a fiber bed at 0.922 porosity) the conductivity values were no longer affected. In the temperature range from 45 to 57°C., the five measurements with at least this minimum heat flux level indicated a 2% increase in conductivity for the nylon beds.

The effect of bed temperature was also observed with Bed N-2 at lower porosity levels under maximum heat flux conditions. These results are included in Fig. 13

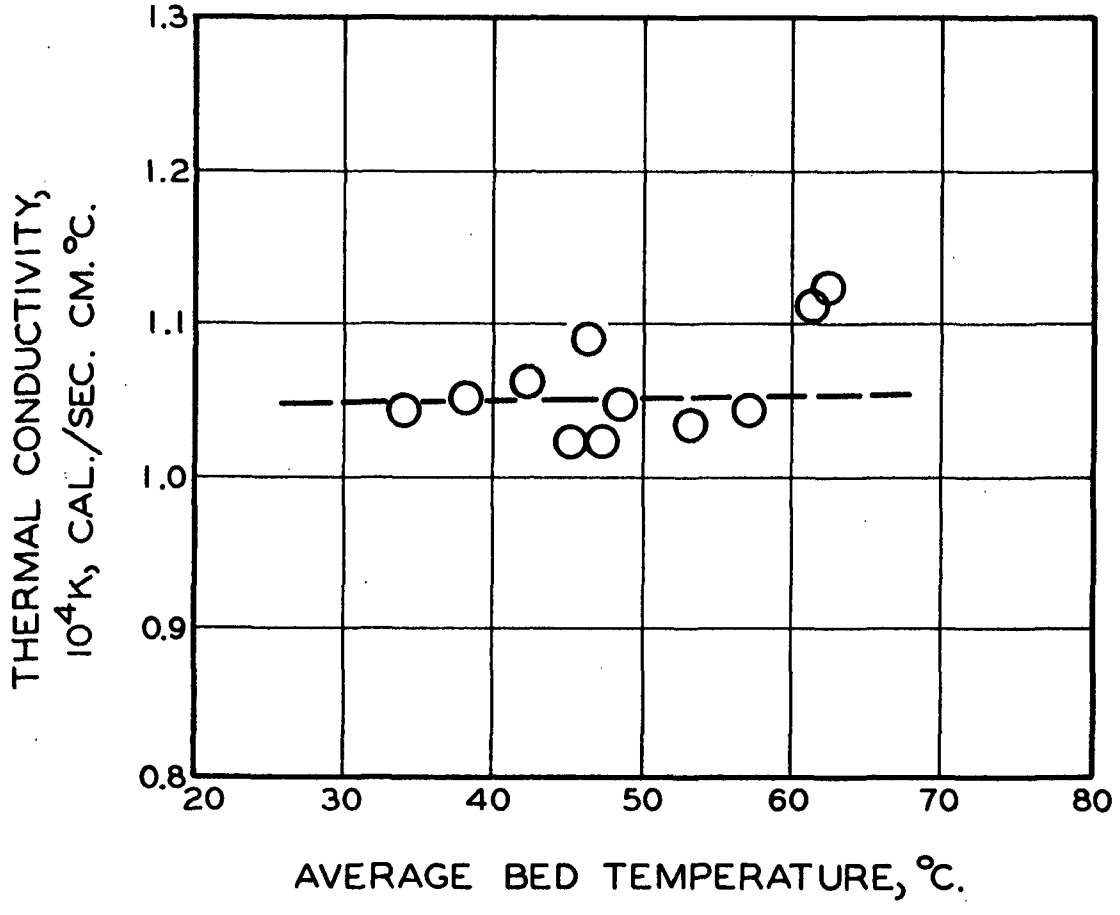

Figure 12. Temperature Study of Dry Nylon Fiber Beds at a Porosity of 0.922

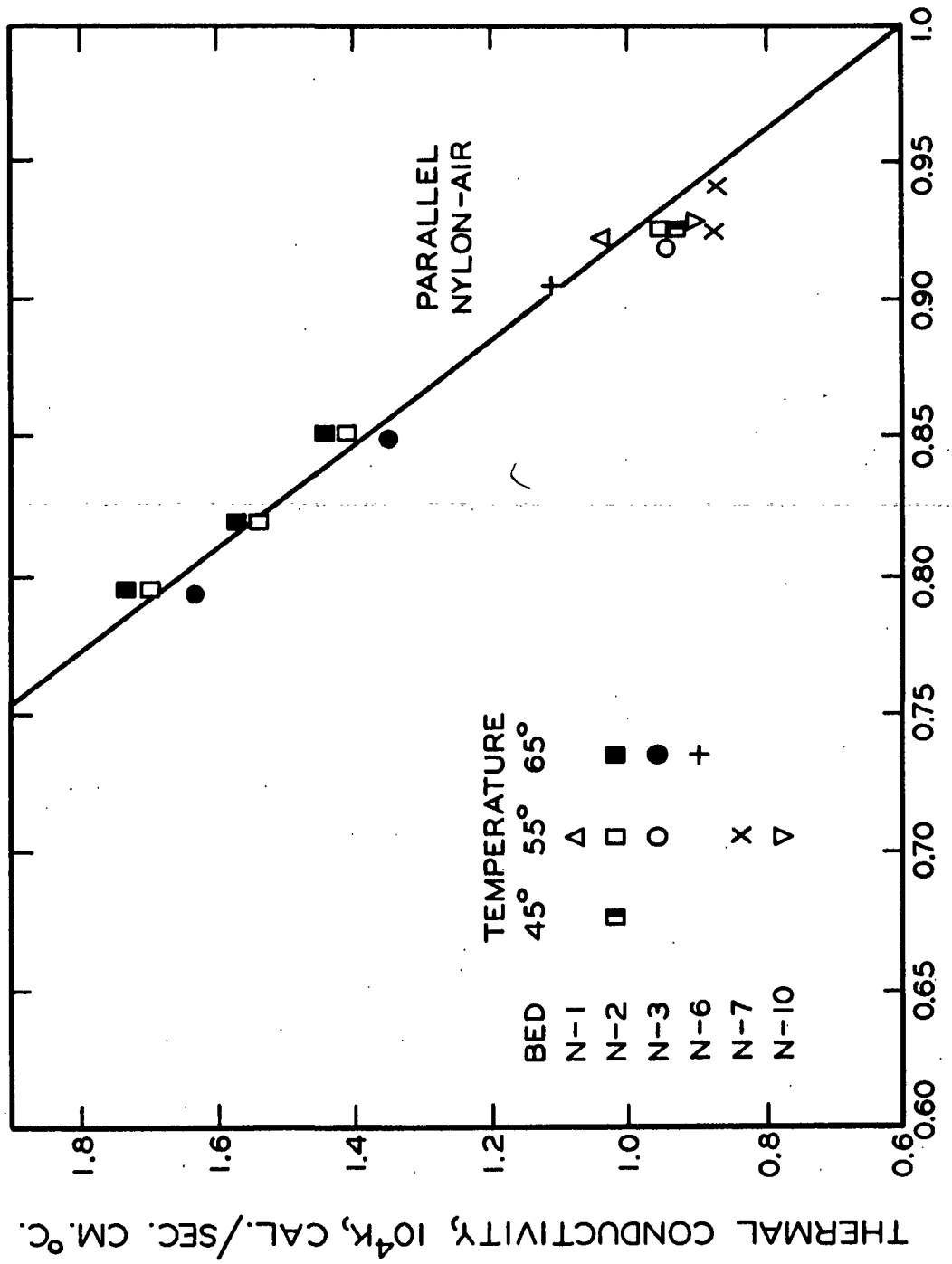

Figure 13. Conductivity of Dry Nylon Fiber Beds—3 Denier, 2.78 mm. Fiber

along with the effect of porosity. On this basis, a temperature coefficient of approximately 0.002×10^{-4} cal./sec.cm.°C.^{2} was attributed to the nylon beds in the 45 to 65°C. temperature range. Further efforts with temperature and heat flux variation were not attempted due to the small effect which was observed; and, therefore, the remainder of the dry bed studies were conducted at 55°C., under maximum heat flux conditions.

The reproducibility of any conductivity measurement was found to be within 1% for a given bed at specific operating conditions. The variation between nylon beds was found to be dependent on the level of porosity. Looking at Fig. 13, the decrease in bed porosity produced a marked increase in the conductivity of the nylon beds. At the higher porosities, a 10% variation in the beds was apparently observed; but this was reduced to less than 5% as the porosity was lowered.

It should be noted that the load limit of the C-clamp compression arrangement was reached when the nylon beds were reduced to 0.8 porosity. Therefore, a superior reproducibility of results should probably not be expected at the maximum compression conditions. For instance, an error in the thickness of a nylon bed of 0.01 inch at a porosity of 0.8 would produce a 3% error in porosity which in turn would cause a 5% change in conductivity.

Two changes in fiber size were investigated by approximately doubling the fiber diameter, i.e., from 3 denier to 15 denier, and also by doubling the fiber length, i.e., from 2.78 mm. to 5.54 mm. The conductivity response for the different nylon fiber beds is presented in Fig. 14. As a basis for comparison, the results predicted from the parallel phase distribution equation

$$K = \epsilon K_g + (1-\epsilon)K_s \qquad (1)$$

are included in Fig. 13 and 14.

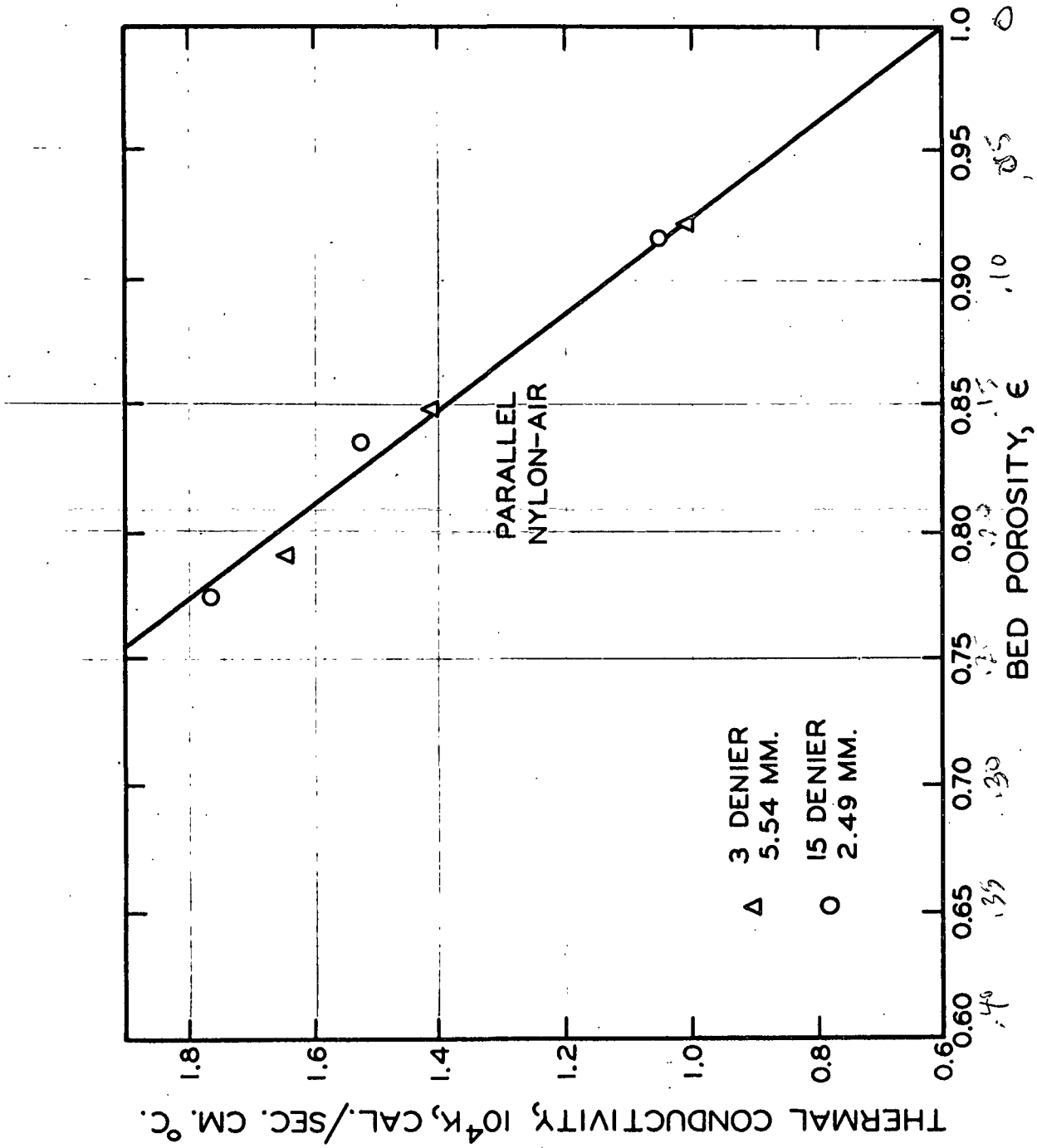

Figure 14. Conductivity of Dry Nylon Fiber Beds—Fiber Size Study

The changes in fiber dimensions did not produce any significant alteration in the conductivity response of the nylon beds. This observation compares favorably with the conductivity data reported for granular materials in which particle size plays an insignificant role.

DRY GLASS FIBER BEDS

The glass fibers had a conductivity value which was four times the conductivity of the nylon fibers. It was anticipated that this increase in fiber conductivity would reveal the effect of this variable on the response of the over-all bed conductivity. The results of the conductivity measurements on the glass fiber beds are given in Table V and plotted in Fig. 15.

First, it is noted that poor reproducibility between glass fiber beds was encountered. As much as a 20% difference in conductivity was found between beds. Formation differences are most likely the reason behind such variation because the glass fibers had a very definite tendency toward flocculation during the formation procedure. Also, structural differences can occur when the glass fibers begin to be broken during compression.

Comparison of the glass and nylon data reveal very little difference in conductivity values at these porosity levels. However, when comparing both sets of data with the parallel phase distribution predictions, the response of the two systems appears to be quite divergent. On this basis, the glass and nylon systems have other differences besides the stated difference in fiber conductivity, e.g., the compressibility of the fiber beds.

It has been mentioned that the glass fibers were broken during compression. An examination of the fiber length distribution of Bed G-5 revealed that after

TABLE V

DRY GLASS FIBER BED STUDIES

Run No.	Fiber Bed Temp., °C.	Fiber Bed $\Delta\underline{T}$, °C.	$\frac{\Delta T}{\text{Ratio}}$	Porosity	Bed Conductivity, 10^4K, cal./sec.cm.°C.	
Bed G-1—13.7 μ—2.76 mm. Length—12.09 g. Weight						
G-1	55	50.5	4.80	0.971	1.45	0.90
G-2	55	43.3	3.33	0.956	1.42	0.88
G-3	55	27.7	1.23	0.916	1.983	1.23
G-4	55	19.6	0.74	0.898	2.72+	1.69
Bed G-2—13.7 μ—2.76 mm. Length—13.77 g. Weight						
G-5	55	50.0	4.62	0.966	1.500	0.93
G-6	55	43.3	2.93	0.950	1.613	1.00
G-7	56	28.0	1.19	0.904	2.05	1.27
G-8	56	23.0	0.915	0.883	2.21	1.37
Bed G-4—13.7 μ—2.76 mm. Length—13.81 g. Weight						
G-9	56	48.7	4.22	0.958	1.323	0.82
G-10	53	41.8	3.32	0.949	1.386	0.86
Bed G-5—13.7 μ—2.76 mm. Length—13.14 g. Weight						
G-12	55	48.5	5.20	0.968	1.34	0.83
G-13	55	42.8	3.33	0.951	1.383	0.858
G-11	56	38.2	2.60	0.941	1.449	0.897
G-14	55	38.1	2.62	0.941	1.438	0.89
G-15	55	33.4	1.95	0.925	1.524	0.945
G-16	56	31.1	1.51	0.908	1.613	1.00
G-17	55	26.2	1.17	0.889	1.720	1.065

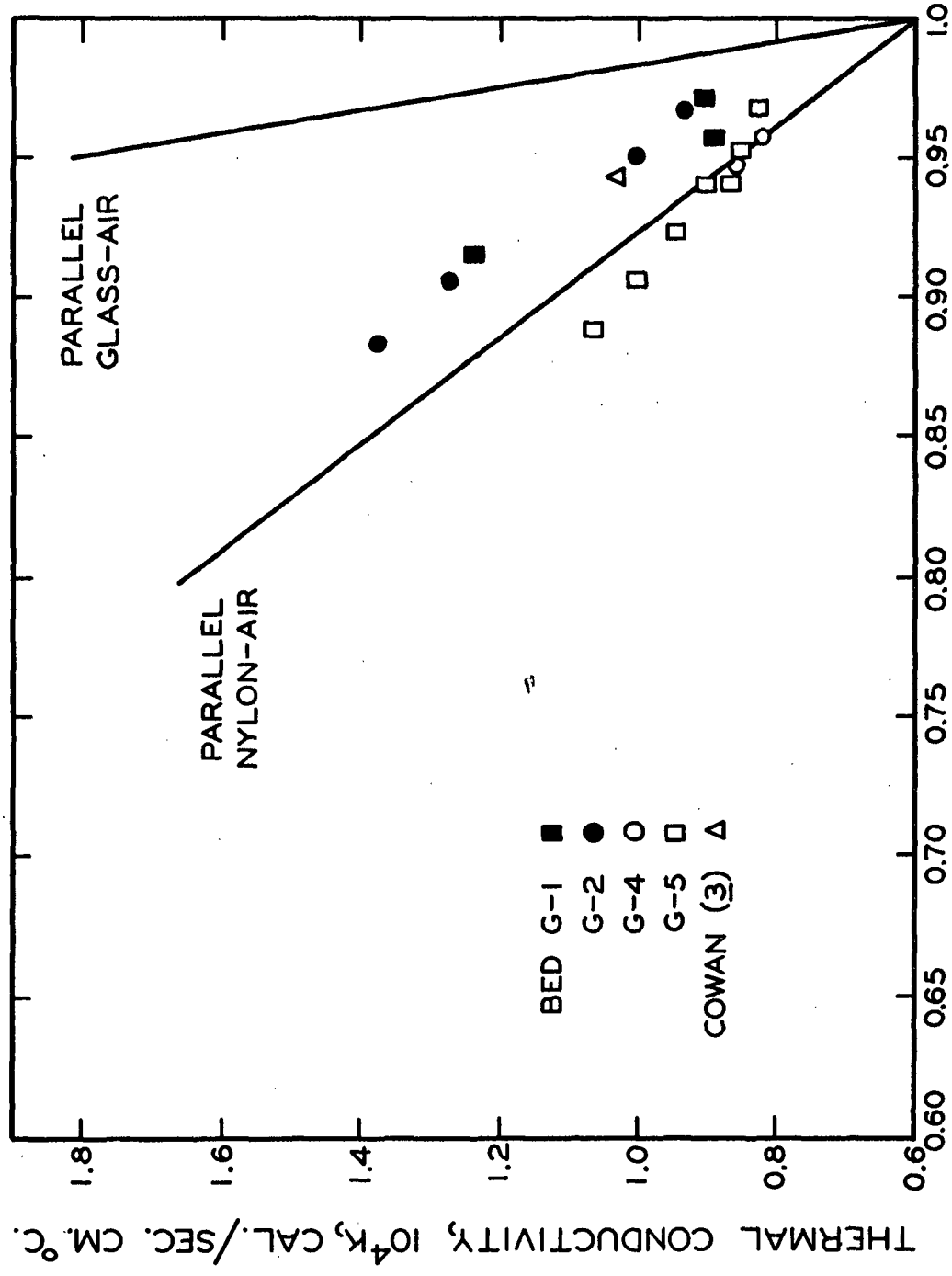

Figure 15. Conductivity of Dry Glass Fiber Beds

compression to 0.89 porosity, as many as one-third of the fibers in the bed may have been broken*. Jones' (42) compression data on glass fiber beds was terminated at a porosity of 0.94 due to the rapid increase of the load on the bed and the increasing significance of fiber breakage. Therefore, porosity reductions below 0.94 may be considered to be produced by considerable fiber breakage and repositioning in addition to compression.

DRY DACRON FIBER BEDS

Because of the widely different compressibility characteristics of the glass and nylon systems, an intermediate system, dacron-air, was selected. The dacron fibers, with a larger elastic modulus, produce a less compressible system than nylon and at the same time do not have the complex fiber-breakage phenomena associated with the glass system. A more ideal, intermediate system would have had a fiber conductivity value greater than nylon, but such a system was not available.

Table VI gives the conductivity results for the dacron system, and these results are also presented in Fig. 16. Two fiber lengths were utilized, but no differences in conductivity response were observed in the two beds formed from the different size fibers. This observation corresponded to the effect of fiber size in the nylon system.

The conductivity response to porosity changes in the dacron beds appears to be similar to the response observed with the nylon system. As the porosity was reduced, the experimental data coincided with the values predicted by the parallel phase distribution equation for dacron and air.

*The average fiber length before compression was 2.76 mm. The total fiber length of the 466 counted fibers after compression was 962 mm. This total length was equivalent to 349 fibers before compression. Therefore, 117 new fibers were formed by breaking.

TABLE VI

DRY DACRON FIBER BED STUDIES

Run No.	Fiber Bed Temp., °C.	Fiber Bed $\Delta\underline{T}$, °C.	$\frac{\Delta T}{\underline{T}}$ Ratio	Porosity	Bed Conductivity, $10^4\underline{K}$, cal./sec.cm.°C.	
Bed D-1—5 Denier—2.04 mm. Length—11.88 g. Weight						
D-1	55	47.7	3.96	0.934	0.873	1.408
D-9	56	38.1	2.55	0.902	0.915	1.476
D-10	56	33.0	1.87	0.875	0.986	1.592
Bed D-2—5 Denier—5.30 mm. Length—11.95 g. Weight						
D-2	55	47.2	4.95	0.947	0.873	1.406
D-3	56	44.7	4.01	0.933	0.865	1.395
D-4	55	41.5	3.25	0.919	0.878	1.416
D-5	55	36.8	2.58	0.901	0.905	1.460
D-11	55	32.0	1.85	0.875	0.996	1.609
D-12	55	28.3	1.40	0.847	1.08	1.740

Very evident in the dacron results was the minimum in the conductivity-porosity relationship. This phenomenon was present in the other fibrous system which was observed at the higher porosity levels, and, also, this condition has been reported for other porous systems. Generally, investigators have attributed this phenomena to convection and radiation. The discussion of this situation will be included in a later section.

OIL-SATURATED FIBER BEDS

The conductivity results for the glass, nylon, and dacron fiber beds which were fully saturated with dioctyl phthalate oil are presented in Fig. 17. These two-phase results are not very extensive, but they add a great deal to the analysis of the two-phase systems since they represent systems with lower solid-fluid conductivity ratios.

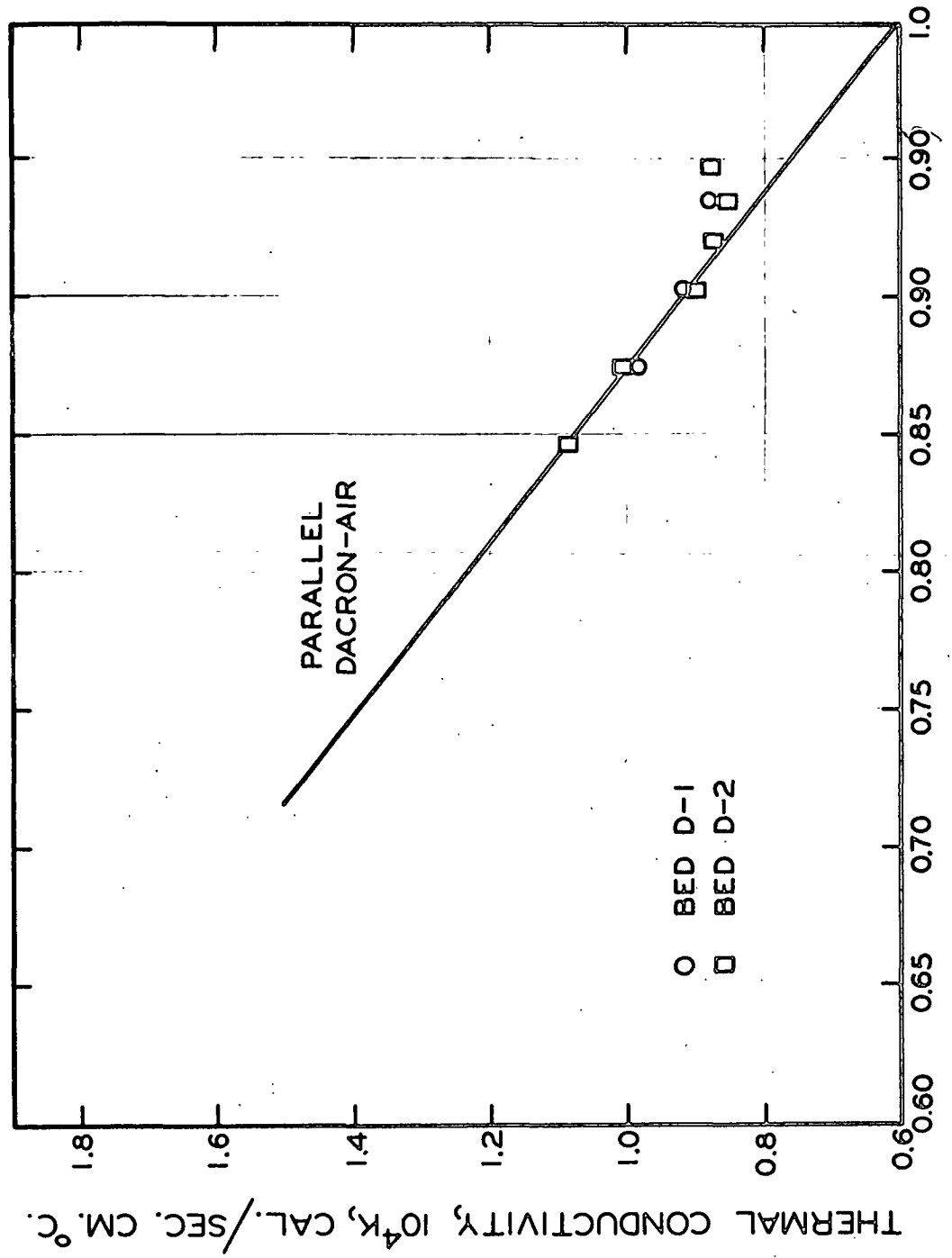

Figure 16. Conductivity of Dry Dacron Fiber Beds

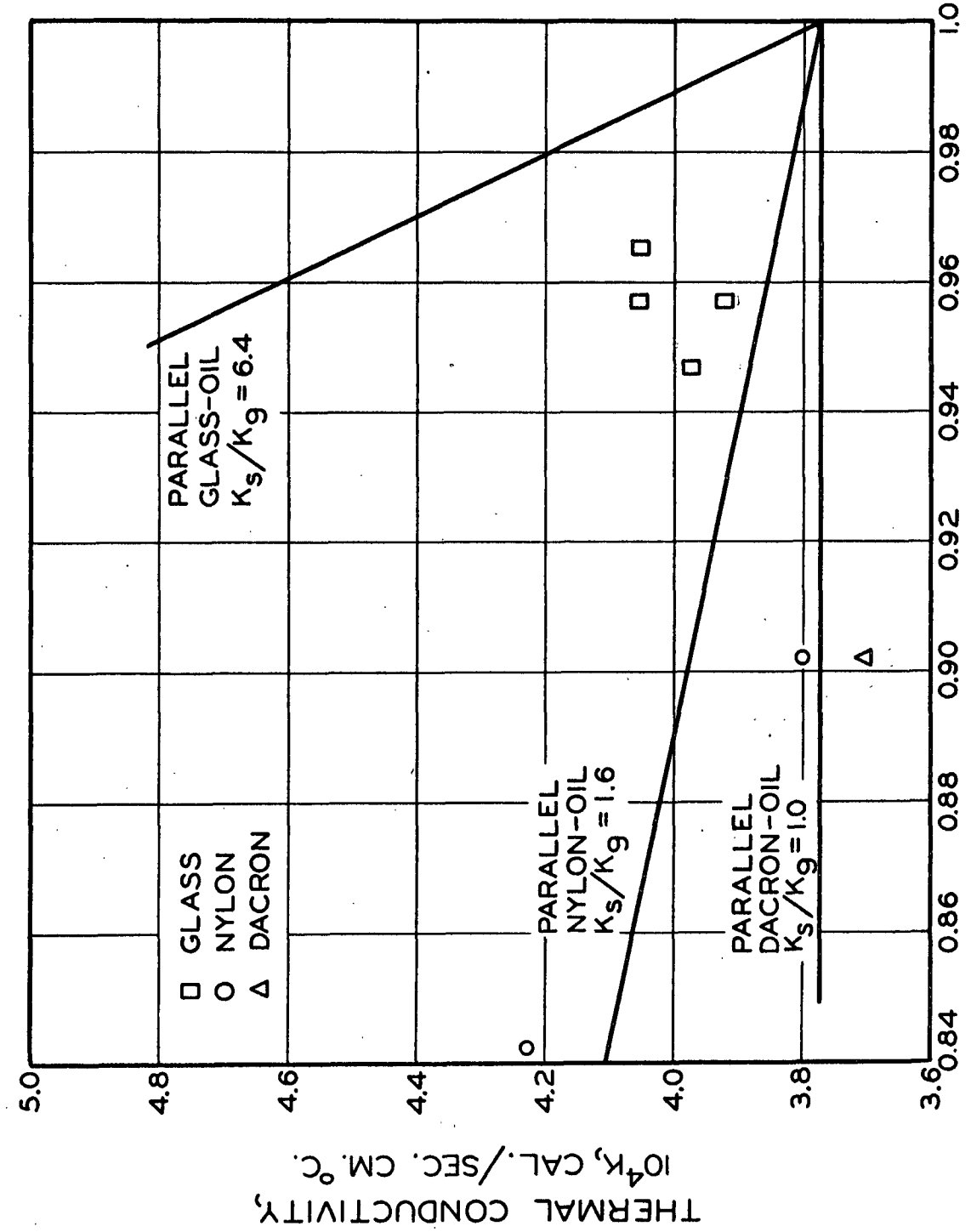

Figure 17. Conductivity of Oil-Saturated Beds

The fully saturated nylon and dacron systems behave like the nylon-air and dacron-air systems in that they align with the parallel phase distribution predictions. It is significant to note that the results for the glass-oil system fall below the predicted values, although not as much as with the glass-air system. Apparently, the replacement of the air with the more conductive oil (reduction of the solid-fluid conductivity ratio) has produced a significant change in the proportion of heat flux in the structure of the highly conductive glass fibers. However, even the reduction of the solid-fluid conductivity ratio has not produced a response in the glass system which is comparable to the viscoelastic fiber systems.

ANALYSIS OF TWO-PHASE RESULTS

CONVECTION AND RADIATION MECHANISMS

With the usual porous materials at normal temperatures, the mechanism of heat transfer is taken to be conduction, and most predictions of composite thermal conductivity assume that convection and radiation are negligible except under specific conditions. In the regions of high porosity encountered with the fibrous systems, there is good evidence that mechanisms of heat transfer in addition to conduction are important.

Although the dry fiber bed conductivity results in the very high porosity range (greater than 0.95) are not very extensive, the conductivity-porosity relationships appear to level off around 0.95 porosity. This tendency is most evident in the results for the dacron fiber beds which were presented in Fig. 16. If conduction were the only mechanism of heat flow in these higher porosity regions, the conductivity values should consistently decrease as the porosity is increased because the volume occupied by the lower conductivity air increases. Other workers with fibrous materials have also encountered this phenomenon.

Finck (5) has reported that the conductivity of various fibrous materials passed through a minimum in the bulk density range of 0.05 to 0.08 g./cc. (corresponds to a porosity range of approximately 0.94 to 0.96).

Baxter (52) indicated that the apparent conductivity of wool felt increased rapidly in the bulk density region below 0.1 g./cc. (porosities greater than 0.92).

The above observations were made with the heat flux passing downward through the highly porous specimen, which corresponded to the conditions of this study. With the heat flux downward through the specimen, the over-all density gradient

in the fluid was such that mass movement from the cold regions to the warm regions of the specimen was retarded. Generally speaking, this condition inhibits the influence of convection. Baxter and Finck also reported that a variation of the direction of heat flux in the highly porous materials did not significantly influence the apparent conductivity results.

Investigation of the influence of radiation on the apparent conductivity of highly porous materials at low temperatures has been limited. Finck found that aluminum powder in a fiber mat influenced the conductivity of a fiber mat only at a bulk density lower than 0.016 g./cc. (porosity greater than 0.99) with the specimen at room temperature.

The apparent conductivity due to radiation, K_r, can be defined as the rate of heat transfer by radiation per unit area divided by the temperature gradient, and this has been expressed by Russell (21) in the form

$$K_r = 4\sigma C T_a^3 p \qquad (22)$$

where σ is the radiation constant (1.36×10^{-12} cal./sq.cm.sec.°K^4), C is the constant depending on the emissivity and the geometry of the surfaces of the air space, T_a is the absolute temperature, and p is the thickness of air space. Assuming that the constant, C, is approximately unity for nonmetallic materials, the radiation contribution to the heat transfer in the pore space can be calculated as a function of temperature and the thickness of the air space. These results are shown in Table VII.

The influence of the radiation effect on the apparent conductivity of the air spaces in the bed is almost wholly transmitted to the over-all conductivity of the bed since the fiber bed has such a high porosity.

TABLE VII

APPARENT CONDUCTIVITY DUE TO RADIATION

Thickness of Air Space, cm.	$10^4 K_r$, cal./sec.cm.°C.	
	55°C.	75°C.
0.01	0.019	0.023
0.02	0.038	0.046
0.03	0.058	0.069
0.10	0.192	0.230
Air conductivity	0.62	0.65

The main problem in evaluating this information is the knowledge of the actual size of the pore spaces in the fiber bed. Cowan (3) utilized the capillary pressure-saturation data on glass fiber beds at 0.945 porosity with the assumption of a hydraulic radius model in his calculation of pore sizes. He reported an average pore diameter of 0.002 to 0.003 cm. in the beds.

The fibers utilized in this study were larger than Cowan's; therefore, a larger pore diameter value would be expected. The effective air spaces in the bed would have to be about ten times the values calculated from the capillary pressure data of Cowan in order to produce an appreciable radiation effect as illustrated in Table VII. Nevertheless, the effective thickness of the air spaces in the bed that are associated with radiative heat transfer may not be adequately represented by the capillary pressure calculations.

On the basis of the above discussion, the influence of heat transfer mechanisms other than conduction at porosities around 0.95 appears to be negligible. However, a closer look at the phenomena may provide some insight. The thermal

conductivity of the solid component and the gaseous component in the porous system are generally quite different. Therefore, the temperature gradient in the solid will be different from the gradient in the pore space. This was illustrated in Fig. 2. Obviously, if the pore space is of sufficient size, this condition will allow convection to occur and become significant in the high porosity regions. This type of convection occurs in the pore space and not as an over-all mechanism where mass movement takes place between the surfaces of the bed. Therefore, a change in direction of heat flux would not give any indication of the extent of this convective mechanism.

The magnitude of the convective movement in the pore space would be dependent on the surface area of the fiber as well as the distance between fibers and the relative conductivity of the fiber and gas components. Therefore, the porosity region in which this type of convective mechanism of heat transfer becomes significant will be dependent on the characteristics of the porous system involved.

The radiation contribution cannot be overlooked, despite the previous calculations. As the bed becomes more and more porous, the possibility for a significant influence of radiation becomes more pronounced. Indeed, the system characteristics play the major role in determining the critical region of influence.

In order to observe the possibility of radiation in the fiber system, the emissivity of the hot plate surface was altered by making measurements with and without the aluminum foil. Also, measurements were made on the conductivity of air in order to determine the effect of the emissivity of the surfaces. These results are shown in Table VIII.

The alteration of the hot-surface emissive characteristics produced the expected, large change in the apparent conductivity of the air. The contribution

of radiation to the over-all heat transfer through the air layer was quite evident.

TABLE VIII

HOT SURFACE EMISSIVITY STUDY

Run No.	Hot Surface Conditions	$10^4 K$, cal./sec.cm.°C.
Air—thickness of 0.25 inch		
A-2	Aluminum foil[a]	0.72
A-5	Copper plate[b]	0.92
Dacron Fiber Bed D-2—porosity of 0.947		
D-2	Aluminum foil[a]	0.88
D-14	Aluminum foil[a]	0.87
D-13	Copper plate[b]	0.90

[a]Normal run conditions. Foil total emissivity approximately equal to 0.05.

[b]Clean, but unpolished copper plate with total emissivity approximately equal to 0.5.

With the dry fiber bed, the changes associated with the emissive characteristics of the hot surface were expected to have little effect on the over-all conductivity of the bed. However, the conductivity results for the fiber beds had indicated that mechanisms, in addition to conduction, aided in the heat transfer at the higher levels of porosity. The 3% increase in the apparent conductivity of the dacron fiber bed when the aluminum foil was removed is probably significant and indicative of the role that radiation begins to play at the higher levels of porosity.

Additional observations of fibrous systems in the higher porosity regions will be necessary before the relative magnitude of the effects of convection and radiation can be acquired.

PREDICTION EQUATIONS

Valuable information has been obtained by applying the two-phase conductivity equations for spherical particles in a continuous fluid to the study of the heat transfer characteristics of granular systems. Since particle geometry is generally not considered to be a critical factor in the heat flow in a porous system, these equations, which were discussed in the Literature Survey section, were utilized in the analysis of the dry fiber bed conductivity results.

The predicted results are presented with the experimental values in Fig. 18, 19, and 20. Air-phase conductivity was taken as 0.6×10^{-4} cal./cm.sec.°C.

Maxwell's noninteracting system [Equation (4)] underestimated all of the conductivities of the fiber beds. Even at these higher porosity levels his model system is not realistic.

The cubic lattice models of Russell [Equation (6)] and Woodside [Equation (7)] correspond quite well with the glass system results, but underestimate the nylon and dacron system. The primary characteristic of these ideal systems at the high porosity levels is that the particles do not touch, and, therefore, solid-solid contact is of little importance to the over-all heat flow in the model. Apparently, the heat-transfer characteristics of the glass fiber bed are adequately described by this type of arrangement.

deVries' relationship, Equation (5), was applied to the fibrous system by assuming that the fiber length and diameter were the major and minor axes of an ellipsoid in order to calculate the particle shape factors in the equation. The predictions from deVries' equation also gave inconsistent results: overestimated the glass system and underestimated the nylon and dacron systems.

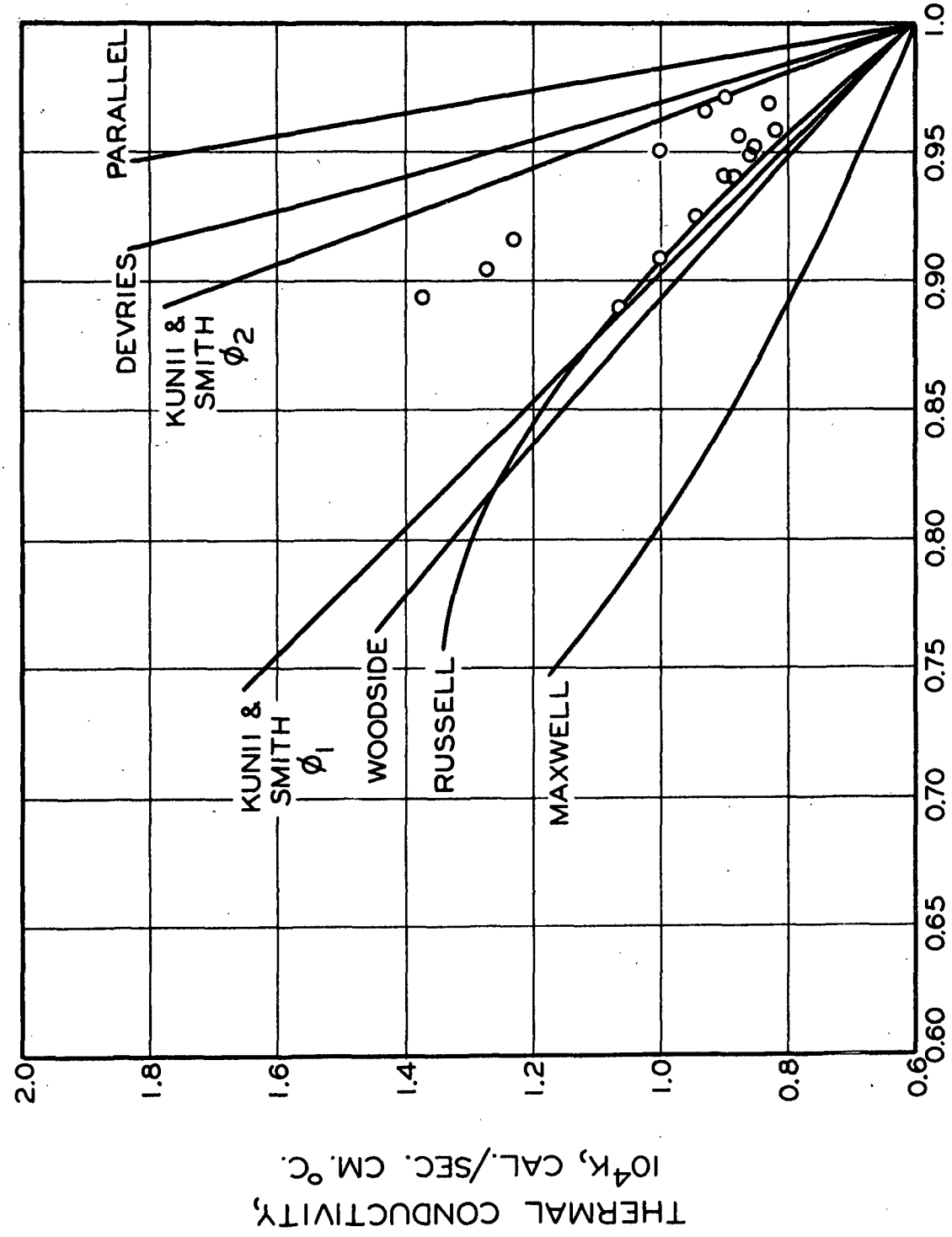

Figure 18. Predicted and Experimental Conductivity Results for Glass-Air Systems

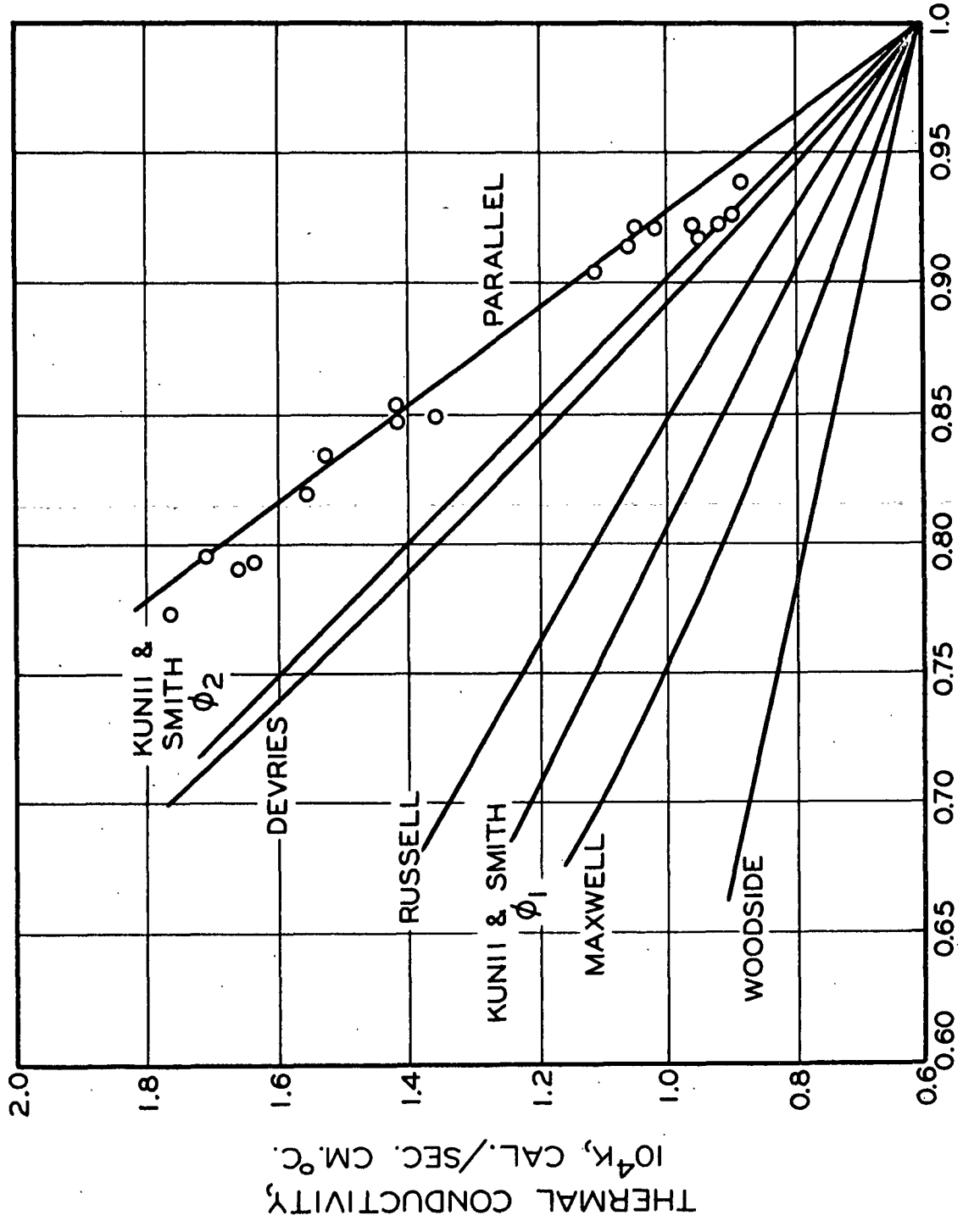

Figure 19. Predicted and Experimental Conductivity Results for Nylon-Air Systems

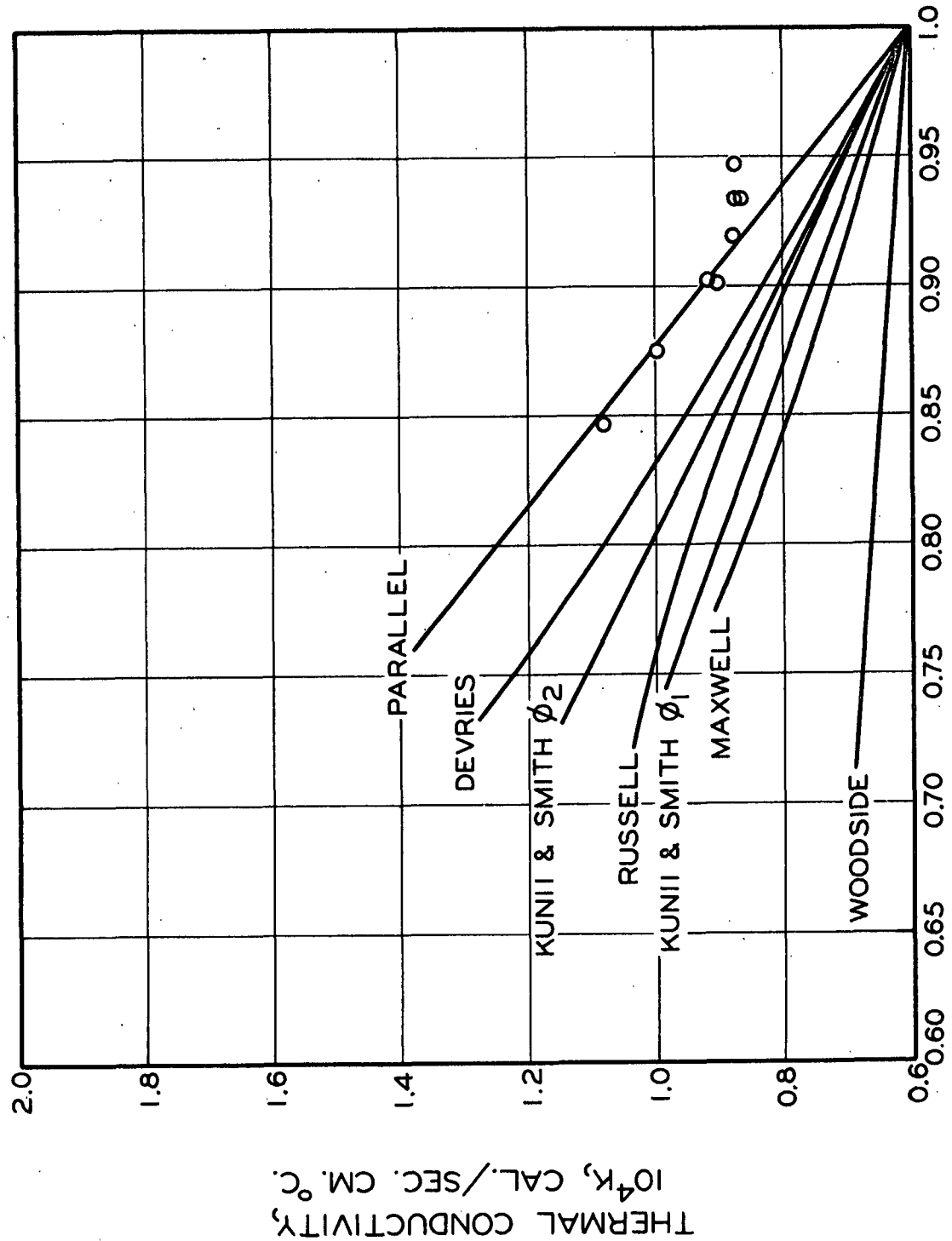

Figure 20. Predicted and Experimental Conductivity Results for Dacron-Air Systems

Apparently, some of the variables in the fibrous system are not accounted for. This situation was more emphatically revealed when the relationship of Kunii and Smith was studied.

Kunii and Smith's final expression took the form of Equation (9) which neglected the effect of the actual solid-solid contact area and only considered the influence of the fluid filaments adjacent to the contact. The effective thickness of the fluid filament, ϕ, was computed by Kunii and Smith for various values of solid-fluid conductivity ratios with two types of structural geometry for the system:

(1) ϕ_1 for loose packing of spheres (approximately 3 contacts/particles), and

(2) ϕ_2 for close packing of spheres (approximately 14 contacts/particle).

The application of Equation (9) to the fibrous system also involved two other parameters. For calculation purposes, the distance between adjacent particle centers was taken to be the particle diameter, and, therefore, β became unity. The effective length of the cylindrical fiber was calculated as shown in Appendix II which indicated that γ was equal to $\pi/4$.

Use of the fluid filament factors, ϕ, for the spherical particles as calculated by Kunii and Smith allowed estimates of the fiber bed conductivities to be made, and these values are shown in Fig. 18, 19, and 20 with the other predictions.

The highly porous structure of the fiber bed should correspond to the loosely packed structure of the spherical particles, provided the solid-solid particle contact is not important. However, only the glass fiber results were adequately predicted by the Kunii and Smith ϕ_1 factor, while the nylon and dacron results were greatly underestimated. On the other hand, the close packing factor, ϕ_2,

should overestimate the results for the highly porous fiber bed. This was true for the glass system, but not for the deformable fiber systems.

The obvious conclusion from the use of the Kunii and Smith relationship was that the influence of the contact region was more pronounced with the dacron and nylon systems than with the glass system. This also had been the indication with the other predicted values though only the Kunii and Smith relationship allowed this difference to be distinguished.

Apparently, the heat-transfer characteristics of the glass fiber system correspond in detail to the model utilized by Kunii and Smith. This includes the neglect of the solid-solid contact contribution to heat flow in the solid structure. The fact that glass has a very high modulus of elasticity supports the concept that the fiber-fiber contact area will be extremely small, and that there will be little deformation at the contacts when the glass fiber beds are compressed. As a consequence, the heat flux in the solid structure of the glass system passes through the fluid filaments adjacent to the contact, and Kunii and Smith have included this contribution in their analysis.

With the dacron and nylon systems, a picture consistent with Kunii and Smith's model cannot be acquired. The predicted values correspond only when the effect of the contact region is maximized in the model.

A close-packed structure does not correspond with the structure of the fiber bed. However, the close-packed model with the reduced resistance in the contact region provided the best conductivity predictions for the nylon and dacron fiber beds. Kunii and Smith found adequate correlation with their predictions for a wide range of solid-fluid systems, and, therefore, it is not adequate to attribute

the fibrous system situation to a reduction in the solid-fluid conductivity ratio. Apparently, the only other significant effect lies with the solid-solid contact.

A finite contact area would greatly reduce the resistance to heat flow in the solid structure, and with deformable materials the existence of significant contact area between particles is reasonable. The analysis of the fiber-fiber contact area (Fig. 4) indicated that there was a significant difference between the glass fiber beds and nylon and dacron beds in the porosity regions of this study.

Further illustration is provided if one looks at the conductivity data for the six, two-phase fibrous systems which have been investigated under comparable compressional conditions. Table IX gives the conductivity values for the fibrous systems and, as a basis for comparison, the predicted conductivity values as calculated from the parallel distribution equation are also included.

TABLE IX

COMPARISON OF PREDICTED AND EXPERIMENTAL RESULTS FOR TWO-PHASE SYSTEMS

System	K_s/K_g	Porosity	$10^4 K$, cal./sec.cm.°C. Experimental	$10^4 K$, cal./sec.cm.°C. Predicted[a]
Glass-Air	40.0	0.95	0.86	1.76
Nylon-Air	9.8	0.90	1.14	1.14
Dacron-Air	6.4	0.90[b]	0.91	0.92
Glass-Oil	6.4	0.95	4.0	4.8
Nylon-Oil	1.6	0.90	3.8	4.0
Dacron-Oil	1.0	0.90[b]	3.7[c]	3.8

[a] Equation (1).

[b] Larger compressional stress than in the nylon and glass systems.

[c] Extrapolated value.

As the conductivity ratio K_s/K_g decreases, the thermal characteristics of the components of the bed become similar and the predicted and experimental conductivity values should converge. Apparently, this is the situation—note the two glass systems. However, at the conductivity ratio of 6.4, the dacron-air experimental values compare favorably with the predictions, but the values for the glass-oil system are 20% apart. Even the experimental results for the nylon-air system, which has a larger conductivity ratio than glass-oil, are identical with the predicted values. Therefore, the deformable fiber systems have one or more additional mechanisms of heat transfer which do not influence the glass system to the same degree.

The derivation of the two-phase conduction equation for a compressible system accounted for the possibility of a significant contribution to the heat flow by the particle-particle contact area. The contact resistance term in Equation (11) includes the area of actual solid-solid contact as well as the area of surrounding fluid. One observes that once the contact factor ($h_c \alpha$) becomes large the expression becomes equivalent to the parallel phase distribution relationship, Equation (1). This corresponds to the concept that as the fiber bed is compressed, the fiber-fiber contacts become more significant and the heat flow from one particle to another is maximized. On the other hand, when the heat flow in the solid structure is less than the maximum, the conductivity predicted from Equation (11) is less than the parallel distribution equation. This latter condition should correspond to the regions of higher porosity. However, it is also in the regions of higher porosity that the additional mechanisms of radiation and convection become significant and Equation (11) would not be expected to be sufficient.

For correlation purposes, the experimental data for the dry fiber beds have been utilized to calculate the contact factor ($h_c \alpha$) values in Equation (11).

$$K/K_g = \epsilon + [1-\epsilon]/[(K_g/K_s) + K_g/D_f(h_c\alpha)] \qquad (11)$$

To aid in the calculation of the contact factors at the higher porosity levels, arbitrary curves have been drawn which correspond to the discussion in the previous paragraph. These arbitrary curves are shown in Fig. 21, 22, and 23 with the experimental data for glass (lowest values), nylon, and dacron beds.

There is a definite possibility that the nylon-air data in the porosity region of 0.92-0.94 falls below the maximum conductivity before the additional heat-transfer mechanisms become significant. Consequently, the nylon response in this region is assumed to be similar to the response of the glass-air system throughout.

The dacron-air data do not drop below the maximum conductivity value before the contribution of mechanisms other than conduction become significant. However, the glass-oil data provide a system with the same solid-fluid conductivity ratio, and the presence of the oil in the voids reduces the effect of convection and radiation. The primary difference in the dacron-air and the glass-oil systems is the elastic modulus of the fibers. Looking at Fig. 4, it is apparent that at the porosity level of 0.95 the contact area fractions for the two systems are about equal. In fact, the glass contact area is a little greater because of the larger compressional stress necessary. Therefore, it seems reasonable to combine the glass-oil data with the dacron-air system in order to acquire some estimate of the $h_c\alpha$ values in the higher regions of porosity.

The calculated values for $h_c\alpha$ are presented in Fig. 24 as a function of solid fraction. The nylon and dacron change is what one would expect when the contact area between fibers begins to contribute to the heat flow in the solid structure as the bed is compressed. The glass system contact factor remains at a low level

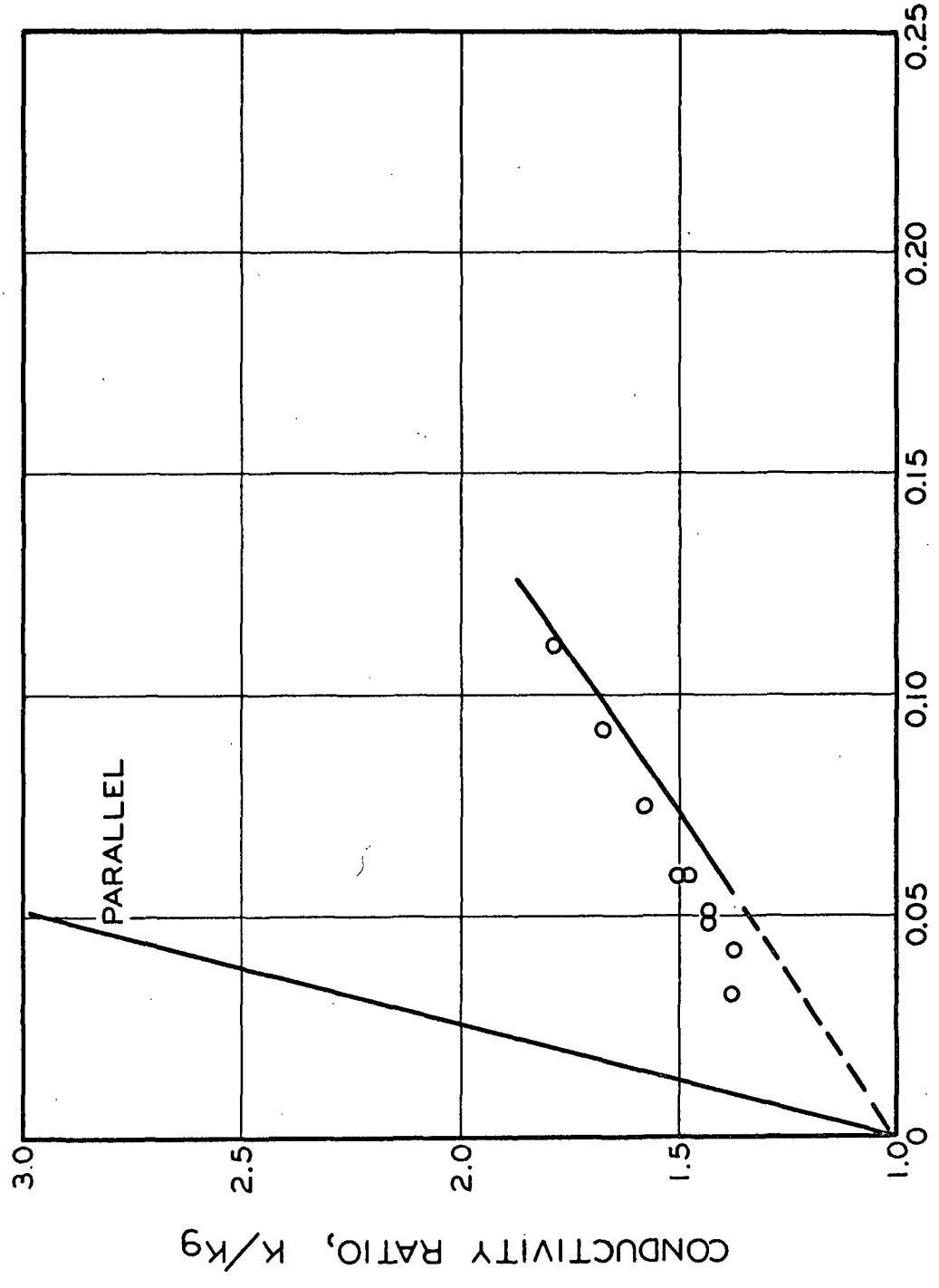

Figure 21. Conduction Curves for the Glass-Air Data

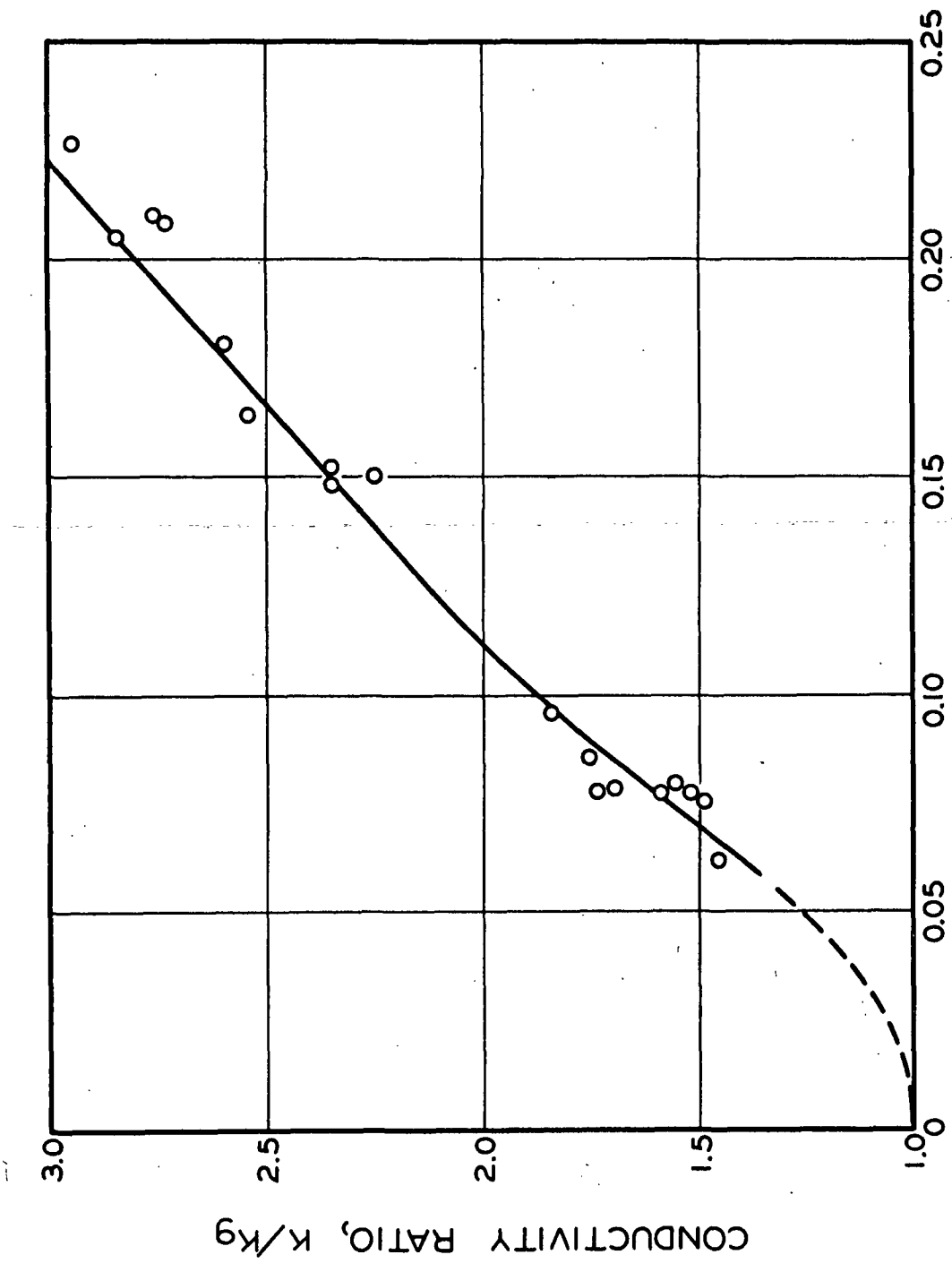

Figure 22. Conduction Curves for the Nylon-Air Data

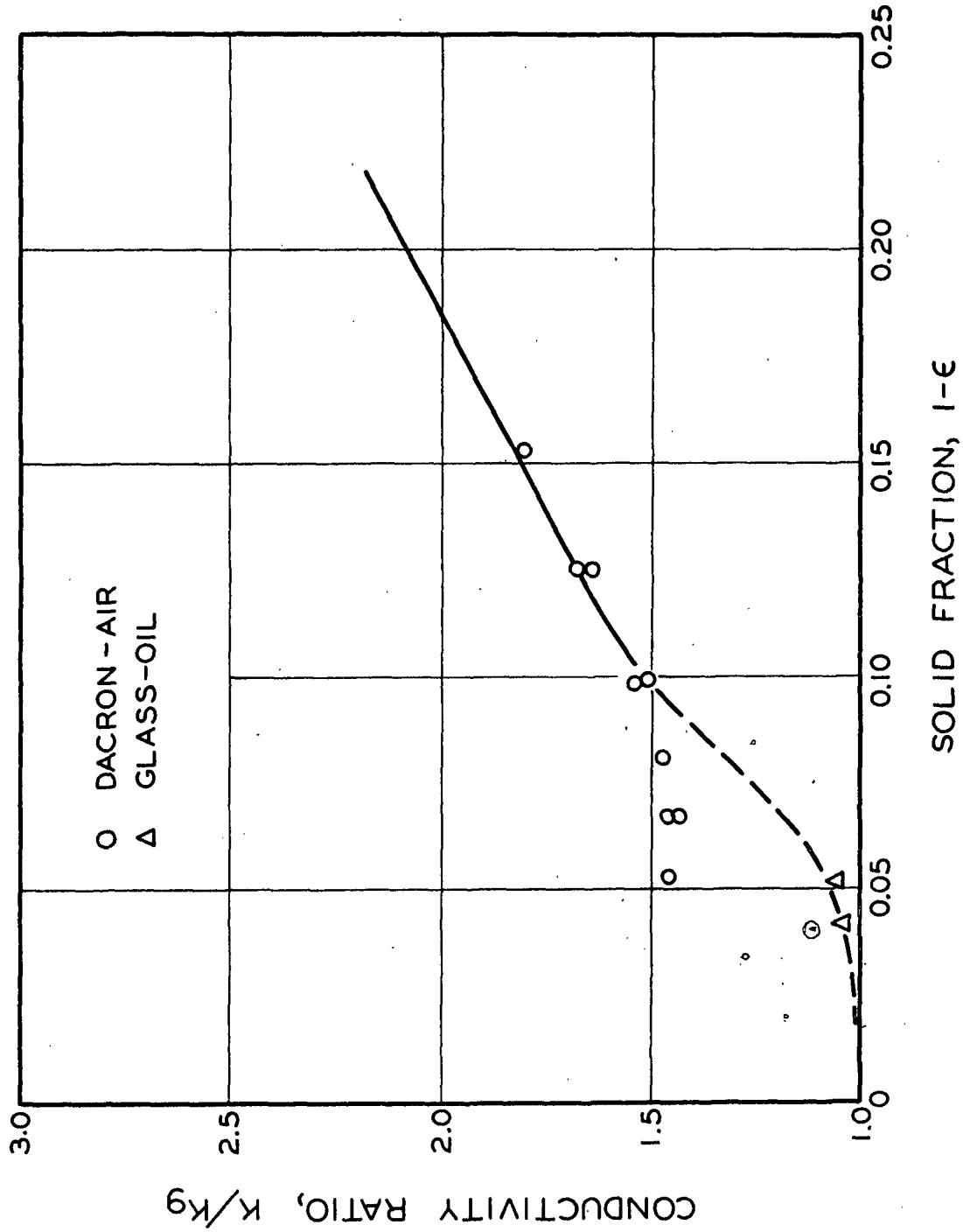

Figure 23. Conduction Curves for the Dacron-Air, Glass-Oil Data

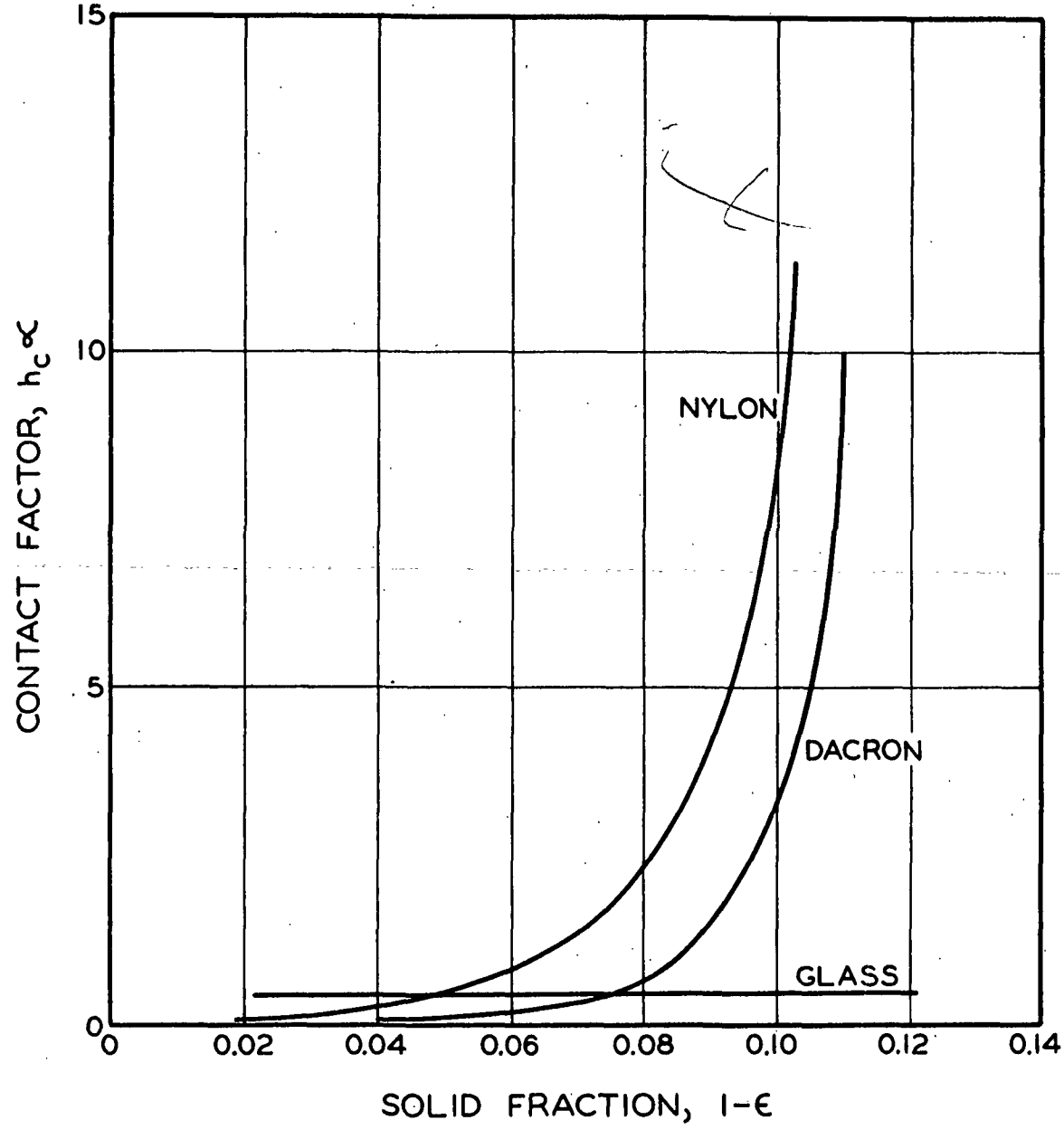

Figure 24. Contact Factor Response

throughout the compression. This observation is consistent with the concept that the heat flow in the fluid film between the glass fibers is controlling since a significant change in this contribution as the bed is compressed is not expected.

At the lower porosity levels, the contact factors for the nylon and dacron systems are primarily dependent on the nature of the solid-solid contact area, and it is expected that the heat flow in the fluid film adjacent to the contact contributes little to the over-all heat flow. When the porosity is increased and the solid-solid contact area is decreased, the nature of the entire contact region, which includes the solid-solid contact area and the fluid film, governs the heat flux in the solid structure.

Apparently, in the glass system, the contact area contribution does not become significant. This is due to the high elastic modulus of the glass and also because fiber breakage occurs. The decrease in the resistance of the fluid film adjacent to the contact as the porosity is reduced is small, especially at these high porosities. Therefore, the decreased resistance of the contact region of the glass-air system is not sufficient to maintain a large heat flux in the solid structure. Consequently, the over-all conductivity of the glass fiber bed does not increase rapidly when the porosity is reduced.

The division of the contact factor into the contributions of the solid-solid contact area and the fluid filament surrounding the contact is difficult. However, if some assumptions concerning the response in the different systems are made one can continue with the analysis.

First, the expression for the conductivity of porous materials when the heat flow in the solid structure is divided as discussed above, is

$$K/K_g = \epsilon + \frac{(1-\epsilon)}{\frac{1}{\frac{\delta}{\phi} + \frac{D_f(h'_c\alpha')}{K_g}} + \gamma K_g/K_s} \qquad (23)$$

where γ and ϕ are effective lengths for the solid particle and the fluid film, respectively; δ and α' are the fractional areas for the fluid filaments and solid-solid contacts, respectively; and h'_c is the heat transfer coefficient for the solid-solid contact area.

If it is assumed that the solid-solid contact area in the glass fiber system does not contribute to the over-all conductivity of the bed, Equation (23) can be utilized to calculate the δ/ϕ value for the glass system. If δ is taken as unity and γ as 0.785 (Appendix II), the ϕ value for glass-air is 0.10.

It was concluded that in the nylon system the contact area contribution was more significant than the fluid filament value. If it is assumed that the fluid filament contributions in the glass and nylon systems are the same, then the ϕ value for nylon will also be 0.10. Using this value in Equation (23), the contact term can be computed for the nylon-air system. The results of these calculations are presented in Table X for high and low porosity levels in the nylon system.

TABLE X

COMPARISON OF FLUID FILAMENT AND CONTACT RESISTANCES IN NYLON-AIR SYSTEMS

Porosity, ϵ	Fluid Filament, ϕ	Contact Term, $[K_g/D_f h'_c \alpha']$	K/K_g, neglecting ϕ	K/K_g, experimental result
0.80	0.10	0.028	2.68	2.80
0.95	0.10	0.455	1.04	1.26
0.80	0.15	0.025	2.73	2.80
0.95	0.15	0.181	1.14	1.26

At the low porosity regions the neglect of the fluid filament contribution in Equation (23) does not introduce a significant error in the calculated conductivity of the nylon-air system. However, at the higher porosity where the fiber-fiber contact area would be less significant, the fluid filament contribution cannot be neglected in the prediction.

Looking at the calculations of Kunii and Smith for the $\emptyset$ values for the system of spherical particles, and also observing the calculations made in Appendices I and II, the $\emptyset$ values for nylon-air are at least 50% greater than the glass-air values. A better estimate of the $\emptyset$ value for nylon-air, based on the empirically determined value of 0.10 for glass-air, would be 0.15. This value was utilized in Equation (23) for nylon-air and these results are also presented in Table X. The conclusions are similar, but the neglect of the fluid filament value does not introduce as much error at the high porosity level as was previously observed.

Alteration of the assumed values of δ and γ in Equation (23) would change the magnitude of the calculated values, but the above discussion would still be applicable.

From the combined contribution of the fluid filament and the contact area ($\underline{h}_c \alpha$ as shown in Fig. 24), the response of the heat-transfer coefficient, $\underline{h}_c$, for the contact region was calculated by using the fiber-fiber contact area fractions, α', as given in Fig. 4. The calculated, contact heat-transfer coefficients for the nylon-air, dacron-air, and glass-air systems are presented in Fig. 25 as a function of the bed solid fraction.

The response of the heat-transfer coefficient for the nylon and dacron systems is what one would expect for a bed in which the fiber-fiber contact area

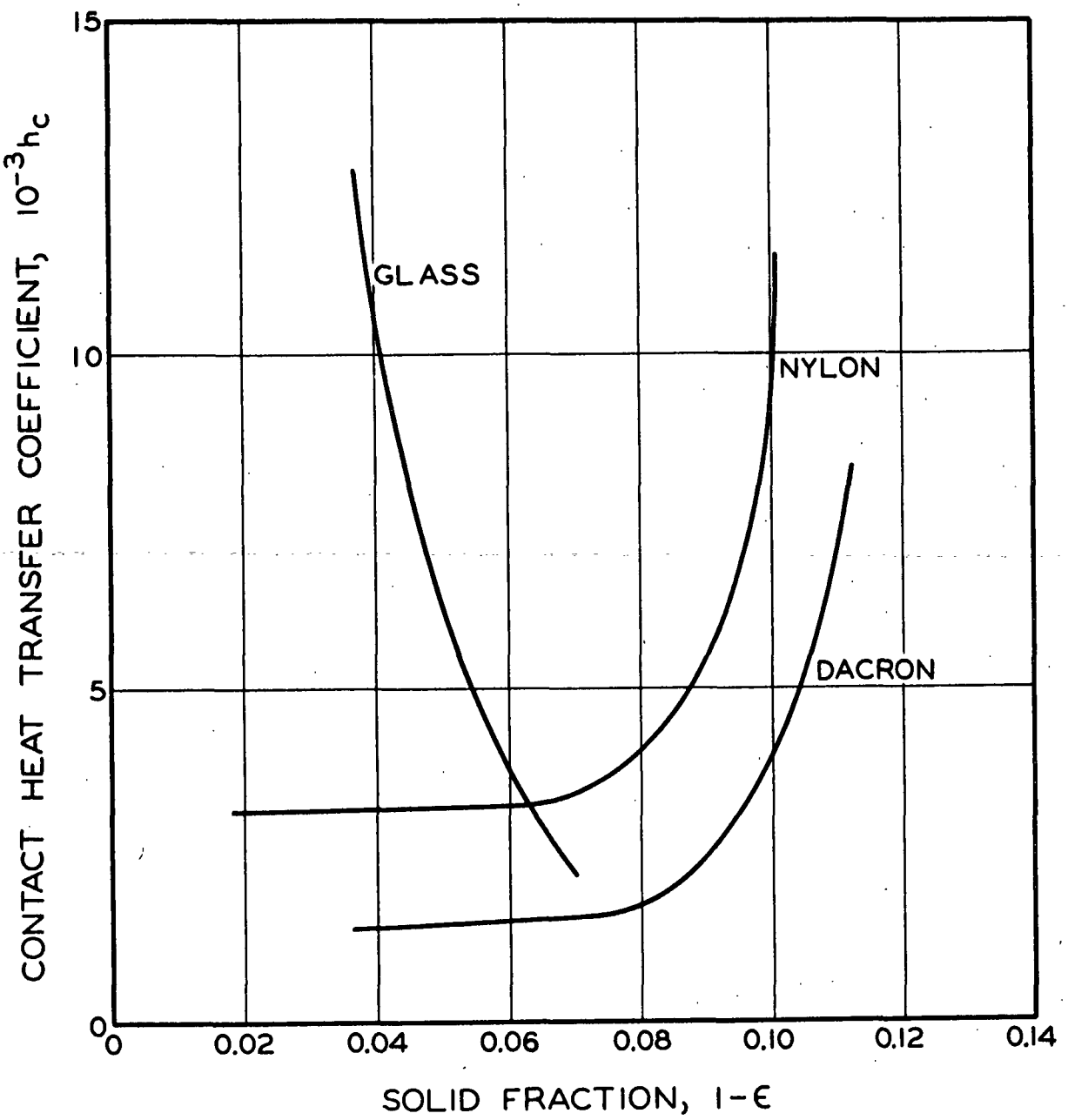

Figure 25. Contact Heat Transfer Coefficient Response

becomes important as the bed is compressed. Better contact between fibers allows more heat to flow in the solid structure as indicated by the decreased resistance in the contact region. Therefore, it appears that the use of the fiber-fiber contact area fraction, α', allows a consistent computation of the heat-transfer coefficient in the deformable fiber systems.

The response of the glass heat-transfer coefficient is not consistent with the result expected if the fiber-fiber contact area was involved in the heat flow in the solid structure of the bed. In that case, one would expect the heat-transfer coefficient to remain constant or to increase as the porosity was reduced. The calculated decrease in h_c indicates that the area of fiber-fiber contact represented by α' is not indicative of the significant portion of the contact region. Therefore, the fluid filaments surrounding the contacts must conduct the heat flowing in the solid structure. These areas of fluid change very little as the porosity is reduced, particularly at these high levels of porosity.

The heat-transfer coefficient, h_c, is probably dependent on the nature of the composite system and the conductivity of its components. An empirical correlation of contact coefficients has been given by Wilhelm, et al. (8). Porosity and solid conductivity were used as the measurable parameters affecting the coefficient, but no direct experimental evidence to clarify the situation was offered. Therefore, more than qualitative discussion is probably futile.

The heat-transfer area associated with the contact region also has nebulous characteristics. The picture presented by Woodside and Kuzmak (Fig. 2) illustrated that some portion of the pore space was involved with the heat transfer in the solid structure. Woodside and Messmer (15) reported that a distance

one-sixth the particle radius from the contact accounted for the important contact region in their granular system. A similar concept provided the basis for Kunii and Smith's analysis. All are empirical adjustments to provide a consistent correlation. The added fiber-fiber contact area contribution in the deformable fiber system simply enlarges the scope of this type of analysis.

THREE-PHASE CONDUCTIVITY RESULTS

The partial saturation study utilized two fibrous systems—nylon and glass. These systems were maintained at two average porosity levels; 0.90 and 0.85 for the nylon, 0.96 and 0.95 for the glass. The primary variable studied was degree of saturation, s, which is defined as the fractional amount of the void volume in the bed which contains liquid. The liquid in this study was the nonvolatile oil, dioctyl phthalate.

The calculated degree of saturation is an average value determined by weight and it is assumed that the liquid is uniformly distributed throughout the network. Obviously, the specific saturation at a given location in the bed may vary from this average, but it is believed that this variation is small, especially as related to the heat-transfer characteristics of the bed.

Maintaining a temperature gradient in a partially saturated porous bed produces a surface tension gradient* in the liquid network and redistribution of the liquid occurs. Preliminary measurements with two beds laminated together indicated that redistribution of the oil from one bed to the other was not extensive. Subsequent measurements of the conductivity of the partially saturated fiber beds indicated that a change in the temperature gradient across the bed did not significantly alter the conductivity of the bed. These observations were made at several levels of saturation with as much as a 50% change in the temperature gradient.

The errors associated with the thermal conductivity measurements in the partial saturation study were the same as with the dry bed study. About 1% variation was observed for individual measurements. Small differences in porosity

*Dioctyl phthalate surface tension at 20°C. was 33 dynes/cm. A surface tension variation with temperature of 0.1 dyne/cm.°C. is normal.

were partially responsible for the 5 to 15% variation between beds at a given saturation. Also, as much as a 5% variation was encountered with a given bed when remeasured at a specific saturation level after the bed has been taken through a complete saturation-desaturation cycle. The best reproduction of measurements was acquired if the changes in saturation were accomplished with the bed porosity at or near the desired porosity for measurement. This was especially applicable to the measurements at the lower levels of saturation.

PARTIALLY SATURATED NYLON FIBER BEDS

Eight nylon fiber beds were used in the partial saturation study. The conductivity results at the two porosity levels are shown in Fig. 26 and 27 as a function of saturation. A complete summary of the operating conditions and the conductivity results are given in Table XI in Appendix III.

In Fig. 26 and 27, the parallel phase distribution equation for nylon-oil-air is plotted as a basis for comparison and subsequent analysis. This equation can be written as

$$K = (1-\epsilon)K_s + \epsilon s K_\ell + (1-s)\epsilon K_g \qquad (24)$$

where K_ℓ is the liquid conductivity and s is the average saturation.

The replacement of the air in the fiber network with the more conductive oil produced an immediate change in the conductivity of the nylon bed. At the upper levels of saturation the conductivity of the bed did not increase as rapidly as the saturation was increased. This produced a leveling off of the conductivity-saturation relationship at saturations above 0.8. This was particularly noticeable with the 0.85 porosity bed.

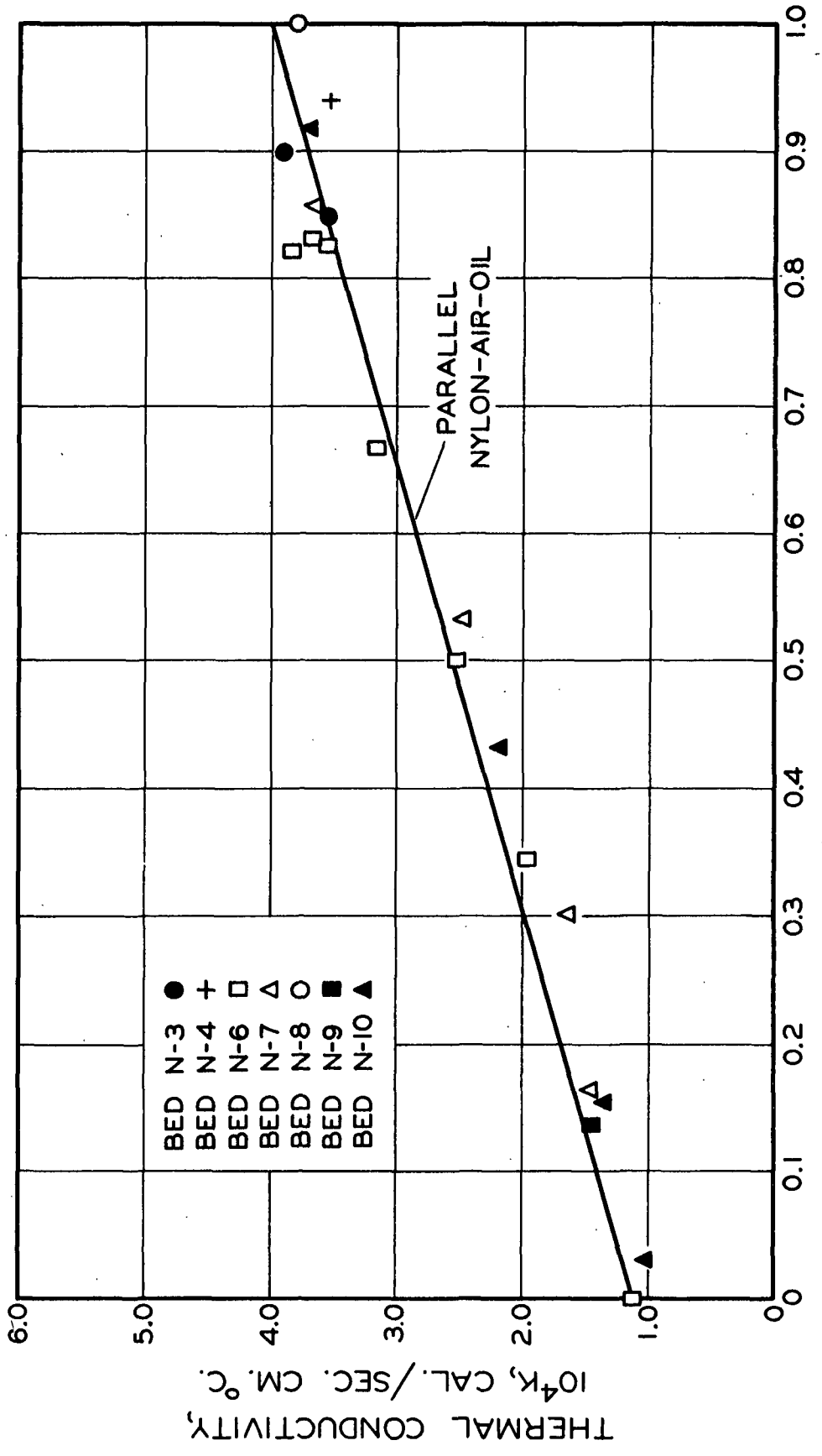

Figure 26. Partial Saturation Results: Nylon-Air-Oil, Average Porosity 0.90

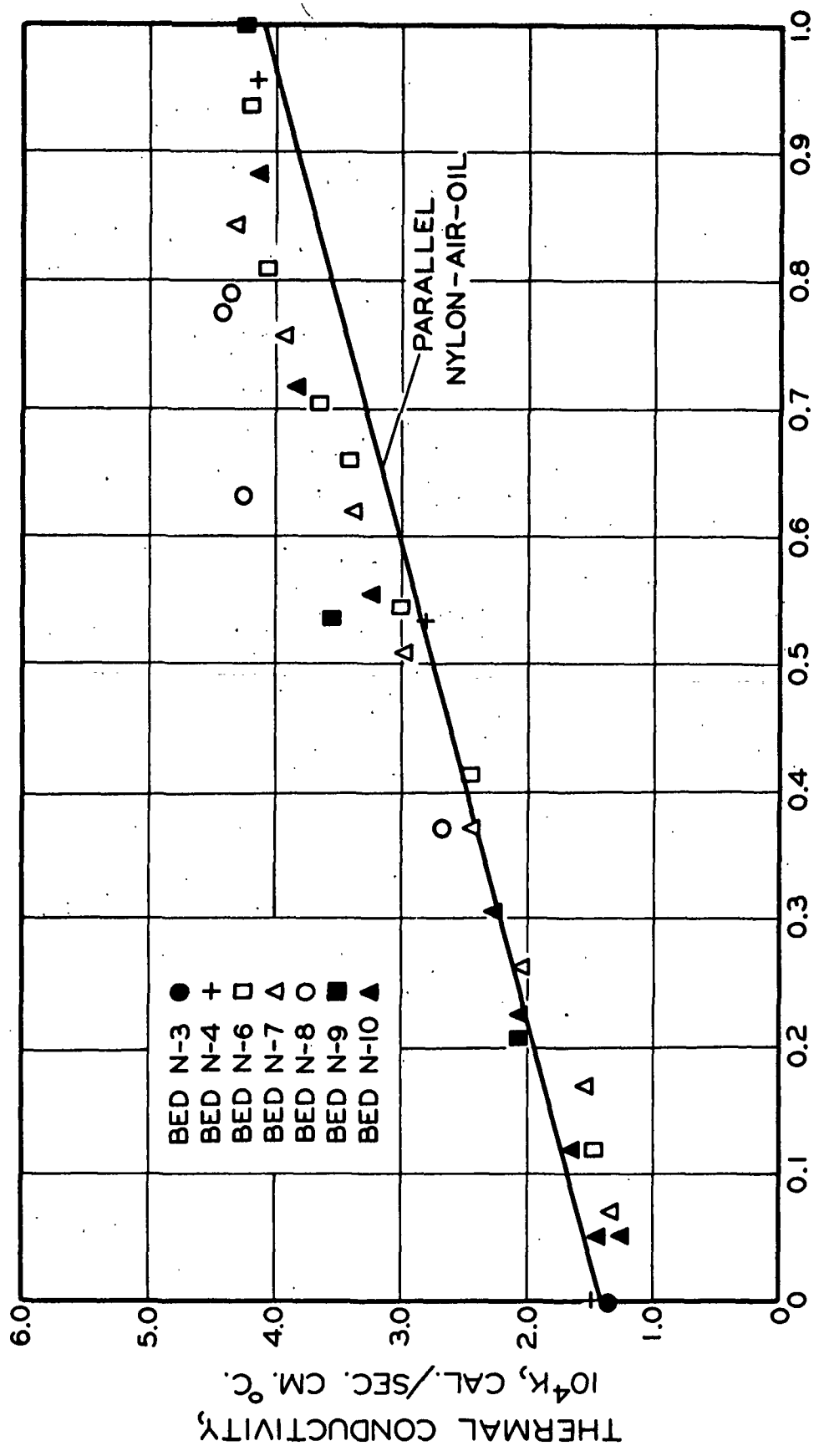

Figure 2Ø. Partial Saturation Results: Nylon-Air-Oil, Average Porosity 0.85

In general, changes in saturation and changes in porosity produced similar conductivity results in the nylon system. Observing the parallel distribution equation predictions, the excellent correlation with the nylon data corresponds with the results for the two-phase study. The introduction of the more conductive oil accomplishes a significant reduction in the solid-fluid conductivity ratio (from 10 to 1.6), and the heat flow in the solid phase would be maximized even if it were not for the appreciable contribution of the solid-solid contact area in the nylon system.

At the lower saturation levels, the conductivity of the system, when the oil is introduced, should lag slightly until the oil becomes the predominant fluid in the pore spaces. The parallel distribution equation accounts for the oil-phase contribution as a whole, but the oil actually is in discrete pockets throughout the bed. Consequently, the contribution of the liquid would not be a maximum one until the saturation is increased. Looking at Fig. 26 and 27, the conductivity values at the lower saturation levels are slightly below the parallel model prediction.

PARTIALLY SATURATED GLASS FIBER BEDS

The conductivity versus saturation results for the glass fiber systems are presented in Fig. 28 and 29. A complete summary of the operating conditions and conductivity results is given in Table XII of Appendix III.

The conductivity change of the glass system as the oil was introduced was much more pronounced than in the nylon system. In the saturation region of 0.4 to 0.8 the conductivity of the glass fiber bed increased very rapidly and then leveled off at saturations above 0.8.

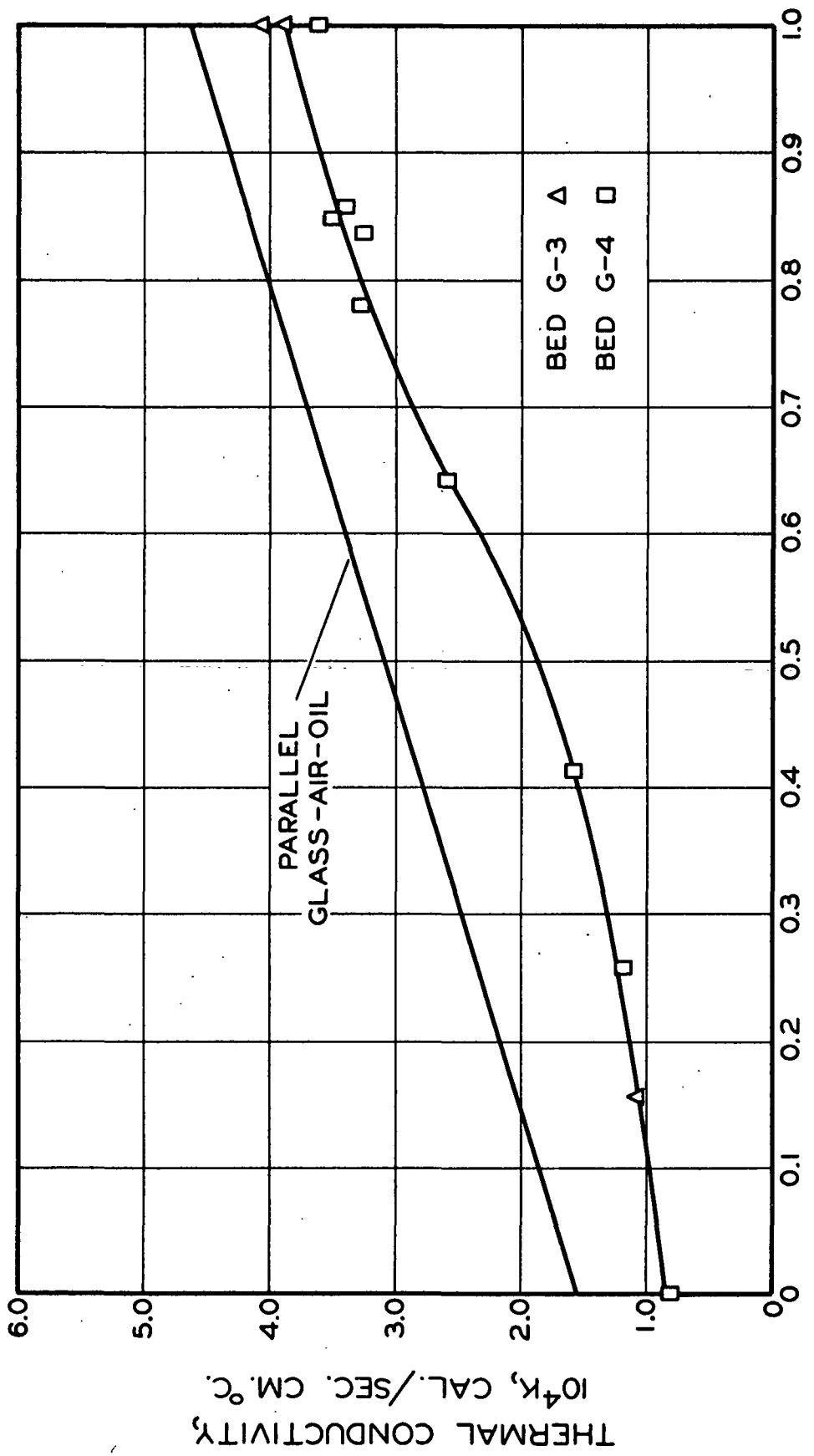

Figure 28. Partial Saturation Results: Glass-Air-Oil, Average Porosity 0.96

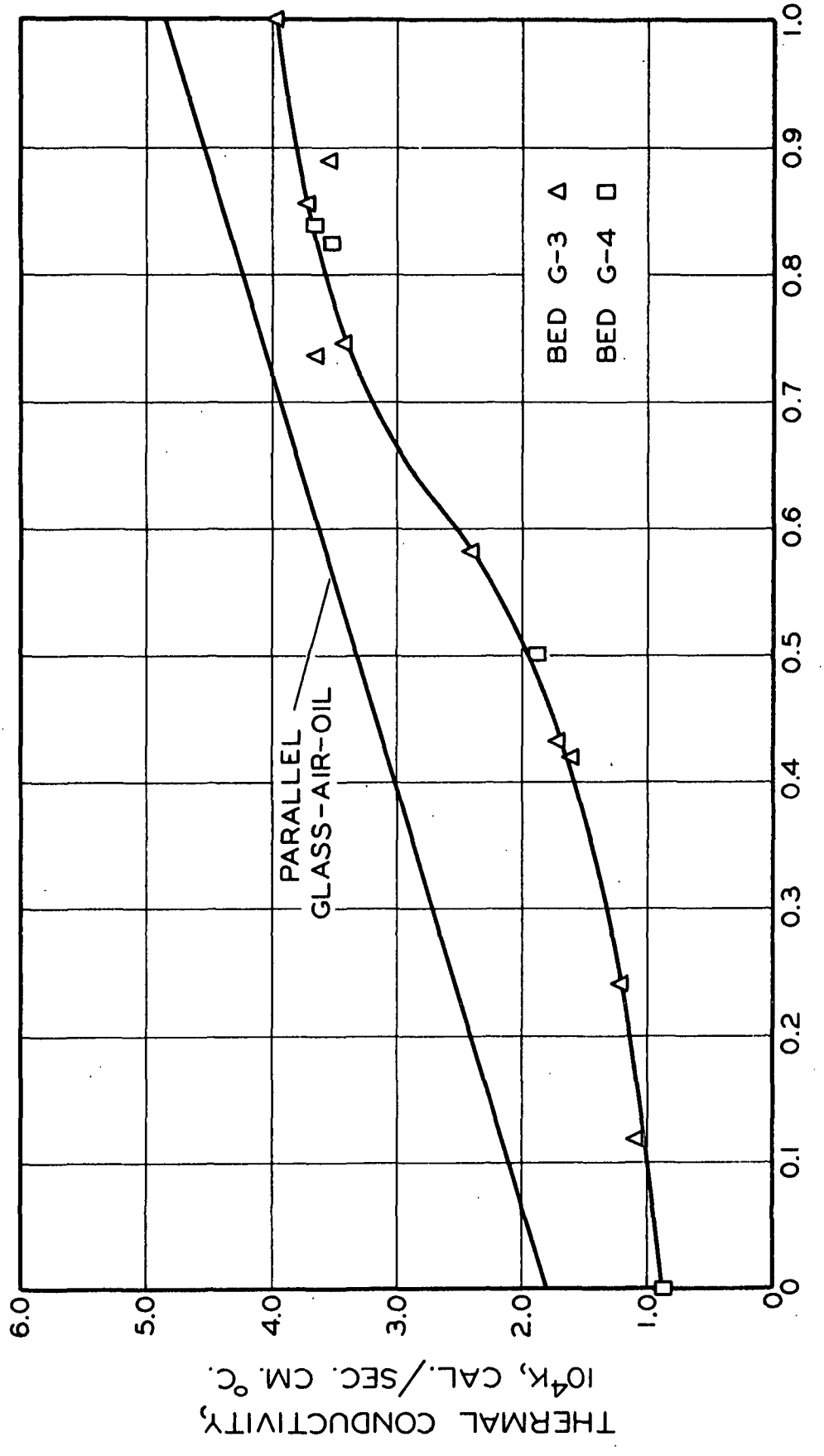

Figure 29. Partial Saturation Results: Glass-Air-Oil, Average Porosity 0.95

It would be expected that the presence of the small amount of the more conductive oil in the contact regions would give rise to an appreciable increase in the conductivity of the fiber system. At the lower saturation levels, the conductivity of the glass fiber bed increases with saturation, but not very rapidly. However, it should be noted that even at the fully saturated conditions, the conductivity results are still 20% below the parallel model. Therefore, the reduction of the solid-fluid conductivity ratio does produce a significant change in the heat flow in the solid structure, but in the initial stages of oil introduction this change is masked by the predominant fluid in the voids—air. When the predominant fluid becomes oil, a rapid increase in conductivity is observed.

In the higher saturation region, the conductivity response levels off also because the relative changes in the system become minor. Even though the less conductive air is being replaced, the effect on the over-all bed conductivity ceases to be important.

ANALYSIS OF THREE-PHASE CONDUCTIVITY RESULTS

PREDICTION EQUATIONS

As in the case of the two-phase results, the conductivity responses of the three-phase systems are consistent if one takes into account the compressional characteristics of the fiber. The contribution of the contact area in the nylon system at porosities less than 0.92 is highly significant and enhances heat flow in the solid structure of the bed. The introduction of the oil does not alter these concepts, and the response of the partially saturated nylon bed is adequately predicted by the parallel model. Any variation in this model should arise at the lower saturation levels where the liquid contribution would not be a maximum. However, this alteration would not be extremely significant.

With the glass system, the description of the configuration of the liquid in the porous network at the lower levels of saturation is necessary in order to account for the liquid contribution. With the glass bed the liquid is more significant since the conductivity contribution of the solid structure is not a maximum. Therefore, a poor assumption about the liquid contribution to heat flow will bring about appreciable discrepancies. This situation is similar to the solid-phase contribution in the two-phase system.

The conductivity relationship which was derived for a three-phase compressible system assumed that the fluid phases were continuous in the network and were parallel paths of heat flow. The equation is

$$K = \epsilon(1-s)K_g + \epsilon s K_\ell + \frac{(1-\epsilon)}{(1/K_s) + (1/D_f h_c \alpha)} \qquad (12)$$

The application of Equation (12) to the partially saturated nylon conductivity data produces the parallel distribution expression because the $\underline{h}_c\alpha$ factor at the porosity levels of 0.90 and 0.85 is calculated to have a value of at least 10.0. Such a value makes the contact resistance term negligible and Equation (12) becomes equivalent to Equation (24).

The application of Equation (12) to the partially saturated glass conductivity data gives the contact factors as shown in Fig. 30. The results of $\underline{h}_c\alpha$ calculations illustrate that Equation (12) does not provide a satisfactory description of the component contributions. Starting with the dry bed, the contact factor would be expected to increase as the oil is introduced. Obviously, Equation (12) allows too much of the heat flow to be attributed to the liquid phase, and the calculated contact factor decreases. Most likely, the liquid phase is initially retained between the fibers and around the contacts, and the heat flow in these regions is increased, thereby increasing the heat flow in the solid structure. Once the liquid occupies a predominant portion of the porous network, a significant contribution to the over-all heat flow in the bed can be attributed to the liquid phase. Then, Equation (12) gives a more realistic prediction as noted in Fig. 30 at saturations above 0.6.

The increased contribution by the contact region when the air is replaced by the oil is shown by the increased value of $\underline{h}_c\alpha$ at the high saturation levels and also by the increase in the contact factor as the porosity is reduced.

A contributing influence to the discrepancies in Equation (12) is the gas-phase contribution. When the air becomes discrete pockets dispersed in the porous network, the model system is erroneous.

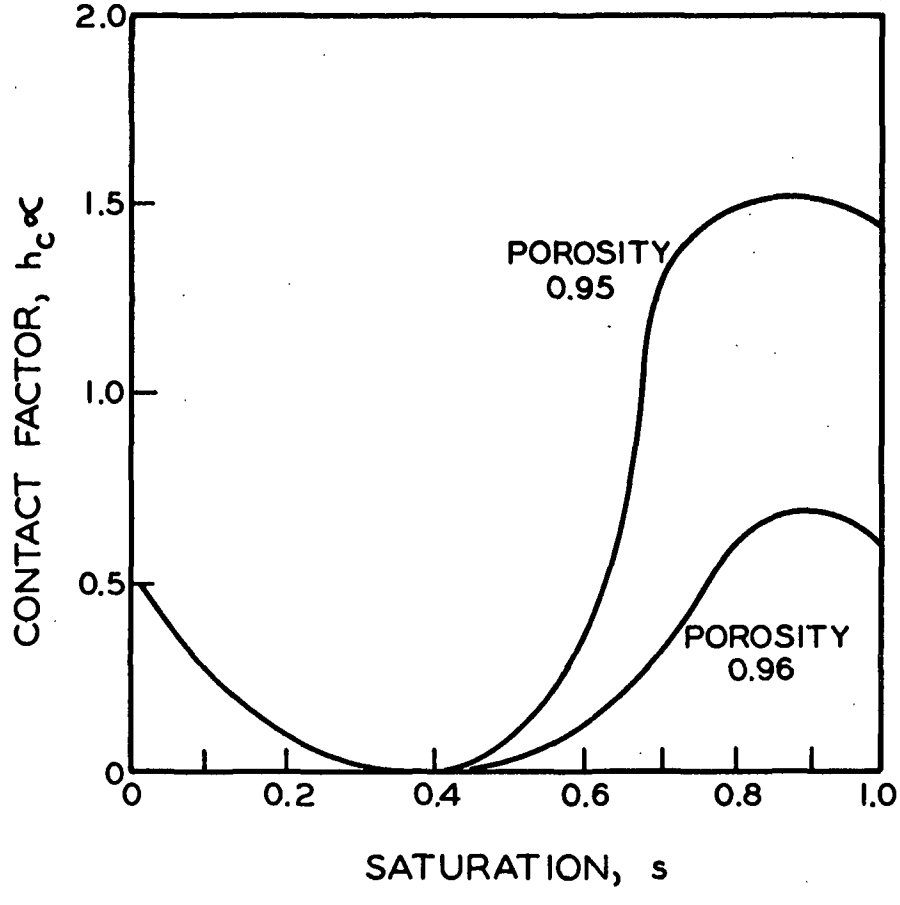

Figure 30. Contact Factor for Glass-Air-Oil System

The increased complexity of the system geometry has made the weaknesses of the model more apparent and, therefore, it is considerably less satisfactory than in the two-phase system.

Eucken (58) utilized Maxwell's relation for the conductivity of an aggregate consisting of one phase in which spheres of the other phases are embedded in deriving an equation for any number of phases. The generalized expression is

$$K = K_c \frac{1 - \sum_i 2V_i(K_c - K_i)/(2K_c+K_i)}{1 + \sum_i V_i(K_c-K_i)/(2K_c+K_i)} \qquad (25)$$

where K_c is the conductivity of the continuous phase and V_i is the fraction volume of the i^{th} phase whose conductivity is K_i.

Equation (25) was utilized to calculate the conductivity of the nylon-oil-air and the glass-oil-air system with (a) the gas phase continuous and (b) the liquid phase continuous. The results for the 0.90 porosity nylon bed and the 0.96 porosity glass bed are given in Fig. 31 and 32, respectively.

In the lower saturation region, with the air as the continuous phase, Equation (25) predicted lower values than were observed experimentally. This is the result of the interaction between particles which was discussed in the two-phase analysis. In the upper saturation region where the oil is the continuous phase, the predictions corresponded reasonably well with the data, especially in the glass system.

The interesting result of these calculations with Eucken's equation is associated with the type of transition which has to occur in the system as the continuous phase shifts from the gas to the liquid and the resultant change in the conductivity response. Also, the shift from the larger solid-fluid conductivity

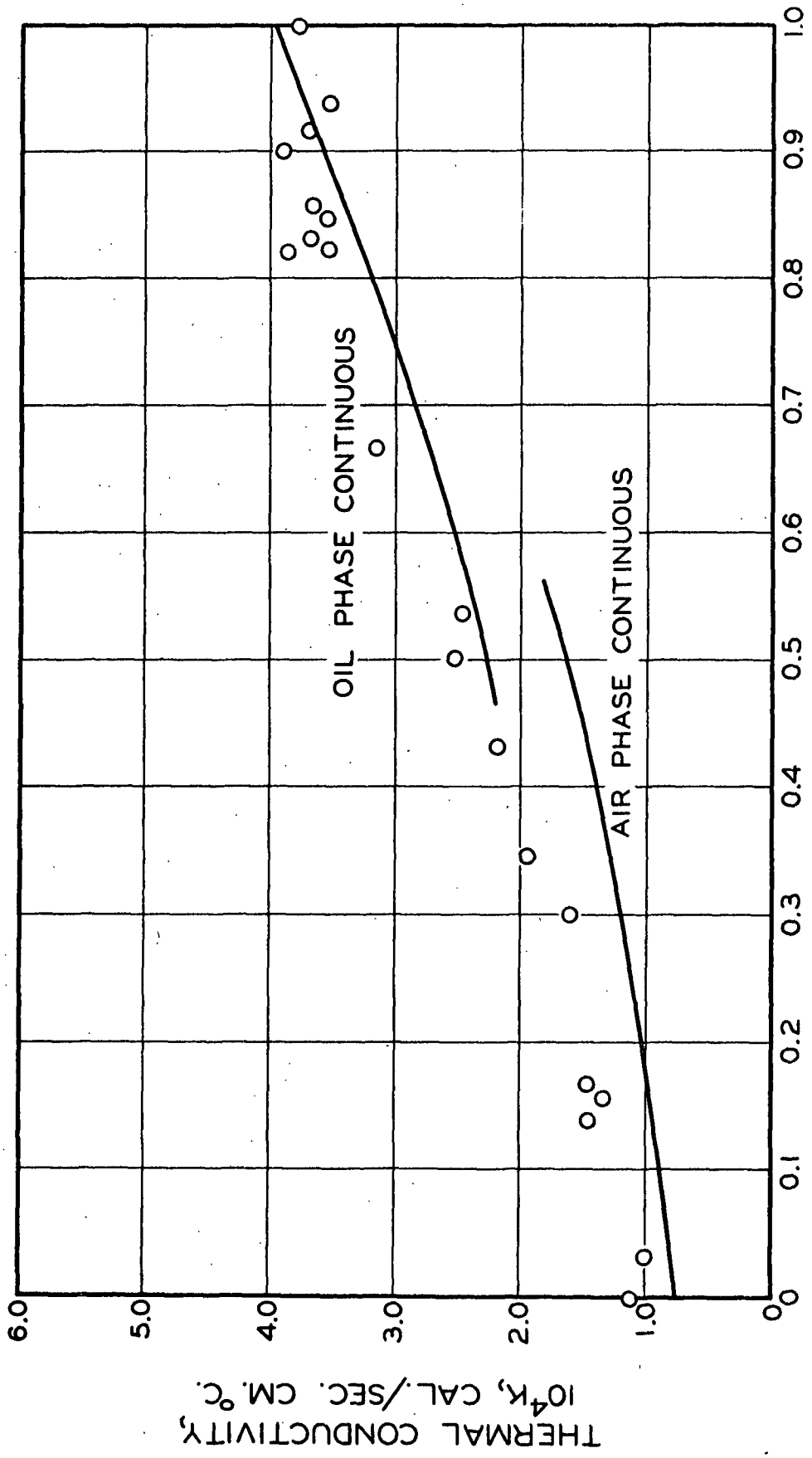

Figure 31. Equation (25) Prediction of Nylon-Air-Oil Results, Porosity 0.90

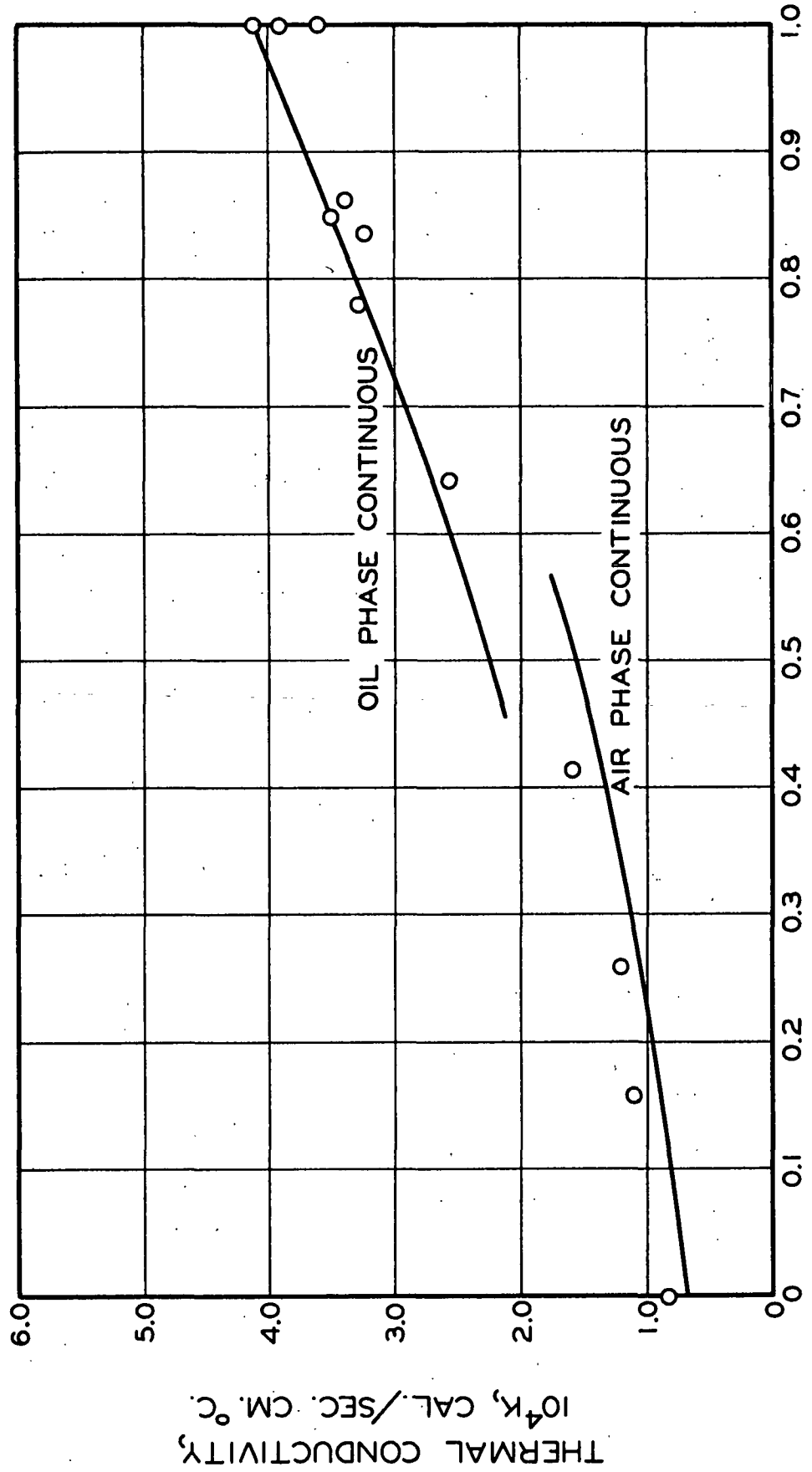

Figure 32. Equation (25) Prediction of Glass-Air-Oil Results, Porosity 0.96

ratio produces an appreciable change in the correlation. In the nylon case, where the oil-saturated bed is almost a homogeneous network, Equation (25) closely predicts the conductivity value as would be expected. In the glass case, the solid-fluid ratio is reduced considerably in going from the air-continuous to the oil-continuous system (from 40 to 6.5). Also, the particle interaction is not as significant. The net result of these factors produces an excellent correlation in the upper saturation levels for the glass system.

SYSTEMS WITH A VOLATILE LIQUID PHASE

The extension of the information acquired in the partial-saturation study with a nonvolatile oil to the more applicable systems with a volatile liquid phase presents a great many difficulties. These difficulties arise primarily from the inadequate understanding of the mechanisms involved in the heat transfer in the porous material. Therefore, no generalized correlation is satisfactory in all cases, and further efforts with other fiber systems with various solid-liquid-gas conductivity ratios are necessary in order to provide a definite correlation in the general case.

The purely conductive characteristics of a given porous system may be estimated quite well under certain circumstances. If the system has a low value of the solid-fluid conductivity ratio, the most consistent estimate can be acquired with the parallel distribution equation. Cowan (3) utilized the parallel model for his analysis of the glass-water-air system in order to estimate the pure conduction conductivity values for his partially saturated beds. From the information previously discussed on the two-phase systems, it can be said that the conductivity of the glass-water system, which has a solid-fluid conductivity ratio of 1.65, would be adequately predicted by the parallel model, but that the glass-air system would be overestimated.

Cowan observed that the glass-air system was overestimated by the parallel model, and he utilized an effective glass conductivity value of 7.5×10^{-4} cal./sec.cm.°C. in his calculations. This type of modification placed restrictions on the parallel model which are similar to the empirical treatments which were utilized in this study. Looking at the conductivity results reported by Cowan and Herminge (33) as shown in Fig. 1, it is obvious that the pure conduction contribution is only a fraction of the total heat flow in the glass-water-air system. Consequently, an inadequate estimate of the pure conductivity in the lower saturation regions will not produce an appreciable error in the over-all, apparent conductivity prediction of the system with a volatile liquid phase.

Considering other fibrous systems, such as paper, which have deformable fibers one would expect a good prediction of the conduction contribution to heat flow to be acquired from the parallel phase distribution equation. The solid-fluid conductivity ratios in the wood fiber-water-air system are low, but more important, the fiber-fiber contact areas are significant and should greatly enhance the heat flow in the fiber network. The internal geometry of both the fiber and the fiber network are complex. Consequently, it is fortunate that the use of the phase distribution equation in such instances may provide an adequate estimate of the conductivity.

The estimates of the vapor movement contribution to heat flow by Philip and deVries (29) and Herminge (33), produced good results in their systems. However, the exact nature of the vapor diffusion and the associated diffusivity in porous systems has yet to be determined and the value of the heat transfer attributable to this mechanism awaits this information.

SUGGESTIONS FOR FUTURE WORK

The confirmation of the contribution of the fiber-fiber contact areas to the heat flow in the solid structure of a fiber bed under compression could be acquired with measurements in vacuo. Subsequent work concerning the incidence of fiber-fiber contacts and the amount of contact area would contribute markedly to the understanding of heat flow in fibrous systems.

A thorough investigation of the extremely high porosity regions of porous materials with variation of temperature, temperature gradient, fiber surface characteristics, pore size, and pore saturant would provide a better insight as to the nature and contribution of the radiation and convection mechanisms.

Additional efforts with a wider range of solid-fluid conductivity ratios would provide a broader basis for a generalized correlation of effective conductivities for both two and three-phase porous systems.

Measurements of conductivities as well as the observation of temperature gradients in the pore spaces of idealized model fiber systems would provide information on the effect of structural geometry in addition to providing a basis for a more fundamental analysis of the composite conductivities.

ACKNOWLEDGMENTS

The author sincerely appreciates the guidance and encouragement provided by his thesis advisory committee during the course of this study and wishes to thank the chairman of the committee, Mr. S. T. Han, and the members, Drs. J. A. Van den Akker, R. W. Nelson, and W. L. Ingmanson.

The successful construction of the apparatus was due to the skill and experience of Mr. H. Marx of The Institute of Paper Chemistry Machine Shop.

Dr. H. E. Robinson, Chief of the Heat Transfer Section of the National Bureau of Standards, provided invaluable advice concerning procedures utilized in conductivity measurements and also made available information on apparatus construction and the conductivity of various materials.

Mr. P. P. Pritulsky of the Textile Fibers Department of E. I. du Pont de Nemours and Company, Inc. provided the information on the conductivity of dacron fibers.

NOMENCLATURE

a = semiaxis of the elliptical contact area, cm.

A = cross-sectional area of bed, sq. cm.

A_c = single fiber-fiber contact area, sq. cm.

C = constant depending on emissivity and geometry of pore space

C_L = number of fiber-fiber contacts per layer

C_t = total number of fiber-fiber contacts in the fiber bed

d_m = maximum thickness of fluid filament between crossed cylinders, cm.

d_{av} = average thickness of fluid filament between crossed cylinders, cm.

D = diffusion coefficient of water vapor in air, sq.cm./sec.

D_f = fiber diameter, cm.

E = modulus of elasticity, g./sq.cm.

g_i = particle shape factor

G = total compressional load on fiber bed, g.

h_c = heat transfer coefficient for total contact region, cal./sec.sq.cm.°C.

h'_c = heat transfer coefficient for fiber-fiber contact area, cal./sec.sq.cm.°C.

H = bed thickness, cm.

K = effective thermal conductivity of system, cal./sec.cm.°C.

K_c = thermal conductivity of continuous phase

K_g = thermal conductivity of gas or fluid phase

K_i = thermal conductivity of i^{th} phase

K_ℓ = thermal conductivity of liquid phase

K_r = apparent thermal conductivity due to radiation

K_s = thermal conductivity of solid phase

K_v = apparent thermal conductivity due to vapor diffusion

ℓ_g = effective length of fluid filament in direction of heat flow, cm.

ℓ_s = effective length of solid particle in direction of heat flow, cm.

L = number of layers in fiber bed

m = transcendental function

n = transcendental function

n_c = effective number of contacts per half particle

N = normal load on single fiber-fiber contact, g.

p = thickness of pore space, cm.

p_o = partial pressure of water vapor, atm.

P = compressional stress on fiber bed, g./sq.cm.

P_a = atmospheric pressure, atm.

q = heat flow rate, cal./sec.

Q = heat flux,cal./sec.sq.cm.

Q_s = heat flux in solid phase, cal./sec.sq.cm.

R = fiber radius, cm.

s = average bed saturation, liquid volume/void volume

T = temperature, °C.

T_a = absolute temperature, °K.

ΔT = total temperature drop, °C.

ΔT_c = temperature drop across contact region

ΔT_s = temperature drop across solid phase

V_g = fractional volume of gas phase, gas volume/total bed volume

V_i = fractional volume of i^{th} phase, phase volume/total bed volume

V_s = fractional volume of solid phase, solid volume/total bed volume

w = side of projected intersection of crossed fibers, cm.

W = weight of fiber bed, g.

x = distance from cylinder axis, cm.

x_o = distance from cylinder axis to boundary of fluid filament, cm.

$\underline{Y}$ = fiber length, cm.

$\underline{Z}$ = ratio of solid conductivity to fluid conductivity

Greek Letters

α = ratio of area of total contact region to total solid area

α' = ratio of area of fiber-fiber contacts to total solid area

β = ratio of distance between particle centers to particle diameter

γ = $\underline{\ell}_s/\underline{D}_f$

δ = ratio of area of fluid filament to total solid area

ϵ = bed porosity, void volume/total volume

θ = angle between axis and differential element, radians

θ_o = angle between axis and boundary of fluid filament, radians

λ = latent heat of vaporization, cal./g.

ξ = Poisson's ratio

ρ = density of fiber, g./cc.

ρ_o = density of saturated water vapor, g./cc.

σ = radiation constant, cal./sec.sq.cm.°K.^{4}

τ = auxiliary angle determining transcendental function

ϕ = $\underline{\ell}_g/\underline{D}_f$

ω = angle between intersecting fibers

LITERATURE CITED

1. Dreshfield, A. C., Jr. A study of transverse moisture distribution and movement during hot-surface drying of paper. Doctor's Dissertation. Appleton, Wis., The Institute of Paper Chemistry, 1956. 175 p.

2. Han, S. T., and Ulmanen, T., Tappi 41, no. 4:185-9(1958).

3. Cowan, W. F. An investigation of the hot surface drying of glass fiber beds. Doctor's Dissertation. Appleton, Wis., The Institute of Paper Chemistry, 1961. 168 p.

4. Heilman, R. H., Mech. Eng. 52, no. 7:693-8(1930).

5. Finck, J. L., Bur. Standards J. Research 5:973-84(1930).

6. Bogaty, H., Hollies, N. R. S., and Harris, M., Textile Research J. 27:445-9 (1957).

7. Takamura, Y., J. Phys. Soc. Japan 8, no. 5:674-6(Sept.-Oct., 1953).

8. Wilhelm, R. H., Johnson, W. C., Wynkoop, R., and Collier, D. W., Chem. Eng. Progr. 44, no. 2:105-16(1948).

9. Waddams, A. L., J. Soc. Chem. Ind. (London) 63:206-10(1944).

10. Aberdeen, J., and Laby, T. H., Proc. Roy. Soc. (London) 113A:459-77(1926).

11. Kannuluick, W. G., and Martin, L. H., Proc. Roy. Soc. (London) 141A:144-58 (1933).

12. Griffiths, —., Dept. Sci. Ind. Research (Brit. Gov.) Food Invest. Special Rep. No. 35, 1929.

13. Saunders, O. A., Phil. Mag. 13:1186-8(1932).

14. Schuhmann, T. E. N., and Voss, V., Fuel. 13:249-56(1934).

15. Woodside, W., and Messmer, J. H., J. Appl. Phys. 32, no. 9:1688-99(Sept., 1961).

16. Strickler, H. S., J. Chem. Phys. 20:1333(1952).

17. Orr, C., Jr., Ind. Eng. Chem. 47:356(1955).

18. Strickler, H. S., Ind. Eng. Chem. 46:828(1954).

19. Weiniger, J. L., and Schneider, W. G., Ind. Eng. Chem. 43:1229(1951).

20. deVries, D. A., Mededel. Landbouwhogeschool Wageningen 52:1-73(1952).

21. Russell, H. W., J. Am. Ceram. Soc. 18:1-5(1935).

22. Topper, L., Ind. Eng. Chem. 47, no. 7:1377-9(1955).

23. Woodside, W., Can. J. Phys. 36:815-23(1958).

24. Webb, J., Nature 177:989(1956).

25. Kunii, D., and Smith, J. M., A.I.Ch.E. Journal 6, no. 1:71-8(1960).

26. Deissler, R. G., and Eian, C. S., Nat. Advisory Comm. Aeronaut., RM E52C05, 1952.

27. Schotte, W., A.I.Ch.E. Journal 6, no. 7:63-7(1960).

28. Austin, J. B., Symposium on thermal insulating materials, Philadelphia, ASTM, 1939.

29. Philip, J. R., and deVries, D. A., Trans. Am. Geophys. Union 38, no. 2:222-32 (1957).

30. deVries, D. A., Bull. inst. intern. froid., Annexe 1952-1:115-31(1952).

31. Woodside, W., and Cliffe, J. B., Soil Sci. 87:75-82(1959).

32. Woodside, W., and deBruyn, C. M. A., Soil Sci. 87:166-73(1959).

33. Herminge, L., Tappi 44, no. 8:570-5(Aug., 1961).

34. Gemant, A., J. Appl. Phys. 21:750-2(1950).

35. deVries, D. A., Nature 178:1074-5(1956).

36. Webb, J., Nature 178:1074-5(1956).

37. Nissan, A. H., Kaye, W. G., and Bell, J. R., A.I.Ch.E. Journal 5, no. 1: 103-10(1959).

38. Bell, J. R., and Nissan, A. H., A.I.Ch.E. Journal 5, no. 3:344-7(1959).

39. Woodside, W., and Kuzmak, J. M., Trans. Am. Geophys. Union 39, no. 4:676-80 (1958).

40. Onogi, S., and Sasaguri, K., Tappi 44, no. 12:874-80(Dec., 1961); J. Japan. Tappi 4:233-8(1957).

41. Finch, R. B., Textile Research J. 21, no. 6:383-92(1951).

42. Jones, R. L. An investigation of the effect of fiber structural properties on the compression response of fibrous beds. Doctor's Dissertation, Appleton, Wis., The Institute of Paper Chemistry, 1962. 158 p.

43. Arnold, E. Light scattering in fibrous sheets. Doctor's Dissertation. Appleton, Wis., The Institute of Paper Chemistry, 1961. 139 p.

44. Ilvessalo-Pfaffli, M., and Alfthan, G. V., Paper and Timber 39, no. 11:509-16(1957).

45. Du Pont. Identification of fibers in textile materials, Bulletin X-156, Dec., 1961.

46. Du Pont. Textile Fibers, Technical Information, Bulletin N-54, Jan., 1956.

47. Wilder, H. D. Personal communication, 1962.

48. Pritulsky, P. P. Personal communication, 1962.

49. Owens-Corning. Textile fiber materials for industry, June, 1961.

50. Bates, O. K., Ind. Eng. Chem. 25:431-7(1933).

51. Hercus, E. O., and Laby, T. H., Proc. Roy. Soc. (London) 95A:190-210(1919).

52. Baxter, S., Proc. Phys. Soc. (London) 105-18(1946).

53. Fluker, B. J., Texas Eng. Exp. Sta. News 8, no. 1:3-7(1957).

54. Pratt, A. W., and Ball, J. M. E., J. Inst. Heating Ventilating Engrs. 24: 201-26(1956).

55. Gier, J. T., Dunkle, R. V., and Bevans, J. T., Refrig. Eng. 66, no. 3:39-42 (1958).

56. Mischke, C. R., and Farber, E. A., Wisconsin, Univ. Eng. Exp. Sta., Res. Rep. No. 5(1956).

57. Somers, E. V., and Cyphers, J. A., Rev. Sci. Instr. 22, no. 8:583-6(1951).

58. Eucken, A., Forsch. Gebiete Ingenieurw., VDI-Forschungsh. 353(March-April, 1932).

APPENDIX I

ANALYSIS OF ALIGNED CYLINDERS

The two-component system to be analyzed consisted of solid, cylindrical fibers and a stagnant fluid. The stagnant fluid was considered as the continuous component filling the void spaces of the system. The fibers were considered as perfect cylinders of diameter, D_f, and of length, Y.

The relationships derived by Kunii and Smith (25) were used as a guide during the initial analysis, and similar heat transfer mechanisms were assumed to be operable in this system as in their system of spherical particles. The mechanisms were:

1. Heat transfer through the void space by conduction.
2. Heat transfer through the solid particle by conduction.
3. Heat transfer through the contact surface of the particles.
4. Heat transfer through the fluid filament adjacent to the contact surfaces.

Using these mechanisms, which neglect radiation and convection, an expression for the effective over-all conductivity of the two-component system was derived.

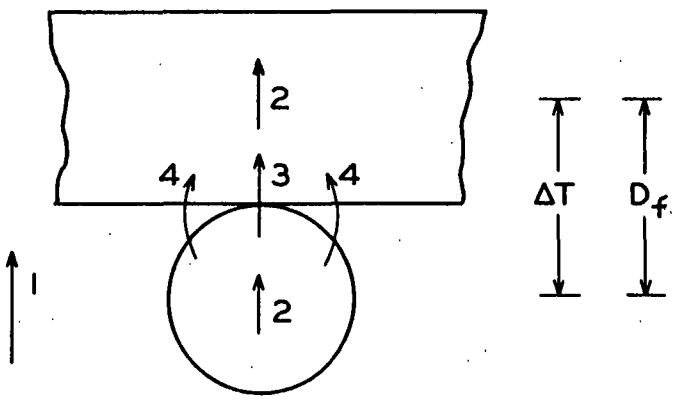

Assume that Mechanism 3 and Mechanism 4 are in parallel, Mechanism 2 is in series with combined 3 and 4, and Mechanism 1 is in parallel with combined 2, 3, and 4.

The over-all heat flux = $K\Delta T/D_f$ = (heat flux in voids)+(heat flux in solid) (28)

(heat flux in voids) = $K_g \epsilon \Delta T/D_f$ (29)

(heat flux in solid) = Q_s (30)

with,

$$\Delta T = \Delta T_s + \Delta T_c \tag{31}$$

where ΔT_s = temperature drop in solid

ΔT_c = temperature drop near contact

Then

$$\Delta T_s = Q_s/(K_s/\ell_s)(1-\epsilon) \tag{32}$$

$$\Delta T_c = Q_s/[(K_g/\ell_g) + h'_c][1-\epsilon] \tag{33}$$

where ℓ_s = effective length of solid resistance

ℓ_g = effective length of fluid filament resistance

h'_c = heat transfer coefficient for solid-solid contact

Combining Equations (28) through (33) and letting $\gamma = \ell_s/D_f$ and $\phi = \ell_g/D_f$ gives

$$K/K_g = \epsilon + \frac{(1-\epsilon)}{1/(1/\phi + D_f h'_c/K_g) + \gamma(K_g/K_s)} \tag{34}$$

If the heat transfer through the contact is neglected

$$K/K_g = \epsilon + (1-\epsilon)/(\phi + \gamma K_g/K_s) \tag{35}$$

The value of $\emptyset$ can be calculated using several techniques. Although the exact technique of Kunii and Smith was not detailed in their article, the same results can be obtained for their system by using the following method.

The initial attack was on the simplified case with the cylinders parallel and having line contact. A single contact is considered. Heat flow is parallel to the axis between particles. The basis of the technique is the definition of the heat flow through differential elements of the model solid-fluid system, the summation of the elements, and the application of the assumed resistances.

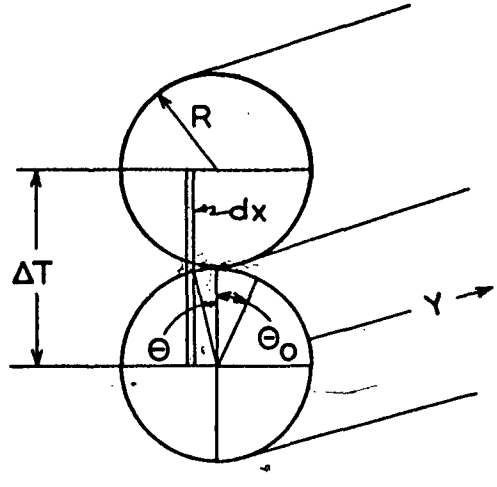

$x = R\sin\Theta$

$dx = R\cos\Theta d\Theta$

Y = FIBER LENGTH

R = FIBER RADIUS

ΔT = TEMPERATURE DROP

Heat flow through solid:

$$dq = \frac{K_s(2Ydx)\Delta T_s}{(2\ R\cos\theta)} = K_s Y \Delta T_s d\theta \qquad (36)$$

Heat flow through fluid filament:

$$dq = \frac{K_g(2Ydx)\Delta T_c}{2(R-R\cos\theta)} = K_g Y \Delta T_c \frac{\cos\theta d\theta}{(1-\cos\theta)} \qquad (37)$$

with $\Delta \underline{T} = \Delta \underline{T_s} + \Delta \underline{T_c}$

then

$$\Delta T = \frac{dq}{K_s Y d\theta} + \frac{dq(1-\cos\theta)}{K_g Y \cos\theta d\theta} \tag{38}$$

Solving for dq, simplifying, and letting $Z = K_s/K_g$

$$dq = \frac{K_s Y \Delta T \cos\theta d\theta}{Z-(Z-1)\cos\theta} \tag{39}$$

The total heat flow rate is

$$q = K_s Y \Delta T \int_0^{\theta_o} \frac{\cos\theta d\theta}{Z-(Z-1)\cos\theta} \tag{40}$$

Integrating

$$q = \frac{K_s Y \Delta T}{(Z-1)} \left[\frac{2Z}{\sqrt{2Z-1}} \left(\tan^{-1} \sqrt{2Z-1} \quad \tan\theta_o/2 \right) - \theta_o \right] \tag{41}$$

An alternate expression in terms of the resistance to the two mechanisms

$$q = \frac{(2YR\sin\theta_o)\Delta T}{(\ell_s/K_s) + (\ell_g/K_g)} = \frac{Y\sin\theta_o \Delta T}{(\gamma/K_s) + (\phi/K_g)} \tag{42}$$

Equating (41) and (42) and solving for ϕ gives

$$\phi = \frac{(1-1/Z)\sin\theta_o}{\left[\frac{2Z}{\sqrt{2Z-1}} \left(\tan^{-1} \sqrt{2Z-1} \quad \tan\theta_o/2 \right) - \theta_o \right]} - \frac{\gamma}{Z} \tag{43}$$

Letting n_c = number contacts for one half of a single particle and assuming $(1/n_c)$ to be the fractional amount of heat passing through a single contact and adjacent fluid filament then,

$$1/n_c = 2x_o Y/2RY = \sin\theta_o \qquad (44)$$

With close packing of cylinders below, the total number of contacts equals 3.

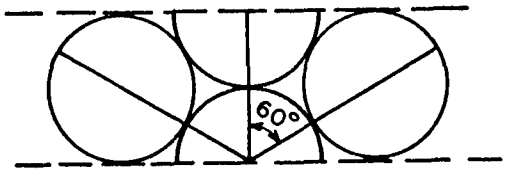

However, correcting for orientation of the two contacts 60° from the axis between particles, $\underline{n}_c = 1 + 2(\cos 60°) = 2$. Using $\sin\theta_o = 1/2$ and $\gamma = \pi/4$ (see Appendix II) Equation (43) was utilized to acquire the following results:

with $\underline{Z} = 10$ for nylon-air, $\emptyset = 0.052$

with $\underline{Z} = 40$ for glass-air, $\emptyset = 0.029$

Using Equation (35), the predicted values for the nylon and glass fiber beds are shown in Fig. 33. In the nylon case the values are lower than experimental, while the glass values are larger as was expected. Both predictions closely align with the Kunii and Smith $\emptyset_2$ prediction for close-packed spheres.

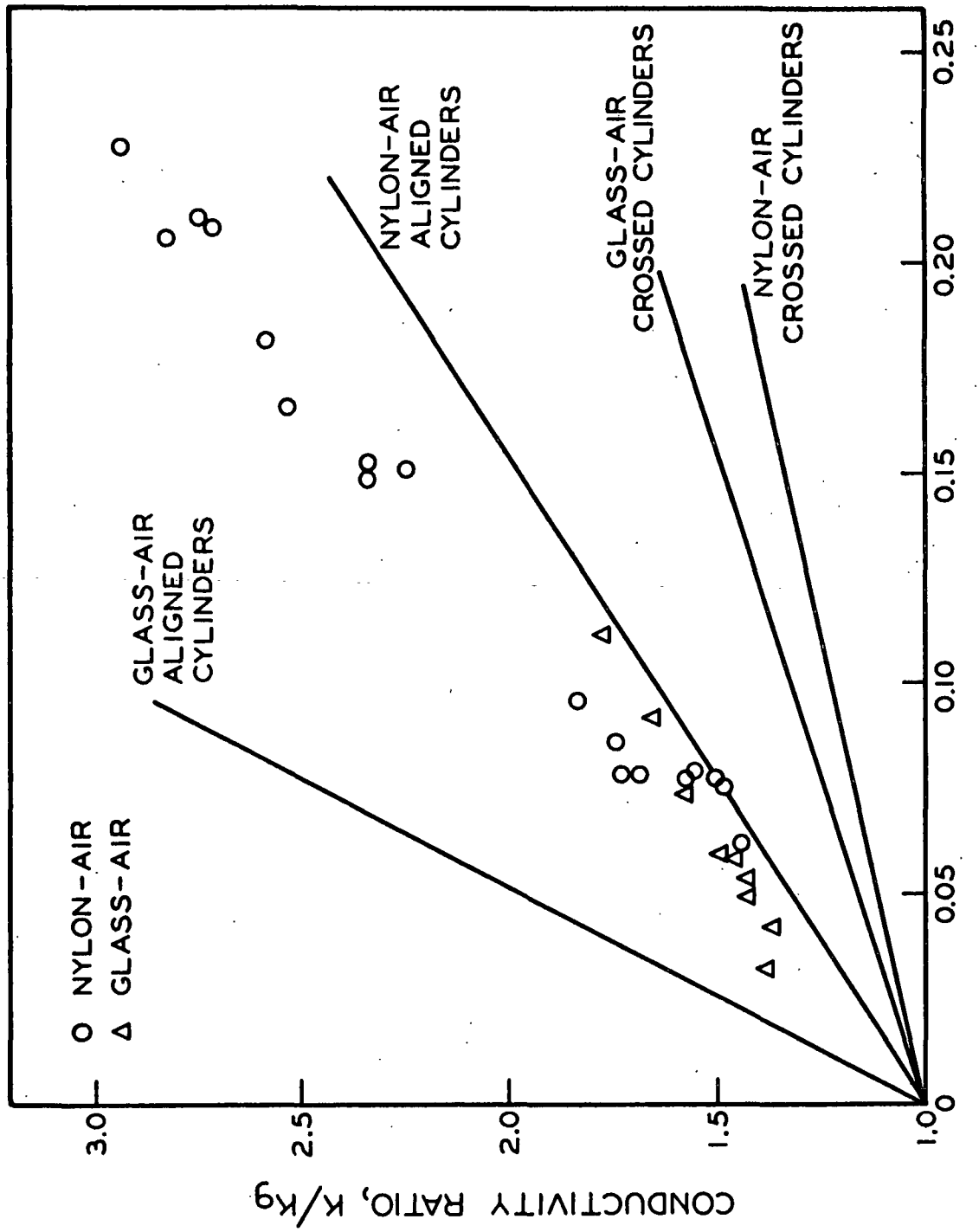

Figure 33. Conductivity Versus Solid Fraction

APPENDIX II

ANALYSIS OF CROSSED FIBERS

The evaluation of $\emptyset$, as given in Equation (35) of Appendix I, for crossed fibers presented geometrical considerations which were impractical. The evaluation of the effective resistance of the solid phase and the fluid filament was accomplished by changing to a projected cross section of fibers intersecting with axes perpendicular.

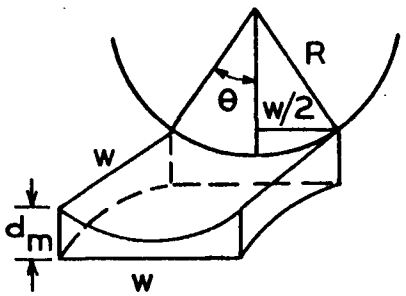

$\underline{w}$ = side of projected area of fiber crossing

$\underline{R}$ = radius of fiber

$\underline{w}^2$ = projected area of fiber crossing

$\underline{d}_m$ = maximum thickness of fluid filament volume

$\underline{d}_{av}$ = average thickness of fluid filament volume

$$\text{total volume} = d_m w^2 = w^2(2R - 2\sqrt{R^2 - w^2/4}) \tag{45}$$

$$\text{volume of cylinder sections} = wR^2(2\theta - \sin 2\theta)$$

$$= 2R^2 w \sin^{-1}(w/2R) - w^2\sqrt{R^2 - w^2/4} \tag{46}$$

$$\text{fluid filament volume} = \text{total} - \text{cylinder sections}$$

$$= 2Rw^2 - w^2\sqrt{R^2 - w^2/4} - 2R^2 w \sin^{-1}(w/2R) \tag{47}$$

$\underline{d}_{av}$ = fluid filament volume/projected area

$$d_{av} = 2R - \sqrt{R^2 - w^2/4} - (2R^2/w)\sin^{-1}(w/2R) \qquad (48)$$

if $\underline{w} = 2\underline{R}$, then $\underline{d}_{av} = 2\underline{R}(1-\pi/4)$

then if $\underline{d}_{av} = \underline{\ell}_{\underline{g}}$, $\emptyset = 1-\pi/4 = 0.215$

if $\underline{\ell}_{\underline{s}} = 2\underline{R}-\underline{d}_{av} = 2\underline{R}\pi/4$, then $\gamma = \pi/4 = 0.785$

Using these values in Equation (35) produces results which are much too low as illustrated in Fig. 33.

APPENDIX III

PARTIAL SATURATION STUDIES

TABLE XI

NYLON FIBER BEDS[a]

Run No.	Fiber Bed Temp., °C.	Fiber Bed $\Delta\underline{T}$, °C.	$\Delta\underline{T}$ Ratio	Saturation	Bed Conductivity, $10^4\underline{K}$ cal./sec.cm.°C.
Bed N-3—Porosity 0.903					
NOS-15	56	16.1	0.607	0.898	3.86
NOS-16	55	16.6	0.655	0.847	3.57
Bed N-4—Porosity 0.909					
NOS-18	56	16.6	0.661	0.940	3.54
Bed N-4—Porosity 0.849					
NOS-21	56	10.5	0.365	0.956	4.16
NOS-22	55	14.5	0.533	0.535	2.85
Bed N-6—Porosity 0.905					
NOS-28	55	16.3	0.645	0.830	3.63
NOS-29	57	17.2	0.659	0.826	3.56
NOS-24	55	15.6	0.612	0.818	3.83
NOS-25	56	17.2	0.743	0.666	3.15
NOS-26	56	20.2	0.937	0.500	2.50
NOS-27	53	21.6	1.190	0.344	1.97
Bed N-6—Porosity 0.853					
NOS-30	56	10.5	0.362	0.937	4.19
NOS-32	56	11.1	0.378	0.808	4.02
NOS-33	56	11.9	0.416	0.705	3.65
NOS-31	55	12.4	0.447	0.660	3.40
NOS-34	56	13.8	0.510	0.543	2.98
NOS-35	55	15.7	0.628	0.412	2.42
NOS-36	55	22.4	1.046	0.120	1.45

TABLE XI (Continued)

NYLON FIBER BEDS[a]

Run No.	Fiber Bed Temp., °C.	Fiber Bed $\Delta\underline{T}$, °C.	$\frac{\Delta T}{\text{Ratio}}$	Saturation	Bed Conductivity, $10^4\underline{K}$ cal./sec.cm.°C.
Bed N-7—Porosity 0.909					
NOS-38	55	16.7	0.650	0.850	3.60
NOS-39	55	21.5	0.953	0.532	2.46
NOS-40	56	27.4	1.395	0.300	1.68
NOS-41	57	30.7	1.600	0.161	1.46
Bed N-7—Porosity 0.859					
NOS-43	55	10.8	0.360	0.840	4.31
NOS-45	56	11.6	0.387	0.757	3.92
NOS-57	55	12.6	0.452	0.618	3.36
NOS-47	55	14.3	0.508	0.508	2.99
NOS-49	54	16.5	0.625	0.368	2.43
NOS-42	54	18.6	0.748	0.260	2.03
NOS-52	56	23.5	0.994	0.167	1.53
NOS-54	56	25.7	1.125	0.070	1.35
Bed N-8—Porosity 0.902					
NOS-19	56	15.9	0.622	1.0	3.77
Bed N-8—Porosity 0.850					
NOS-17	55	10.2	0.349	0.787	4.35
NOS-11	56	10.2	0.346	0.777	4.40
NOS-12	66	12.7	0.345	0.777	4.41
NOS-7	55	10.0	0.355	0.632	4.28
NOS-8	64	12.4	0.353	0.632	4.31
NOS-14	56	15.0	0.570	0.370	2.66
Bed N-9—Porosity 0.898					
NOS-5	45	21.6	1.61	0.136	1.45
NOS-3c	57	29.0	1.61	0.136	1.45
NOS-4	64	34.0	1.60	0.136	1.46

TABLE XI (Continued)

NYLON FIBER BEDS[a]

Run No.	Fiber Bed Temp., °C.	Fiber Bed ΔT, °C.	$\frac{\Delta T}{\bar{T}}$ Ratio	Saturation	Bed Conductivity, $10^4 \frac{K}{\bar{T}}$ cal./sec.cm.°C.
Bed N-9—Porosity 0.842					
NOS-13	64	13.0	0.359	1.0	4.23
NOS-10	53	11.4	0.432	0.533	3.52
NOS-9	64	14.4	0.431	0.533	3.53
NOS-6	56	18.0	0.726	0.204	2.09
Bed N-10—Porosity 0.906					
NOS-44	55	16.1	0.632	0.915	3.70
NOS-46	55	23.6	1.080	0.430	2.17
NOS-48	56	30.5	1.675	0.154	1.40
NOS-50	56	36.6	2.29	0.030	1.02
Bed N-10—Porosity 0.855					
NOS-53	55	10.9	0.370	0.883	4.10
NOS-55	55	11.4	0.398	0.717	3.81
NOS-56	56	13.4	0.468	0.553	3.24
NOS-58	56	17.6	0.681	0.304	2.23
NOS-59	55	17.7	0.743	0.218	2.04
NOS-60	55	20.8	0.925	0.117	1.64
NOS-61	55	23.1	1.040	0.050	1.46
NOS-51	55	25.2	1.200	0.050	1.27

[a]All beds from 3-denier fibers, 2.78 mm. long, except Bed N-4 with 5.54-mm. fibers.

TABLE XII

GLASS FIBER BEDS

Run No.	Fiber Bed Temp., °C.	Fiber Bed ΔT, °C.	$\frac{\Delta T}{\text{Ratio}}$	Saturation	Bed Conductivity, $10^4 K$ cal./sec.cm.°C.
Bed G-3—Porosity 0.965					
GOS-1	65	25.1	0.860	1.0	4.05
GOS-13	55	22.6	1.002	1.0	3.46
Bed G-3—Porosity 0.957					
GOS-2	55	17.7	0.732	1.0	3.92
GOS-20	55	17.6	0.707	1.0	4.05
GOS-26	58	39.0	2.600	0.157	1.10
Bed G-3—Porosity 0.947					
GOS-3	56	15.5	0.590	1.0	3.97
GOS-28	56	16.8	0.662	0.887	3.54
GOS-25	56	16.3	0.638	0.852	3.70
GOS-4	56	17.6	0.680	0.747	3.44
GOS-23	55	15.3	0.635	0.735	3.69
GOS-16	55	21.2	0.969	0.581	2.42
GOS-5	56	28.6	1.380	0.428	1.70
GOS-6	55	27.6	1.450	0.418	1.61
GOS-9	55	32.2	1.890	0.242	1.24
GOS-11	55	33.8	2.110	0.118	1.11
Bed G-4—Porosity 0.958					
GOS-7	56	23.1	0.962	1.0	3.60
GOS-24	57	24.6	1.020	0.858	3.40
GOS-10	55	22.4	1.005	0.852	3.45
GOS-12	55	23.7	1.080	0.835	3.21
GOS-15	55	23.4	1.055	0.778	3.29
GOS-17	56	27.6	1.355	0.644	2.56
GOS-18	55	35.4	2.190	0.413	1.58
GOS-22	54	40.1	2.830	0.259	1.22
Bed G-4—Porosity 0.949					
GOS-8	55	19.1	0.789	0.840	3.63
GOS-27	56	19.6	0.810	0.825	3.54
GOS-19	56	29.6	1.520	0.498	1.89

TABLE XIII

DACRON FIBER BED[a]

Run No.	Fiber Bed Temp., °C.	Fiber Bed $\Delta\underline{T}$, °C.	$\frac{\Delta T}{\text{Ratio}}$	Saturation	Bed Conductivity, $10^4\underline{K}$ cal./sec.cm.°C.
Bed D-1—Porosity 0.902					
DOS-1	57	16.3	0.658	0.884	3.56
DOS-2	55	17.0	0.692	0.789	3.38
DOS-3	54	18.2	0.803	0.671	2.98

[a]Fibers—5 denier, 2.04 mm.